

**Constructing a Full-Scale Horizontally-Curved Twin Steel
Trapezoidal Box Girder Bridge Segment to Determine
Redundancies in Fracture Critical Bridges**

by

Timothy J. Barnard, B.S.C.E.

Departmental Report

Presented to the Faculty of the Graduate School of
The University of Texas at Austin
in Partial Fulfillment
of the Requirements
for the Degree of

Master of Science in Engineering

The University of Texas at Austin

December 2006

Copyright

by

Timothy J. Barnard

2006

**Constructing a Full-Scale Horizontally-Curved Twin Steel
Trapezoidal Box Girder Bridge Segment to Determine
Redundancies in Fracture Critical Bridges**

**APPROVED BY
SUPERVISING COMMITTEE:**

Eric B. Williamson

Karl H. Frank

Dedication

To Jesus Christ for providing me strength and to my wife, Kim, and three sons, Joshua, Jacob, and Zachary, for their love, patience, and support during this endeavor.

Acknowledgments

I would like to express my deepest thanks and appreciation to Prof. Eric B. Williamson and Prof. Karl H. Frank for their guidance throughout the course of my graduate studies; it was privilege learning from them. Also, I am grateful to all the faculty members for always being available to answer my questions and for all the much needed advice.

I would like to thank my co-researchers, Catherine Hovell and Jim Sutton, for their hard work, professional attitudes, and friendship during the course of our research. They were wonderful to work with and demonstrated an outstanding work ethic. Others that were vital to the success of this research were Omar Espinoza, Chen Shi, Tanmay Borse, and Rangson Wongjeeraphat for their work on the data collection system. Finally, I would like to thank the host of graduate students that helped cast the concrete foundations and deck for this project.

I would also like to thank the laboratory and administrative staff at Ferguson Laboratory. Dennis Phillip and Blake Stasney were always available to answer questions, give advice, or lend a hand, which enabled our research to stay on schedule. Eric Schell was instrumental in ensuring the high-speed data collection system was setup and functioning properly. A special thanks to Barbra Howard and Ella Schwartz for their kind assistance with acquiring the materials and supplies for the research.

Finally, I would like to thank my family for encouragement and support. None of this would have been possible without them.

December 8, 2006

Table of Contents

CHAPTER 1 – Introduction.....	1
1.1 Introduction	1
1.2 Objectives.....	2
1.3 Scope	3
CHAPTER 2 – Background	4
2.1 Background	4
2.2 Motivation for Research.....	6
CHAPTER 3 – Construction of Test Specimen.....	9
3.1 Introduction	9
3.2 Objectives.....	9
3.3 Repairs to girders	9
3.4 Foundation.....	12
3.4 Bracing	15
3.5 Bridge Deck.....	17
3.6 Rails.....	22
CHAPTER 4 – Instrumentation of the Bridge	26
4.1 Introduction	26
4.2 Objective	27
4.3 Girder Cross-sections	28
4.4 Diaphragms	30
4.5 Deck Reinforcement.....	30
4.6 Shear Studs	32

CHAPTER 5 – Gravity Load Data	35
5.1 Introduction	35
5.2 Objective	35
5.3 Elevation measurements.....	36
5.4 Data Reduction	45
5.4.1 Plate bending	45
5.4.2 Thermal effects.....	46
5.4.3 Data Fluctuations.....	47
5.5 Induced stresses and strains.....	48
5.5.1 Concrete Deck	49
5.5.2 T501 Rail.....	50
5.5.3 Live Load	51
CHAPTER 6 – Conclusion and Recommendations	59
6.1 Summary	59
6.2 Conclusions	60
6.3 Recommendations for Future Research	61
APPENDIX A – Calculations	63
A.1 Elastomeric Bearing Pads.....	63
A.2 Pier Foundation Capacity	68
APPENDIX B – Drawings	76
B.1 Site Plan of Bridge	76
B.2 Foundation Drawings	77
B.3 TxDOT Bridge Structural Details	78
B.4 TxDOT Decking Details	83

B.5 TxDOT Standard T501 Railing Design Details	85
APPENDIX C – Instrumentation Graphs	87
APPENDIX D – Pictures	99
REFERENCES	118
VITA.....	120

List of Tables

Table 3.1: Actual loads per foundation	15
Table 3.2: Average as-built condition of deck prior to casting	18
Table 3.3: Concrete cylinder tests for deck.....	19
Table 3.4: Reinforcing steel test results	20
Table 3.5: Concrete cylinder tests for rail	25
Table 4.1: Shear stud locations	33
Table 5-1: Elevations of foundation corners above benchmark	38
Table 5-2: Load cell calibration	54
Table 5-3: Steel ballast for front axle.....	55
Table 5-4: Live load weights.....	55

List of Figures

Figure 2-1: Aftermath of the Silver Bridge collapse (Charleston Mail 2006)	4
Figure 2-2: Girder fracture on a bridge on I-79 at Neville Island in Pittsburgh, Pennsylvania (Connor, Dexter, and Mahmoud, 2005).....	7
Figure 3-1: (a) Post removal damage of flange and studs prior to shipping to Trinity (b) shear stud damage repaired at Ferguson lab.....	10
Figure 3-2: (a) South end diaphragm top corner connection (b) north end lower corner connection	11
Figure 3-3: New stud welded on to the inner flange of the interior girder.....	12
Figure 3-4: (a) Bearing pad plate and elastomeric layer thickness (b) side view of pad.	13
Figure 3-5: (a) Bottom of north foundation (b) stem wall of south foundaion.	14
Figure 3-6: UTrAp rotations of the girders during deck pour with out external bracing.	16
Figure 3-7: (a) WT Stubs for external cross frames (b) bracing being clamped together prior to welding.	17
Figure 3-8: Tensile test of reinforcing steel.	20
Figure 3-9: Load verses displacement curve for the tensile test on the #4 rebar. .	21
Figure 3-10: Load verses displacement curve for the tensil test on the #5 rebar. .	21
Figure 3-11: (a) Typical T501 rail (TxDOT Bridge Railing Manual, 2206), (b) rebar cage for east rail, (c) formwork for west rail... ..	22
Figure 3-12: (a) Vertical construction joint in west rail at the midspan (b) skewed construction joint north of the centerline in the east rail.....	23
Figure 3-13: Center construction joint on the east rail at midspan.... ..	24
Figure 4-1: Out-of-plan imperfections in the web..... ..	27
Figure 4-2: Instrumented cross-section locations.....	28
Figure 4-3: (a) gages at cut A-A (b) gages at cut B-B.	29
Figure 4-4: (a) single direction strain gage (b) rectangular rosette gage.....	29
Figure 4-5: Inside of the north end diaphragm.....	30
Figure 4-6: Strain gage location for the deck reinforcement.....	31
Figure 4-7: Strain gages on the deck reinforcement and wire placement	31
Figure 4-8: Shear stud strain gage locations.	32
Figure 4-9: (a) Schematic of typical shear stud gage positioning (b) interior girder flange shear stud.....	34

Figure 5-1: (a) Spectra self-leveling laser model LL400 (b) receiver CR500 attached to the measuring rod.....	36
Figure 5-2: Deflection measurement locations..	37
Figure 5-3: Diagram of girder curvature..	39
Figure 5-4: Centerline deflections of interior girder.	40
Figure 5-5: Centerline deflections of exterior girder.....	40
Figure 5-6: Deflections from UTrAp just after deck casting.	42
Figure 5-7: Deflections from finite element model after casting..	42
Figure 5-8: Example of the rotation of the girder cross-section.....	44
Figure 5-9: Cross-sectional rotation of the interior girder along the length.....	44
Figure 5-10: Cross-sectional rotation of the exterior girder along the length.	45
Figure 5-11: Example of thermal effects on the strain.....	47
Figure 5-12: (a) Formwork on bridge (b) deck reinforcing steel..	50
Figure 5-13: .Average microstrains and stresses (ksi) south of midspan after deck casting.....	51
Figure 5-14: Average microstrains and stresses (ksi) after casting rails.....	52
Figure 5-15: (a) (a) Front axle loading (b) rear axle loading	53
Figure 5-16: Load cell connection to crane.....	53
Figure 5-17: Live load position 1.....	56
Figure 5-18: Live load position 2.....	57
Figure 5-19: Third and final live load position.	57
Figure 5-20: Final microstrains and stresses prior to fracture test..	59

CHAPTER 1

Introduction

1.1 INTRODUCTION

The art and science of constructing bridges has been refined over the years with the help of technology and advances in research. The art is displayed through the unique architecture a designer strives to provide a structure that is aesthetically pleasing to the public as they traverse the roadways. The goal of creating an eye-pleasing structure is coupled with the responsibility of ensuring that a bridge will function safely throughout its design life. The expectations for today's bridges have been extended to a design life of 75 years (AASHTO, 2004). It takes a large initial investment to build a bridge and, under the current Federal Highway Administration's mandated inspection criteria, can require a substantial cost to maintain. One factor that contributes to increased maintenance costs for bridges is the use of Fracture Critical Members (FCMs) in their design.

A bridge that is designed or built with a "component in tension whose failure is expected to result in the collapse of the bridge or the inability of the bridge to perform its function" is classified by the American Association of State Highway Transportation Officials' (AASHTO) Load Resistance Factor Design (LRFD) standards as fracture critical (AASHTO, 2004). According to a recent report by the National Cooperative Highway Research Program, this classification is assigned to 11 percent of all steel bridges within the United States (Connor, Dexter, and Mahmoud, 2005). Bridges that fall into this category require thorough inspections at critical details to detect possible failures where the system lacks any redundancy to transfer loads. These inspections are time consuming and add significant costs to the owner's maintenance budget every year. Therefore, it is in the interest of owners (like TxDOT) and bridge designers that a

modeling tool be developed that can determine the inherent redundancies of current fracture critical bridges by accurately predicting their performance after a fracture event.

The opportunity to provide a benchmark for such analytical models presented itself in the fall of 2005 when TxDOT was removing a twin steel trapezoidal box-girder bridge along I-10 in Houston. This type of bridge is considered fracture critical (FC) because losing one of the girders due to a brittle fracture is assumed to cause the entire structure to collapse. This report presents the steps taken to capture data that will aid the study of a twin steel trapezoidal box-girder bridge after a fracture of a bottom flange of one of the girders.

1.2 OBJECTIVES OF THIS REPORT

The objective of this report is to document the design and construction of a full-scale segment of a horizontally curved steel trapezoidal box-girder bridge that can be used to as a calibration tool for future computer analysis models. The following goals were set to maximize the impact of the research:

- design and construct a foundation system for both ends of the bridge that provides sufficient room for deflection of the bridge during the test and allows for the bridge to be supported and repaired for future research.
- design and procure, if necessary, bearing pads on which the box-girders can rest that meet TxDOT requirements.
- construct a bridge deck with a T501 rail, see Appendix B, that is representative of what TxDOT has had built in the past to ensure the test results are meaningful.
- Instrument the bridge to capture critical data in order to calculate stresses at strategic points along the bridge both during construction and fracture testing.

The overarching objective is to provide a useful reference for research into refining analytical models that accurately account for reserve strength due to built-in redundancies and to reduce overall maintenance and inspection requirements.

1.3 SCOPE OF THIS PROJECT

This report includes the development, construction, and setup of a full-scale test specimen that is representative of a steel box-girder bridge currently in use by the Texas Department of Transportation (TxDOT). Chapter 2 includes a brief background review of events that have occurred in the field that provoked questions concerning the need for research on the redundancy that is built into bridges with Fracture Critical Members (FCM). Chapter 3 conveys the history behind the bridge girders used in the test set up along with the design and construction of the foundation, deck, and railing for the girders. Chapter 4 contains the instrumentation plan for the test set up. Chapter 5 discusses the results of the data collected on the bridge prior to testing. Finally, Chapter 6 gives conclusions and recommendations for future research based on the information included in this report.

CHAPTER 2

Background

2.1 BACKGROUND

The collapse of the Silver Bridge that connected the towns of Point Pleasant, West Virginia and Gallepois, Ohio in November of 1967 set in motion changes that have altered the design and maintenance of the nation's bridges. In response to the bridge failure, the government passed the Federal-Aid Highway Act of 1968 and established the National Bridge Inspection Standards (NIBS) (Lovejoy, 2003). These standards placed inspection requirements on publicly owned bridges with the intent of preventing catastrophes like the one mentioned above. Despite government regulation, bridges failures still occur.



*Figure 2.1: Aftermath of the Silver Bridge collapse
(Charleston Daily Mail, 2006)*

The inspection requirements received heavy scrutiny after a corroded hanger pin assembly failed and brought down a bridge span along Interstate Highway 95 that crossed the Mianus River at Greenwich, Connecticut in June of 1983. Similarly, it was concluded that a stress-corrosion-induced fracture had

caused the failure of the Silver Bridge. As a result of these events, attention was given not only to inspection frequency but also to potential weak points in a bridge. One of the problems identified was the lack of redundancy built into bridge superstructures. The lack of redundancy in steel bridges left these types of structures vulnerable to collapse if only one of its members failed in a way that would prevent the member from carrying any load. Such members were identified as *fracture critical* (FC) as defined in the Code of Federal Regulations, Title 23, Part 650, Subpart C-National Bridge Inspection Standards (e-CFR, 2006). The classification FC increased the cost of inspections and maintenance of bridge systems with FC members (FCMs) on the order of 8 percent (Connor, Dexter, and Mahmoud, 2005). In Texas, around \$26 million dollars has been spent annually on bridges that are classified as FC (Kalwalik, 2006). To avoid designing bridges with FCMs requires engineers to provide redundancy to prevent the possibility of collapse. Identifying those redundancies has been an issue that has spurred researchers to look at methods of quantifying the redundancy built into existing structures and new designs.

Past researchers have proposed methods to identify the redundancies of bridge structures through the use of system factors or load multipliers (Ghosn and Moses, 1998). Both approaches quantify the level of redundancy using subjective decisions made by a designer. Ghosn and Moses pointed out that the AASHTO Load and Resistance Factor Design load factor modifiers were influenced by subjective variables like the “operational importance” of a structure, which was determined by the effects a bridge had on the “social, economical, and/or security requirements” if it was out of service. Other researchers have recognized the benefits of a more direct analysis with the aid of a finite element model and full-scale testing.

Researchers from New Mexico State University developed a finite element model and tested a full-scale continuous span twin I-girder bridge in September of 1993 (Idriss, et al., 1995). The bridge segment was part of I-40 that crossed the Rio Grande River in Albuquerque, New Mexico. The researchers' objective was to determine the impact of a near full-depth fracture in one of the bridge girders with a truck load of 82 kips placed on the deck in a position that would cause the most deflection. They began by developing a three-dimensional finite element model to predict the bridge system behavior, and they later used the field test data to validate the analytical results. The researchers found that the bridge remained stable, and the resulting deflections over the 163 ft. span were small, 1.1875 in., under dead loads and applied live loading, even after a 6 ft. crack through the girder's bottom flange and into the web (Idriss, et al., 1995). A similar methodology was used in the testing of the single span simply supported trapezoidal box-girder bridge discussed in this report.

2.2 MOTIVATION FOR RESEARCH

The research conducted up to the present has focused mainly on twin I-girder bridges with little or no redundancy. As pointed out above, the findings of other researchers indicate that, despite a fracture of one of the FCMs, some bridge systems have the reserve capacity to continue to function. Also, experience has shown that bridge fractures occur and go unnoticed for days until the problem is found either incidentally or during an inspection (Connor, Dexter, and Mahmoud, 2005). Such was the case in 1977 when a full-depth fracture occurred on the twin I-girder bridge along I-79 bridge at Neville Island in Pittsburgh, Pennsylvania (Figure 2.2). The results of tests and observations from the field have brought the definition and classification "fracture critical" into question. Because other types of bridge systems and components have been identified as FC, research is needed

to question the validity of that decision and to assist governing agencies in better defining when the classification should be applied.



Figure 2.2: Girder fracture on a bridge on I-79 at Neville Island in Pittsburgh, Pennsylvania (Connor, Dexter, and Mahmoud, 2005).

The cost of hands-on, in-service inspections of bridges with FCMs has been estimated to be 2 to 5 times greater than bridges without FCMs (Connor, Dexter, and Mahmoud, 2005). Twin trapezoidal box-girder bridges have been identified as having fracture critical members because the bottom flanges of the girders are considered to be non-redundant. The higher costs of designing and maintaining this type of bridge system have not been justified, however, because there is a limited understanding of the alternative load paths available within the structure.

Bridge designers, public owners, and researchers still a need to understand the built-in redundancies that provide alternative load paths that keep bridges capable of carrying loads after a full-depth fracture event. The regulations put in place to prevent major collapse and loss of life have become more stringent despite improvements in materials and design processes. Research has shown that the broad definition used to classify “fracture critical members” has not been applied correctly in some circumstances.

The research contained within this report provides information on the construction process and instrumentation of a full-scale trapezoidal box-girder bridge segment that will be tested under a simulated fracture event to help quantify structural redundancies inherent in such bridge system. Also, the system's response during a live load test is discussed. In the next chapter, the construction process is documented to show that the specimen is an adequate representation of a typical trapezoidal box-girder bridge in service throughout the state of Texas. Later chapters describe the instrumentation installed on the bridge and the response to a simulated live load test.

CHAPTER 3

Construction of the Test Bridge

3.1 INTRODUCTION

The construction of the bridge was an enormous task that took the skill and assistance of the TxDOT bridge division and a contractor that was familiar with this kind of work. The quality of construction was guided by TxDOT standards to provide a product that is representative of a typical steel trapezoidal box-girder bridge currently in service around the state. The contractor was selected based on responses during the solicitation phase of the project. With the assistance of TxDOT, the project researchers were able to identify a contractor that was reliable and possessed the ability to construct the deck and railing quickly and safely according to AASHTO and TxDOT standards. The funding for the deck construction came from the FHWA.

3.2 OBJECTIVES

The ultimate goal for construction of the test bridge was to provide a representative sample of a typical bridge section that is currently in use throughout the state of Texas. Looking beyond the immediate goals of the project, every effort was made to make it as simple as possible for researchers to continue to use the bridge to explore areas of inspection and repair with new materials after the initial test. The challenges of meeting these goals began shortly after the girders were removed from service.

3.3 REPAIRS TO GIRDER

During the removal of the bridge girders from I-10, the contractor damaged the flanges and shear studs extensively (Figure 3.1). The girders had to be sent to Trinity steel fabricators in Houston to have the flanges and some shear studs



(a)



(b)

Figure 3.1: a) Post removal damage of flange and shear studs prior to shipping to Trinity b) shear stud damage repaired at Ferguson lab

straightened. The repairs were made mostly by using heat and applying large forces to reshape the distorted steel close to its previous shape. Once Trinity made the repairs possible for the funds that were available, the girders were transported to the Phil M. Ferguson Structural Engineering Laboratory at the J.J. Pickle Research Center campus.

Once placed on the pier foundations, which are discussed in the next section, the girders were assembled. The 7/8-in. diameter A490 bolts that were specified on the structural drawings were installed in the diaphragms that connect the two girders. The bolts were tightened following the *Turn-of-Nut Pretensioning* guidelines from the AISC Steel Construction Specifications (ASCI, 2003). As an internal quality assurance measure, each bolt was marked with a “T” after it was tightened to provide a visual check that all of the diaphragms and top plate bolts were installed correctly (Figure 3.2). Once the girders were secured together, repairs to the girders could be finished.

Repairs to the damaged shear studs were limited to those that were critical to support the bridge after the fracture test. Subsequently, not all the shear studs were straightened or replaced. To determine the critical areas where the shear



Figure 3.2: a) South end diaphragm top corner connection b) north end lower corner connection

studs would need to be repaired, the provisions in the American Concrete Institute (ACI) code 318-02, Appendix D-Anchoring to Concrete, were followed to calculate the amount of shear studs required to support the bridge after fracture. The girders were modeled as simply supported beams with a live load of 72 kips placed at the midspan with the fracture of one of the girders modeled by a hinge in the girder at midspan. The results were then multiplied by a factor of 2 to account for dynamic effects. These preliminary calculations showed that approximately 80 feet or 44 rows of studs, essentially the middle third of the girders, would be needed to transfer the load from the fractured girder to the intact girder.

The middle third of the girders were inspected for the shear studs that showed any sign of damage. There were a total of 29 studs that had been badly damaged, similar to that shown in Figure 3.1b above, or that were bent enough to possibly affect their ability to transfer the load from the concrete deck to the undamaged girder. These studs were cut from the flange, and the surface was ground flat to accept new studs. Shear studs with the same dimensions, 7/8 in diameter and 5 inches tall, were welded on the flanges as close to the old position as possible (Figure 3.3). The studs were attached with a 1/2-in. fillet weld at the



Figure 3.3: New stud welded on to the inner flange of the interior girder

base. The remaining studs were either in good condition or outside the middle third of the girder and were not expected to influence the results of the test.

3.4 FOUNDATIONS

The foundations were designed and constructed to: 1) support the bridge under dead load, simulated live load, and anticipated construction loads before the fracture test; 2) prevent the foundation from sliding along the ground after the exterior girder bottom flange was fractured; 3) prevent the foundation base from settling and overturning during the fracture test; and 3) provide sufficient height to allow the bridge to deflect midspan after the test.

The first task in preparing the supporting structures for the girders was to determine a suitable method of transferring the loads from the girders to the foundations. The original girders were designed with pot bearing pads that were bolted to the bent caps. During the demolition of the bridge in Houston, the contractor cut the bearing plates from the bottom flanges of the girders. Instead of spending the extra time and money to repair the old bearing system, the decision was made to use elastomeric bearing pads based on their use in the field on other box-girder bridge projects such as the US 290 & IH 35 interchange in Austin (Bradberry, et al, 2002). The TxDOT *Bridge Design Manual* was used to

determine the specifications for the bearing pads. The loads from the girders were taken to be the 220 kips per bearing pad specified on the plans (Figure B.3-1). The size was limited to a minimum of 220 square inches by the 1000 psi maximum bearing pressures in the manual. Bearing pads from another research project were found that met the bearing pressure limitations and were used rather than purchasing new ones to prevent delays and save funds. The pads were 22 in. long, 11 in. wide and 3 in. height. They had 9 reinforcing steel plates 1/8 in. thick with 10 layers of neoprene material in 3/16 in. layers top, bottom and in between the steel plates (Figure 3.4).

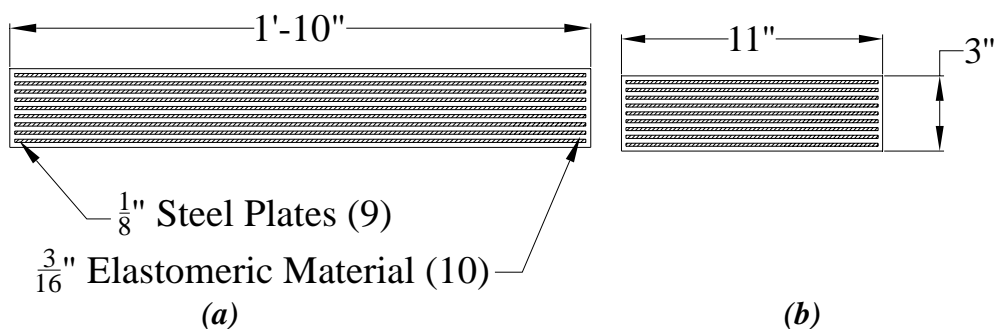


Figure 3.4: a) Bearing pad plate and elastomeric layer thickness b) side view of pad.

The pads were checked against TxDOT and AASHTO standards in order to verify that they would function within the same parameters as expected from those in the field (Appendix A.1). The bearing pads were not designed for the deflections that might be experienced during the fracture test because this is not done in normal bridge design. Once the pads were sized, the foundations were designed.

The pier foundations were designed using the 220 kips per girder specified on the plans plus a horizontal load of 55 kips applied at the top in anticipation of how the bridge might react once the fracture had occurred and the bridge deflected. A bearing pressure of 3,000 lbs per square foot was assumed based on the minimum value allowed by the 2003 International Building Code, section 1804, for the soil at the test site. The base of each pier had a footprint of 170

square feet, which would support 510 kips with the assumed soil pressure. The height was selected such that the girders would be 10 feet above the ground to provide room for instrumentation, installation, and removal of the external braces and deflection after the fracture event. The foundations were built according to the final design, shown in Appendix B in Figure B.2, on site prior to the girders arriving (Figure 3.5).



Figure 3.5: a) Bottom of north foundation b) stem wall for south foundation

The final design weight of each foundation was approximately 121.6 kips. Adding the 440 kips used as a design load brings the total load for each foundation to around 561 kips, which exceeds the assumed soil bearing capacity. A check of the dead loads on the bridge was calculated using the weights of the different bridge components and simulated truck load to determine how conservative the estimated loads were and if settlement would be a concern (Table 3.1). The computations showed that the foundation bearing pressure would not exceed the bearing capacity of the soil, and settlement would not be a concern.

Table 3.1: Actual loads per foundation

Bridge Loads				
Component	Area (Ft²)	Weight (Lbs/Lf³)	Length (Ft)	Total Weight (lbs)
Deck	16	150	120	288,000
Railing	2.20	150	240	79,200
Girder self weight (2 at 60 kips each)				120,000
Simulated Live Load				72,000
Total				561,200
Actual load per foundation				279,600
Total bearing load per foundation				401,200
Bearing pressure per foundation (lb/ft²)				2360
Allowable bearing pressure (lb/ft²)				3000

3.5 BRACING

Bracing was installed to provide torsional stiffness to the girders during construction of the deck and railing. A preliminary analysis of the girders using the UTrap software showed that rotations in the outer girder could be as much as .003 radians without exterior bracing installed. Because the inner girder has less curvature, it is reasonable to expect the rotation to be equal to or less than the outer girder. This observation, along with the UTrap predications, could mean an elevation difference between the top inner flanges of between 0.25 in. and 0.50 in. (Figure 3.6). This differential in elevations would induce stresses in the permanent metal decking that will form the bottom of the slab and result in a variation of the bridge deck thickness. Therefore, the bracing was installed to limit the possibility of the girders rotating. Also, having the bracing installed prior allowing construction loads was consistent with construction practices used in the field.

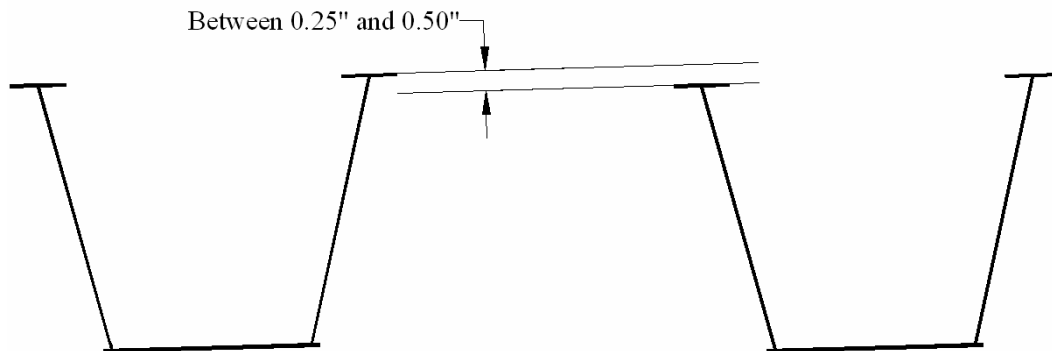


Figure 3.6: UTrAp rotation of the girders during deck pour without external bracing

The braces were fabricated according to the design plans obtained from TxDOT (Figure B.3-4) and were installed at two points between the girders (Figure 3.7). The connection of the cross frames to the girders used a WT 7×21.5 rolled shapes with the flanges bolted to the webs of the girders with 3/4-in. twist off bolts and the cross frames attached to the stem of the WT. The top and bottom cords were made from the same rolled WT 7×21.5 section. To make installation easier and prevent problems aligning the holes, the top and bottom cords were cut and the connection holes drilled in place for the 3/4-in. diameter A325 bolts. The bolts were tightened using the *Turn-of-Nut Pretensioning* mentioned above. The L 5-in. × 3.5-in. × 0.375-in. angles that are used for bracing between the top and bottom cords were clamped in place and welded with a 1/4-in. fillet welds on top and bottom as indicated on the plans. Once the cross frames were in place, construction loads could be applied safely, and the deck could be constructed.



Figure 3.7: a) WT Stubs for external cross frames b) bracing being clamped together prior to welding.

3.6 BRIDGE DECK

The deck was to be constructed to be representative of typical TxDOT construction. The deck drawings (Figure B.4-1) were provided by TxDOT to ensure the deck was configured to represent what is currently in their inventory. During the second project meeting with representatives from TxDOT and the FWHA, questions were raised concerning the 3 in. haunch height called for in the drawing and construction joints in the railing. The 3 in. haunch height would reduce the penetration of the shear studs into the slab and could reduce the pull out strength of the studs. Also, the gap in the railing reduces its ability to contribute to the structural capacity of the section. Because of these reductions in capacity, all the parties agreed that fracture test would provide more information if the bridge was built according to the original design.

Visual inspections were made by TxDOT personnel during construction to ensure standard practices were being followed. After the permanent metal deck forms and the reinforcing steel were installed, measurements of the reinforcing steel spacing were taken 10 feet longitudinally on each side of the centerline to document a representative sample of the as-built condition (Table 3.2).

Table 3.2: Average as-built condition of deck prior to casting

<i>Interior Girder reinforcing steel spacing</i>			
Top Bar (in)	Bottom bar (in)	Vertical (in)	Bottom cover (in)
6.0	6.0	3.4	1.4

<i>Exterior Girder reinforcing steel spacing</i>			
Top Bar (in)	Bottom bar (in)	Vertical (in)	Bottom cover (in)
6.0	6.0	3.5	1.4

<i>Average haunch heights</i>			
Ext Outside (in)	Ext Inside (in)	Int Outside(in)	Int Inside(in)
3.0	3.1	2.9	3.8

The rebar spacing was measured between bars horizontally and vertically for both the top and bottom layers of steel. The spacing of the rebar in all directions fell within the 6-in. specifications on the drawings. The haunch height for the exterior girder flanges averaged 3 inches, but the interior girder haunches averaged 3.8 inches on the inside edge and 2.9 inches on the outside edge of the flange. The difference in height was due to the construction of the formwork on the inside edge of the interior girder flange. The extra height of the interior girder will reduce the shear stud anchorage. This observation suggests that the interior girder will require more shear studs than mentioned previously to carry the load after the exterior girder is fractured. The deck was inspected before, during, and after the pour by TxDOT inspectors to ensure the bridge would represent what is typically done in the field. In fact, it was the express desire of the sponsors and researchers to provide a bridge that would not include any design modifications that were thought to improve the redundancy of the system.

The concrete for the deck was supplied by a local concrete ready-mix company that had an approved design mix for TxDOT class-S-type concrete with a 28-day compressive strength of 4000 psi or greater. The deck was wet cured with blankets and plastic for 10 days to allow the concrete to gain strength and prevent any shrinkage cracking that might result from rapid curing. Two test cylinders that were taken from each of the 9 trucks that delivered the concrete during the deck pour were tested at day 28 or 29. Test results are provided in Table 3.3 below. The cylinder labels represent the truck number and sample. The cylinders had a strength of 4600 psi or higher.

Table 3.3: Concrete cylinder tests for deck

Cylinder	Days of Curing	Strength (psi)	Cylinder	Days of Curing	Strength (psi)
1A	28	4,725	1B	28	4,605
2A	28	5,121	2B	28	5,107
3A	28	5,082	3B	28	4,957
4A	28	4,612	4B	28	4,478
5A	28	4,707	5B	28	4,973
6A	29	4,810	6B	29	4,923
7A	29	4,697	7B	29	4,789
8A	29	4,980	8B	29	4,838
9A	29	5,001	9B	29	4,697

The reinforcing steel used in the deck and rails was comprised of number 4 and 5 bars meeting the requirements of grade 60 steel as specified by TxDOT (Figure B.5-1 and B.5-20). Samples of each type of reinforcement were tested to ensure the tensile strength met the specifications. The specimens were placed in the testing machine (Figure 3.8) and tensile force was applied until brittle fracture

occurred. The load-displacement curves for each steel specimen indicate that both samples had a yield strength at or above 60 ksi, which meets or exceeds the required yield strength (Figure 3.9 and 3.10). The results are listed below in Table 3.4.



Figure 3.8: Tensile test of reinforcing steel

Table 3.4: Reinforcing steel test results

Bar Designation	Nominal Yield Strength F_y (ksi)	Nominal Ultimate Strength F_u (ksi)
#4	60	102
#5	68	101

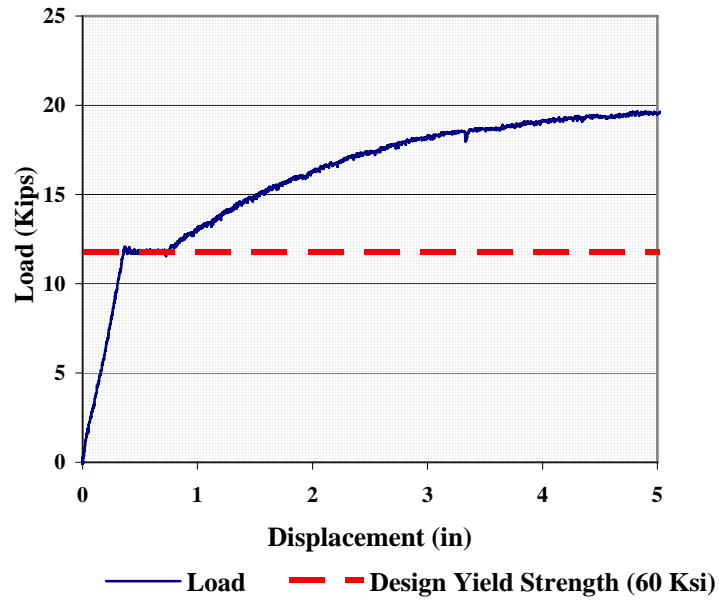


Figure 3.9: Load verses displacement curve for the tensile test on the #4 rebar

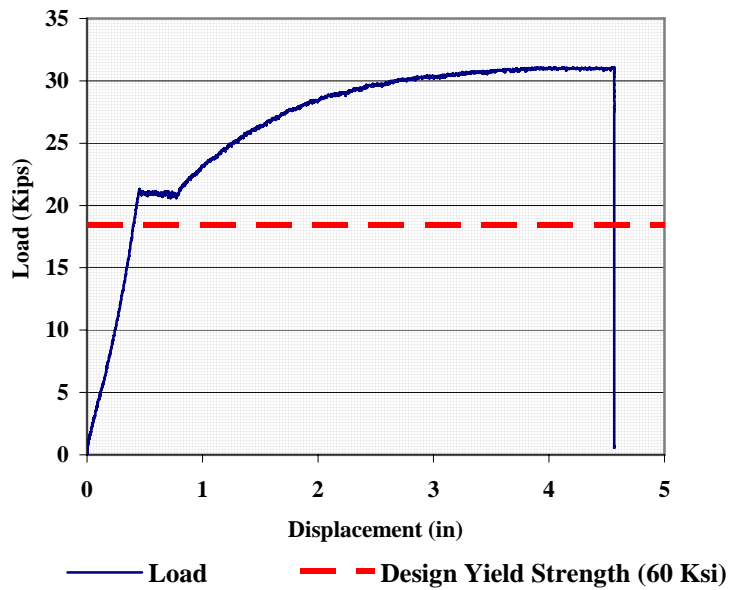


Figure 3.10: Load verses displacement curve for the tensile test on the #5 rebar

3.7 RAILS

The TxDOT standard T501 rail (Figure 3.11) was chosen due to its prevalent use in the field. The rails were constructed according to the details provided by TxDOT with the exception of the optional slotted drains. Because drainage will not affect the performance of the bridge before or after the fracture test, none was provided. The rails were formed and poured in place after the deck had wet cured for 4 days to provide as much strength as possible and still mimic standard practice in the field. The plans call for the rails to be constructed



(a)



(b)



(c)

Figure 3.11: a) typical T501 rail (Bridge Railing Manual, 2006); b) rebar cage for east rail b) formwork for west rail

in panels of lengths ranging from 10 ft. to 33 ft. (Figure B.5-1). The rail panels are to be separated by intermediate wall joints. To maximize the effects of losing the capacity of the exterior girder at midspan, the joints were spaced every 30 feet to ensure the rails would be separated at midspan of the bridge.

The joints were formed by placing 3/4-in. extruded polystyrene foam insulation in the formwork (Figure 3.12). Normally, TxDOT will allow the contractor the option of leaving the insulation in place or removing it and filling the bottom 6 inches of the gap with mortar. The contractor chose to leave the insulation in place for this project. After the formwork was removed, the joints showed signs where the concrete had shifted the insulation and skewed some of the joints slightly. The center joint over the exterior girder had the most deformation (Figure 3.13). The top of the insulation was shifted 3 inches to the north of the centerline of the deck, but the bottom of the joint remained directly at the centerline of the bridge deck.

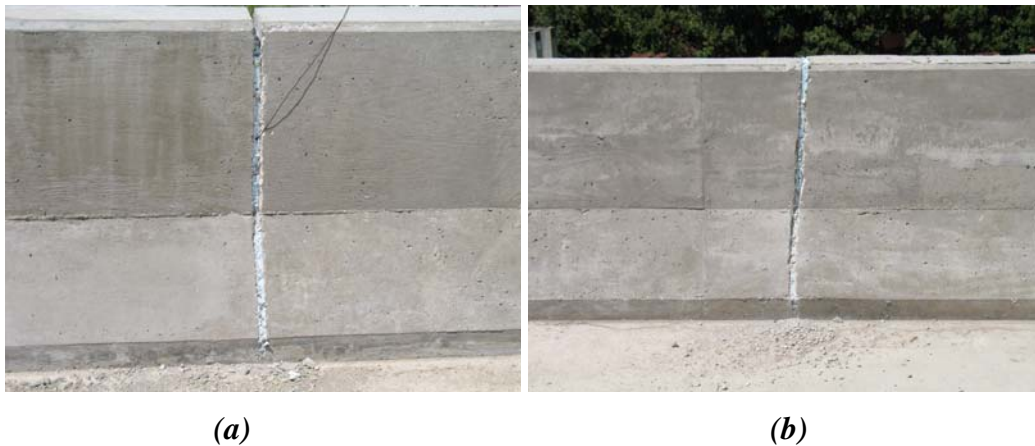


Figure 3.12: a) Vertical construction joint in the west rail at the center b) skewed construction joint north of the centerline on the east rail



Figure 3.13: Center construction joint on the east rail at midspan

The east and west rails were poured at different times because the contractor needed to reuse the forms. The west rail was poured first, and then two days later, the east rail was poured. The concrete that was used in the rails came from the same concrete supplier, but the design was Austin class S as compared to TxDOT class S used for the deck. The difference in the mix design is the aggregate type, but the mix design strength was the same. The cylinder strength tests were performed after the east rail had cured 26 days and the west rail cured for 28 days. The compressive strengths ranged from 4400 to 5747 psi (Table 3.5). During the compression tests on all of the cylinders for the concrete deck, all specimens failed below a peak force of 160 kips the maximum load range selected on the test machine. When testing started on the cylinders for the rails, the testing machine was left on a maximum load range of 160 kips. Unexpectedly, cylinder 2A reached the maximum loading and did not fail. The machine was set to apply a higher load, and testing subsequent tests were performed. The results show that the lowest strength was more than specifications required.

Table 3.5: Concrete cylinder tests for rail

Rail	Cylinder	Days after Casting	Load (lb)	Strength (psi)
West	1A	28	138,800	4,909
West	1B	28	142,400	5,036
West	2A	28	160,000	5,659
West	2B	28	162,500	5,747
East	1A	26	146,800	5,192
East	1B	26	139,100	4,920
East	2A	26	124,400	4,400
East	2B	26	126,200	4,463

All components of the bridge system were built in a manner that was typical for this type of TxDOT project. All materials met or exceeded the specified requirements, and the bridge passed the inspection performed by TxDOT prior to the deck casting. It is expected that the bridge segment will behave similarly to the bridge systems currently in use.

CHAPTER 4

Instrumentation of the Test Specimen

4.1 INTRODUCTION

As stated earlier, once a bridge loses what is considered to be a FCM, by definition, the bridge is expected to collapse or no longer be able to perform its intended function. After suffering a fracture of the bottom flange of the exterior girder, the bridge in this test program will need to redistribute loads to other parts of the bridge. From preliminary computer analysis, it is expected that the deck, end diaphragms, and interior girder will be able to resist the redistributed loads. The strains that will be induced in both interior and exterior girder webs and bottom flanges as the loads are transferred will be measured by a combination of single-directional foil and rectangular 0-45-90 rosette gages located throughout the bridge.

The plates of the box girders came from the field with out-of-plane imperfections in the web that were noticeable (Figure 4.1). Measurements were made by other graduate students to determine the out-of-flatness condition of the webs after they were erected. They recorded out-of-plane displacements of over 1/8-in. in some locations. As the girders are loaded, the imperfections can increase.



Figure 4.1: Out-of-plane imperfections in the web

In order to account for this out-of-plane bending, gages were placed on the both sides of the web and bottom flange plate of the interior and exterior girder cross-sections and on the inside and outside of the end diaphragms. Under the assumption that plane sections will remain plane, the strains through the thickness of the plates will be treated as linear, and the average will be taken as the estimated strain during the data reduction

4.2 OBJECTIVES

The goals of the data collection network developed for this project were as follows: 1) to capture the behavior of the bridge system components as they were loaded, 2) provide data to validate the computer model under development, and 3) provide a baseline for future modeling tools be compared. To accomplish these goals the strain data collected from the bridge will be used to compare with the computer model both during and after the fracture test. The strains will be converted to stresses to compare with the nominal material strengths. The stresses after installation of the formwork, concrete deck, railing, and placement

of the live load will provide a means to calibrate the computational model prior to the fracture event. After the fracture of the exterior girder, observing how the system redistributes load will be used to identify potential points of redundancy that may not be accounted for in the current design process. Knowing how the components of the system interact is crucial to developing an accurate model for future design.

4.3 GIRDER CROSS-SECTIONS

The girders were instrumented at three locations (Figure 4.2). The gages placed near the midspan in the exterior girder were offset 72 in. to the south to limit the damage they would experience during the fracture event. The gages in the interior girder were offset on both sides of the midspan, 70 in. north and 72 in. south, from the transverse centerline of the bridge. The single-direction foil gages are designated with “F” before their number (Figure 4.3a). The rectangular 0-45-90 rosette gages are designated with “R” before their number (Figure 4.3b). The web plates were instrumented with 12 single-direction foil gages 0.2362 in. (6 mm) long with a resistance of 350 ohms (Figure 4.4a). Also, the bottom flanges were instrumented with 6 rectangular 0-45-90, stacked rosette gages 0.2362 in (6 mm) long with a resistance of 120 ohms (Figures 4.4b).

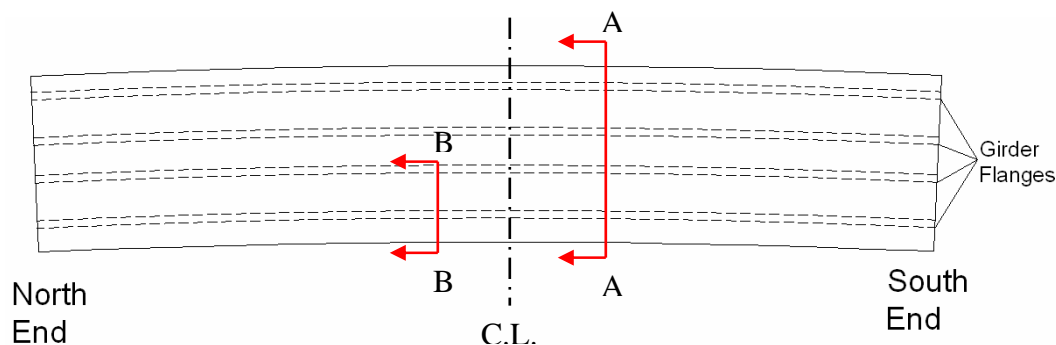


Figure 4.2: Instrumented cross-section locations

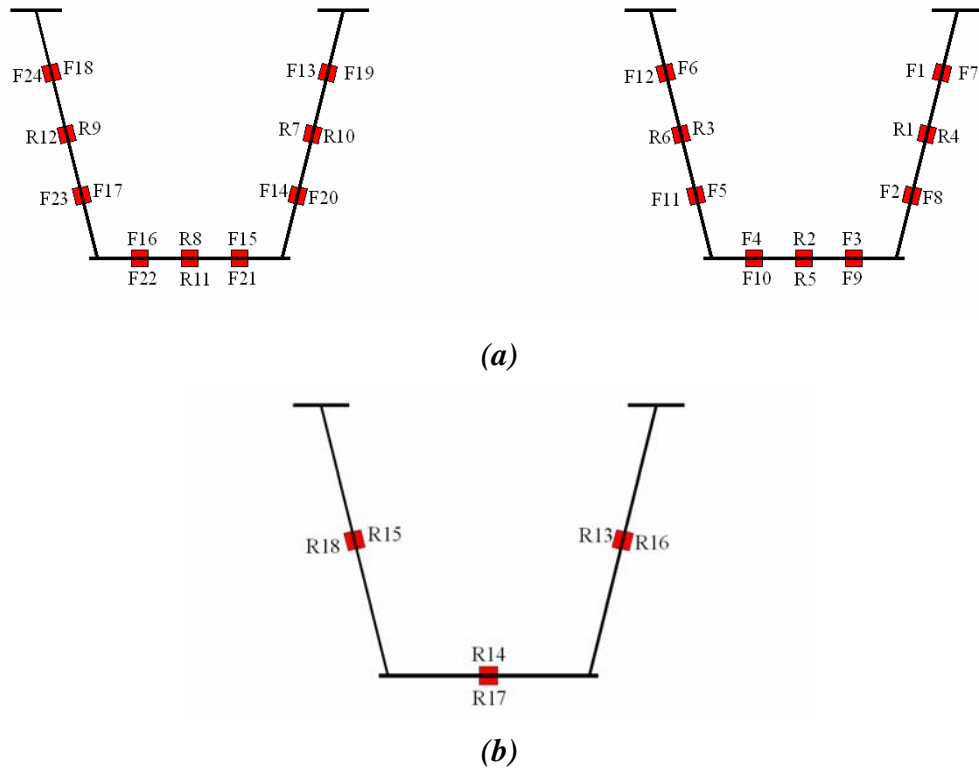


Figure 4.3: a) Gages at cut A-A b) gages at cut B-B

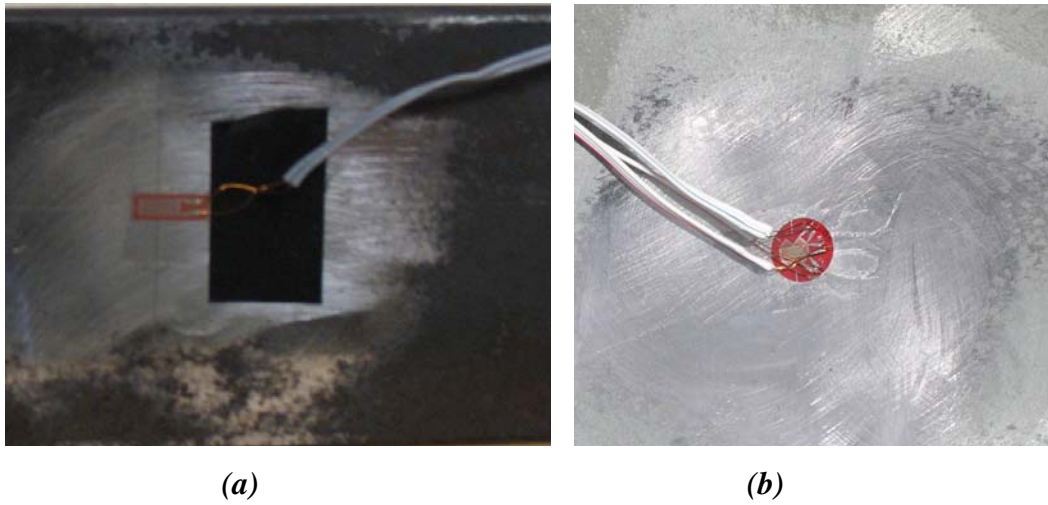


Figure 4.4: a) Single direction strain gage b) rectangular rosette gage

4.4 DIAPHRAGMS

The end diaphragms were expected to transfer some of the load from the exterior girder to the interior girder after the fracture event. The high-speed data collection system to be used during the fracture event had a limited number of available channels. Consequently, the system limitation only allowed 6 channels of data for each diaphragm; which meant two rosette gages for both the north and the south diaphragms. As stated previously, the gages were placed on the inside and outside to account for plate bending. The assumption was made that the shear in the center of the diaphragm would represent the average shear stresses that were transferred between the girders (Figure 4.5).



Figure 4.5: Inside of the north end diaphragm

4.5 DECK REINFORCEMENT

The reinforcing bars in the deck were instrumented at 10 locations to capture the load being transferred from the exterior girder to the interior girder after the fracture event (Figure 4.6). The bars were instrumented with single-direction strain gages like the one pictured in Figure 4.4a. The gages were placed on the bottom of the bars and covered with self-adhesive coating tape to prevent damage

during the deck pouring. Also, the wires were run under the bars to protect them from being walked on by the workers as the deck was being placed, and they were also placed through plastic inserts in the pan decking to prevent them from chaffing on the edges of the hole (Figure 4.7).

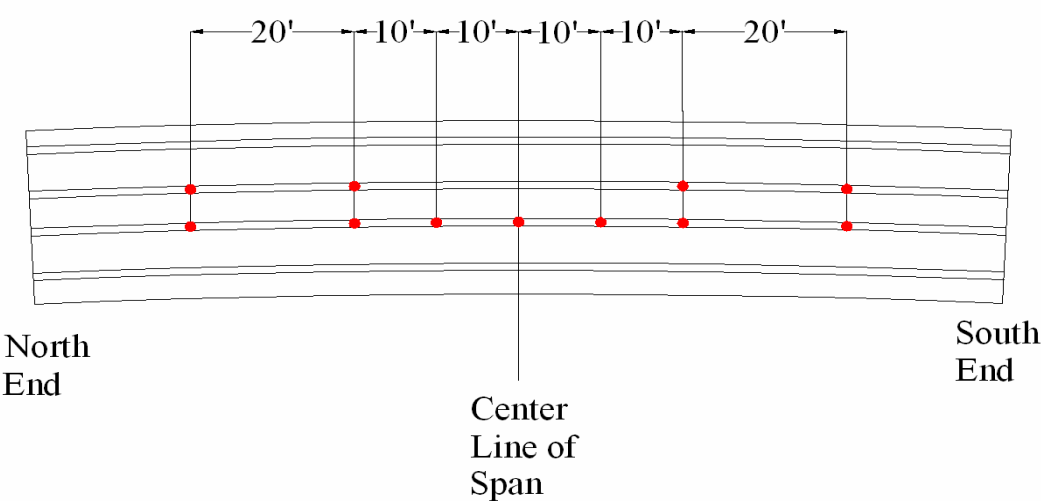


Figure 4.6: Strain gage locations for the deck reinforcement

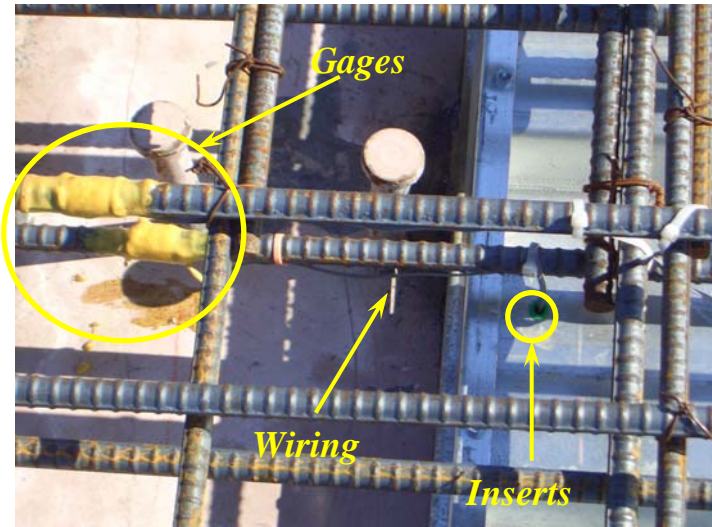


Figure 4.7: Strain gages on the deck reinforcement and wire placement

4.6 SHEAR STUDS

The shear studs were instrumented with bolt gages to measure the tension that develops between the studs and the deck as the girders deflect. The bolt gages were 0.2362 in. (6 mm) in length with a resistance of 120 ohms. As mentioned earlier, 15 out of the 29 damaged studs were instrumented. The studs with gages were placed along the flanges, to the greatest extent possible, where the tension force was expected to exceed the calculated pullout capacity (Figure 4.8). The distance from the centerline and the flange locations are listed in Table 4.1.

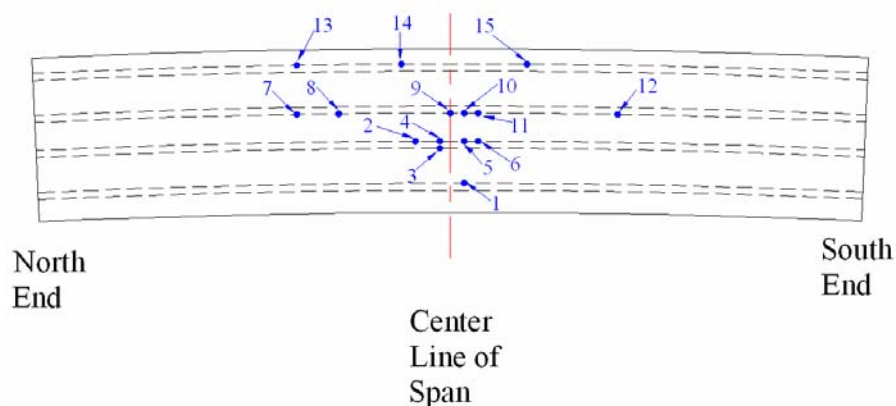
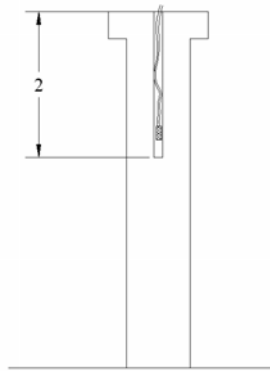


Figure 4.8: Shear stud strain gage locations

Table 4.1: Shear stud locations

<u>Gage Number</u>	<u>Location</u>	<u>Distance from Center (ft)</u>
1	Interior girder West flange	2
2	Interior girder East flange	5
3	Interior girder East flange	1.5
4	Interior girder East flange	1.5
5	Interior girder East flange	2
6	Interior girder East flange	4
7	Exterior girder West flange	22
8	Exterior girder West flange	16
9	Exterior girder West flange	0
10	Exterior girder West flange	2
11	Exterior girder West flange	4
12	Exterior girder West flange	24
13	Exterior girder East flange	22
14	Exterior girder East flange	7
15	Exterior girder East flange	11

The bolt gages were installed in holes 0.7874 in. (2 mm) in diameter. The holes were drilled through the head of the stud, approximately 2 in. deep into the shaft (Figure 4.9a). Using a syringe and needle to avoid air voids, epoxy was injected to hold the gages in place. The holes were injected with epoxy with a syringe and needle to avoid air voids. After the epoxy set, the wires were run down the side of the stud and protected with self-adhesive butyl rubber tape (Figure 4.9b). Also, the wires were run along the bottom of the rebar through plastic inserts in the pan decking to minimize the chance of being damaged during the concrete deck casting.



(a)



(b)

Figure 4.9: a) Schematic of typical shear stud gage positioning b) interior flange shear stud

With the instrumentation provided, the response of the different components that make up the bridge were monitored to give the overall behavior of the bridge during the construction and live load testing. The next section provides the data that was collected and discusses the behavior of the system response.

CHAPTER 5

Gravity Load Data

5.1 INTRODUCTION

The data measured was taken in two phases of the project. First, the construction of the bridge was monitored as the contractor placed the deck and rails. Second, live load testing was conducted to provide information on how the bridge responded as loads were placed at different locations transversely across the deck and to verify the high-speed data collection system gave consistent readings. Each part provided information that was used to gain insight as to how the bridge girders and deck components interact when the bridge is loaded. The deflection measurements and strain data were comparable and allowed for the validation of computer model being designed. The information gained from the bridge during construction and the live load test establish a baseline for future testing for the type of bridge system discussed in this report. The following sections step through the methods used to monitor the systems and the responses obtained.

5.2 OBJECTIVES

The goal during the construction and live load testing was to document the behavior of the bridge system components through observed elevation measurements and strain gage data. The information that was gathered provided a baseline for which computer model designers and other researchers can reference when studying this type of bridge system. Ultimately, the data were used to validate the reliability of the finite element model being developed concurrently with the construction and testing of the bridge system.

5.3 DEFLECTION MEASUREMENTS

The deflections were measured using a Spectra Precision Laser level, model LL400, and CR500 receiver shown below in Figure 5.1 (Trimble 2006). The system was selected because of simplicity and the advertised level of accuracy of $\pm 1/16$ -in. within a distance of 100 ft. Because traditional surveying rods do not allow for the degree of accuracy the system could provide, a measuring rod was constructed using a planed 1 in. by 3 in. wood board 6 ft. in length with a measuring tape strip attached that enabled measurements of 1/16-in. shown in Figure 5.1b. During the surveys, the laser level was positioned close to the center, between the measurement points 11 and 30 shown in Figure 5.2. This position minimized the distance to the measurements points which kept the receiver within the manufacturer's suggested range for the required accuracy.



(a)

(b)

Figure 5.1 a) Spectra self-leveling laser model LL400 b) receiver CR500 attached to the measuring rod

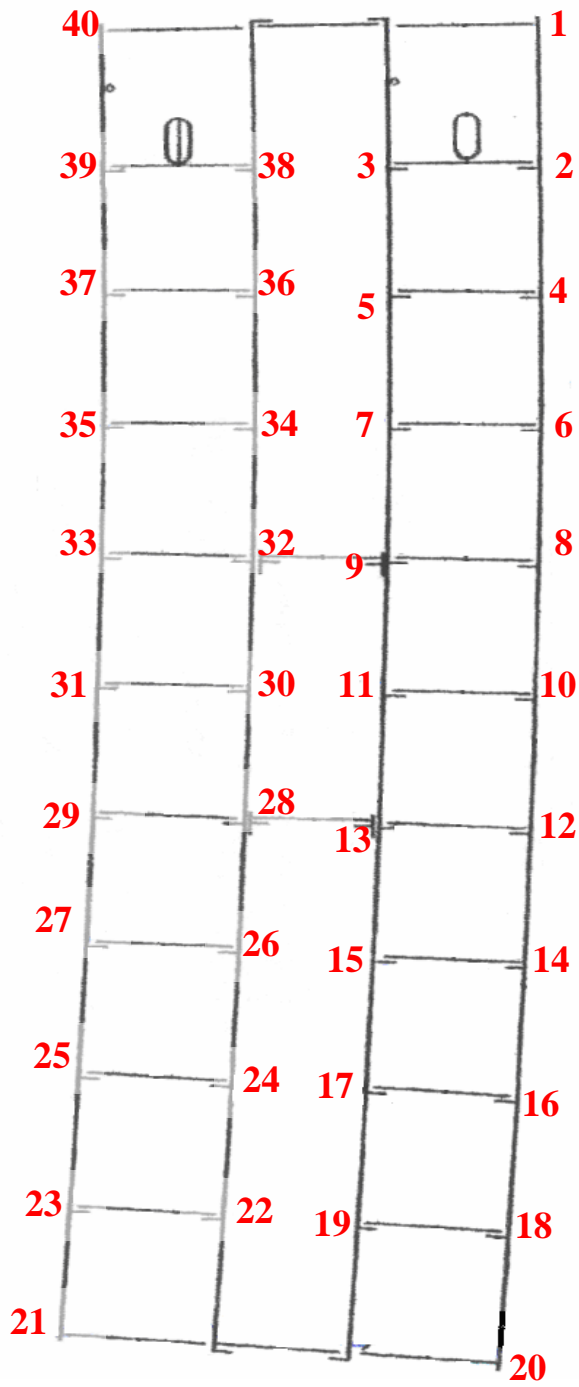


Figure 5.2: Deflection measurement locations

The elevations were all measured relative to a benchmark that was established at the southwest corner of the slab located between the north foundation and the building east of the test site shown in Figure B.1. Also, the elevations of the inside corners of each foundation footing were measured to determine the accuracy of the system over the course of the project. Table 5.1 shows that the measurements for the foundation corners varied from 1/8 to 1/4-in.

Table 5.1: Elevations of the foundation corners above the benchmark

Date	Northeast (in.)	Northwest (in.)	Southeast (in.)	Southwest (in.)
6/19	30.2500	29.5625	23.0625	22.5625
6/23	30.2500	29.1875	22.9375	22.5000
8/1	30.3125	29.5000	23.0625	22.5635
8/7	30.3125	29.5000	23.03125	22.5938
8/18	30.1563	29.2500	23.03125	22.5313
8/31	30.000	29.5625	22.8125	22.3750
10/5	30.000	29.5626	22.6875	22.3125
10/24	29.9375	29.5625	22.5625	22.4325
10/31	29.9375	29.4325	22.5625	22.3750
Max	30.3125	29.5625	23.0625	22.5938
Min	29.9375	29.1875	22.5625	22.3125
Average	30.1250	29.3750	22.8125	22.4531
"+/-" variation	0.1875	0.1875	0.2500	0.1875

The elevations were taken at locations along the girder that corresponded to places where interior bracing frames were installed to provide a simple means of locating the points in the computer model. Measurements on both sides of the bottom flange were recorded as the construction progressed and after the live load was placed for the fracture test to determine the deflections and rotations in the girders.

These elevation measurements were averaged over the width of the bottom flange to determine the centerline elevation. The position of these values relative to the chord that extends for the north to the south bearing pad was calculated using the geometric relationship shown in figure 5.3. The results are plotted in Figure 5.4 for each event.

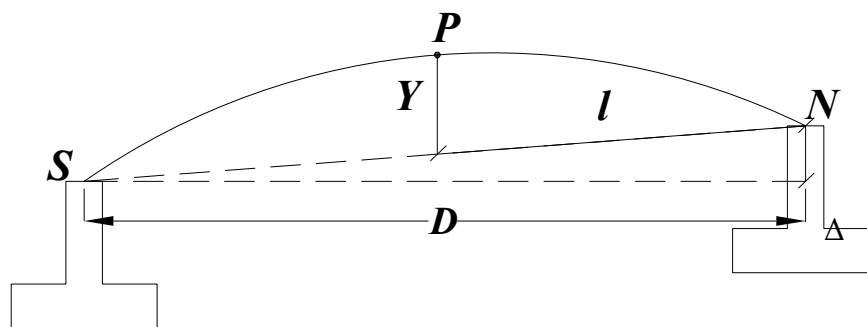


Figure 5.3: Diagram of girder curvature

$$Y = P - \left(\frac{l}{D} \right) \times \Delta - N$$

- Where Y = Distance above the elevation of the north end of the girder
- P = Elevation of the point along the girder
- D = Distance between supports
- Δ = Difference in elevation of the north and south end of girder
- N = Elevation of the north end of the girder
- S = Elevation of the south end of the girder

The initial measurements indicated that the girders had a camber of just over 3.5 in. before placement of the deck. As the construction progressed, the pan decking, formwork, and reinforcing steel were installing to prepare for the deck. After this phase of the construction, the girders deflected about 0.25 in. at the midspan. After the deck was poured, the girders deflected at the midspan of just over 3 in. for the interior girder and almost 4 in. for the exterior girder.

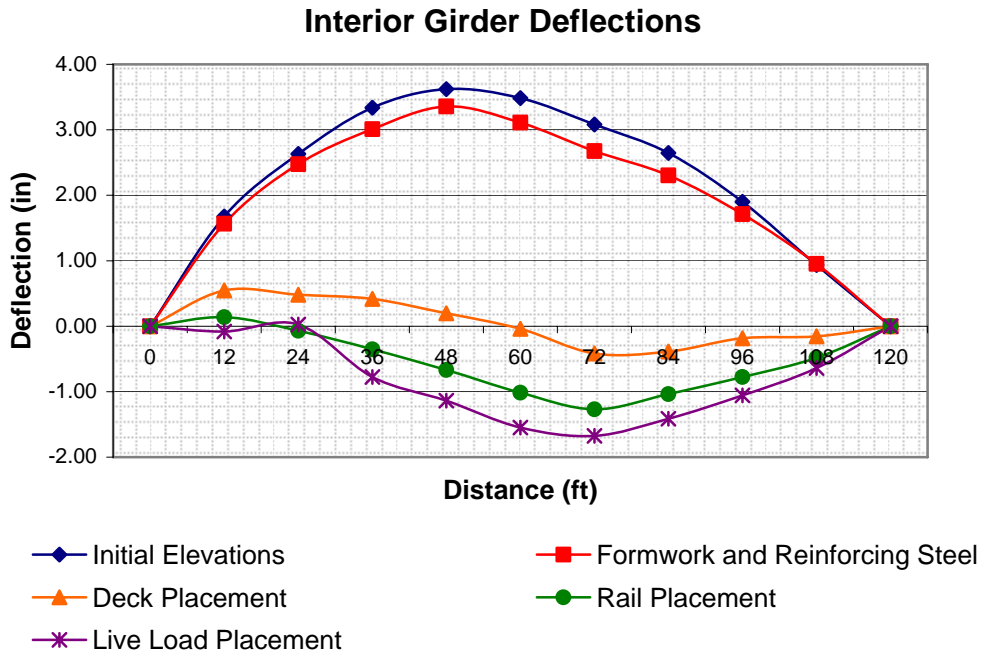


Figure 5.4: Centerline deflections of interior girder

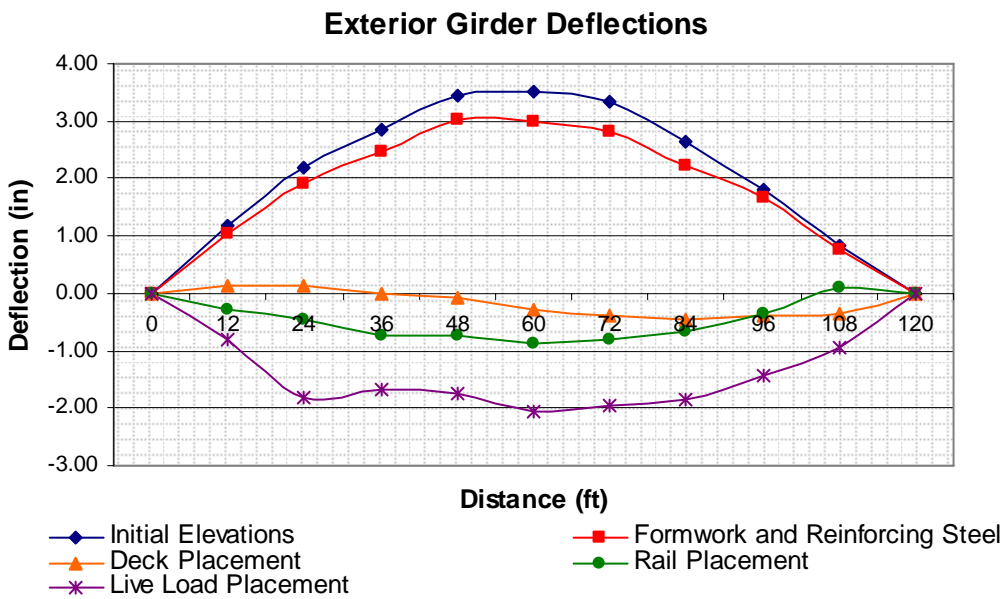


Figure 5.5: Centerline deflections of the exterior girder

The deflection of the exterior girder taken the morning after the deck casting was compared to the deflections obtained by UTrAp, software developed for designing trapezoidal box girders (Figure 5.6), and the finite element model being developed (Figure 5.7). Because the only deflections that UTrAp displays are those for the exterior girder, the interior girder deflections were not discussed. Also, it should be noted that neither model includes any initial camber, the geometry for the base model is slightly different than the actual bridge. To account for this difference, the deflection due to the self-weight was determined for both programs. UTrAp had a deflection due to the self-weight of the girders of 1.11 in. The finite element model predicted a deflection due to self-weight of the girders of 1.27 in. After subtracting the self-weight deflections from the total reponse after the deck was poured, the UTrAp deflection was 4.47 in. and the finite element model was 3.93 in. The observed deflection was 3.82 in. after the deck was poured. The prediction of the finite element model is within 3 percent and the UTrAp model was within 20 percent. The difference in the UTrAp result could be due to the fact that the model did not include stiffness in the deck as the casting took place.

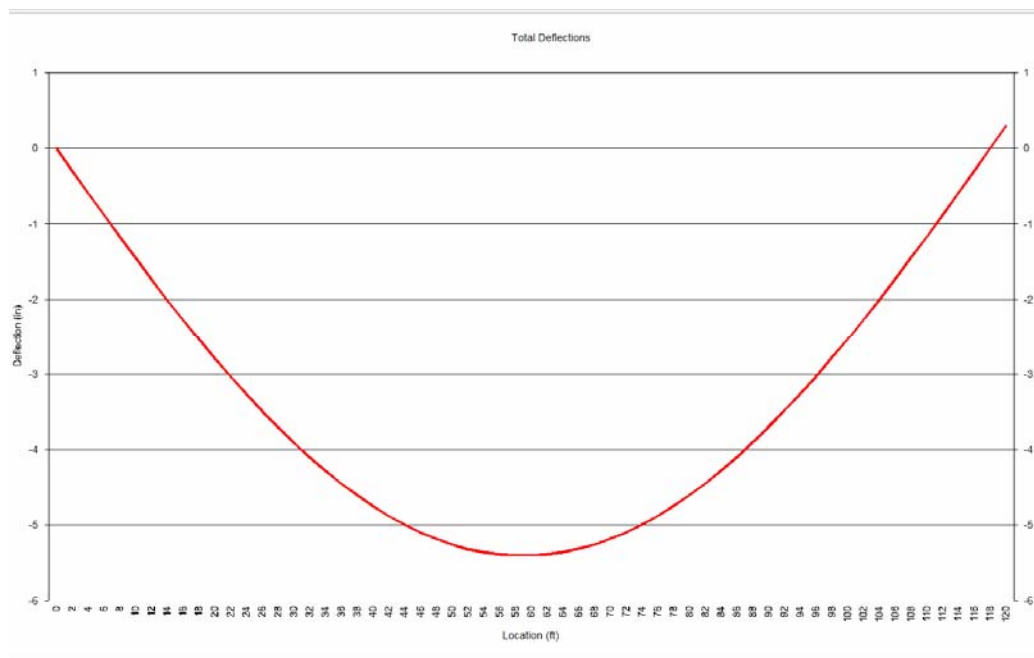


Figure 5.6: Deflections from UTrAp just after deck casting

Deflection Along Length of the Exterior Girder

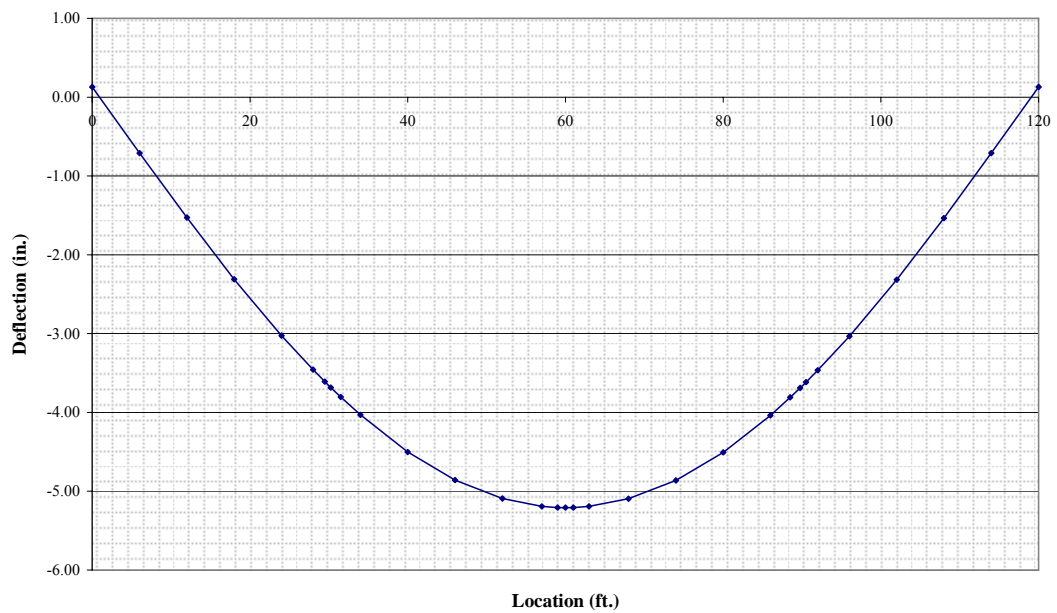


Figure 5.7: Deflections from finite element model after deck casting

The last part of the construction was the installation of the T501 railing on the east and west sides of the bridge. The deflections after this part of the project eliminated all of the initial camber except a small portion on the south end of the interior girder and north end of the exterior girder. The last phase was the live load placement.

The live load placed in the final position, as described later in section 5.5.3, caused a deflection at the midspan of the exterior girder of 5.52 in. below the original elevation. The finite element model predicted a deflection at the midspan of the exterior girder of 4.74 in. after the live load was placed, excluding the deflection due to the self weight of the girders. The finite element model deflection is with 15 percent less of the actual deflection observed. The difference is due to the fact that the finite element model is generally stiffer than the actual bridge.

The rotations in the girder cross sections are calculated assuming that the small angle approximation rule can apply. The angle of rotation is computed as the difference between the centerline averaged elevation and the elevation of the west side of the bottom flange over one-half the width of the bottom flange (Figure 5.8). The rotation is negative for a clockwise rotation and positive for counter-clockwise rotation of the girder. Also, the zero end represents the north side of the bridge. The longitudinal rotations of the girders as forms, deck, rails, and live load are placed on the bridge are plotted in Figure 5.9 and 5.10. The two most noticeable events happen after the formwork is placed on the bridge and the other is after the live load is put on the bridge. After the formwork is placed, both girders switch directions of rotation. This result occurs because of the cantilevered brackets that the contractors use to support their formwork.

Finally, it should be noted that the observed rotations are small and the small displacement assumption to calculate the angles was valid.

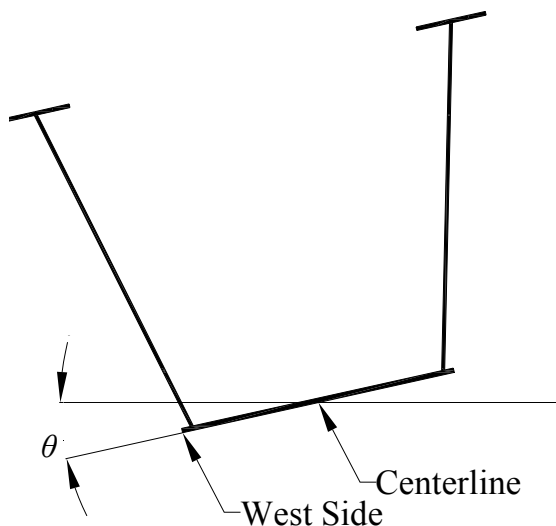


Figure 5.8: Example of the rotation of the girder cross section

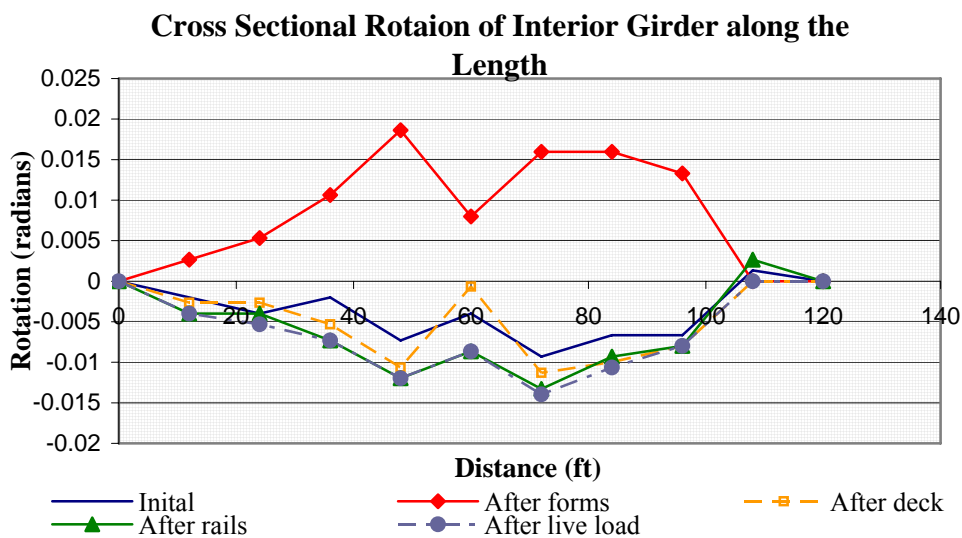


Figure 5.9: Cross sectional rotation of the interior girder along the length

Cross Sectional Rotation of Exterior Girder along the Length

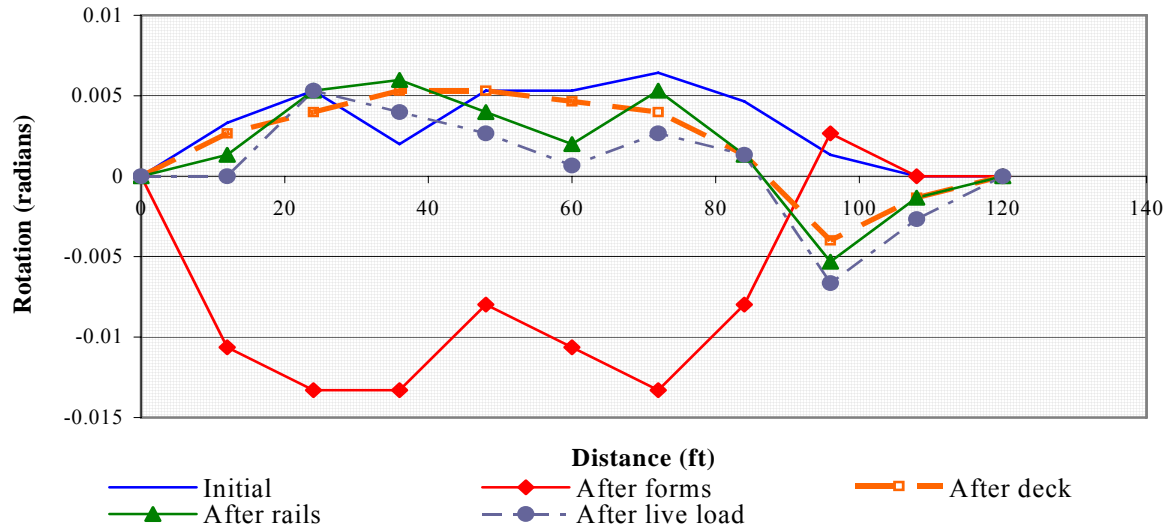


Figure 5.10: Cross sectional rotations of the exterior girder along the length

5.4 DATA REDUCTION

The stain gage data collected showed variations due to bending of the plates from out-of-plane straightness, expansion and contraction from the thermal energy absorbed from the sun, or other reasons explained in the following paragraphs. Each variation was filtered as much as possible to minimize their influence on the strain data and to ensure the final estimates were a reasonable representation of the existing condition in the bridge system.

The data indicated that the strains varied less during the hours of 4:00 A.M. to 6:00 A.M. Because this time period provided the best opportunity to establish an estimated baseline strain, the values were averaged during the 4:00 A.M to 6:00 A.M. time period for several days prior to the casting of the deck to obtain an estimate of the initial zero state of strain in the system components. These

estimated strains were used to determine the increase in strain in the system components for each stage of construction and during the live load testing.

5.4.1 PLATE BENDING

The stresses in the individual plates that make up the bridge system are captured by placing gages on both sides of the plates. As mentioned in the previous chapter, the plates of the webs came from the field with out-of-plane imperfections. As the plates experience stress during loading, the out-of-plane regions are expected to experience bending. As a result, one side would be in compression and the opposite side would be in tension. The assumption is made that the bending will remain elastic and the distribution of the strains across the plate will be linear. Therefore, the strain at the center of the plate will be the average of the strains at the extreme fibers. This strain and its orientation along the longitudinal axis of the bridge will be used to compare with the computer model and to determine the stress in the plate to compare to the expected yield stress of the steel.

5.4.2 THERMAL EFFECTS

The bridge is located in an open area that is fully exposed to the sun. This positioning has allowed the girders to absorb radiant heat. The expansion and contraction as the bridge heats up and cools down can easily be seen in the strain data captured by the gages (Figure 5.11). To compensate for these thermal effects, each channel of data was averaged between each stage of the construction and live load testing.

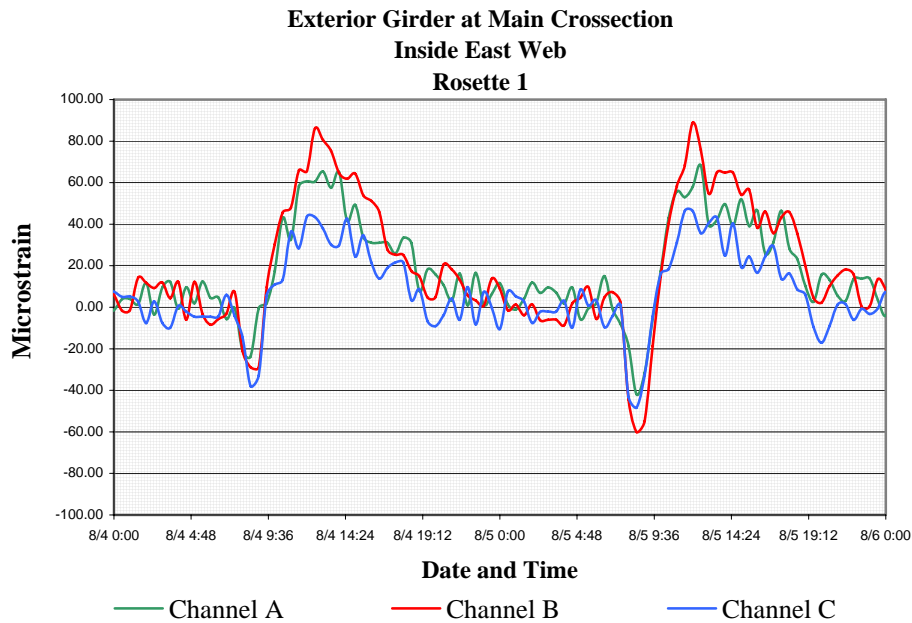


Figure 5.11: Example of thermal effects on the strain

5.4.3 DATA FLUCTUATIONS

The variations in the data in the foil and rosette gages were due to several causes. Construction activities caused the gages of the interior girder to fluctuate days just before, during, and after casting of the deck and rails (Figure C.1). Also, anomalies were attributed to loose wires on the data loggers, gage wires touching the metal girders because of gaps in the heat shrink, missing heat shrink insulation on some of the wiring, or a defective gage. The wires to the data logger were reconnected to the terminal blocks, the exposed wires were covered with electrical tape, and the defective gage was replaced. These corrections fixed most of the gages that were exhibiting abnormal output. A couple of the rosette gages experienced sudden changes that could not be explained or corrected (Figure C.2). Although the gages had a severe change, their values leveled out and remained steady for several weeks prior to the live load testing (Figure C.3). These values

were not used to determine the average change in strain. They were monitored until the data collection systems were switched in preparation for the fracture test and showed to be steady. Because the high-speed system zeroed the readings for each channel when the system was turned on and because the gages gave consistent readings, the decision was made to use gages during the live load test to determine if they would be able to continue to give reasonable results.

The stud gage data collected showed that fluctuations in most of the gages had been reduced to reasonable movement by the middle of September (Figure C.5). Most of the gages exhibited drift and leveled off similarly to shear stud number 2 (Figure C.6). Large fluctuations still persisted in 5 of the 15 gages. Shear studs 1, 7, 11, 13, and 14 all displayed strain variations between 500 and 1100 microstrain. Graphs of gages 11 and 14 show the variations in the data that were recorded (Figure C.7 and C.8, respectively). The other gages performed in an acceptable manner.

5.5 INDUCED STRESSES AND STRAINS

The data collection for the strain gages installed on the bridge began on August 3rd. This date was just after the contractor had started placing the formwork and steel for the deck. Therefore, the strains induced from the self-weight, formwork, and reinforcing steel were not captured by the data collection system. The system sampled the strains every 30 minutes until the day before the deck casting when it was set to sample every 10 minutes. The following day it was reset to sample every 30 minutes. The data collection system was switched over to a high-speed setup capable of sampling at a rate of 500 readings per second in preparation for the fracture test two weeks before the fracture test. Live load testing was preformed to ensure the gages connected to the high-speed system functioned properly. The behavior of the gages that were functioning

properly are described in the following sections, with the exception of the shear studs and reinforcing steel gages.

The shear stud and reinforcing steel gages that generated what was felt to be good data did not show the behavior well enough to be conclusive during the course of the construction and live load placement. The drift in the shear stud data and such small variations after each of the construction events prevented conclusions from being drawn concerning the accuracy of the data. However, the data are expected to be useful during the fracture event where the system is expected to rely on the shear stud capacity to transfer larger loads. The reinforcing steel gages had a similar issue; small changes in strain that a relevant conclusion could not be made about the behavior at this time. Again, the strains that will be induced once the fracture event occurs are expected to crack the concrete deck and engage the reinforcing steel. These gages should be beneficial in describing the behavior of the bridge system during and after the fracture test.

5.5.1 CONCRETE DECK

Construction of the deck began on June 27, 2006. The formwork brackets and forms were erected first, then the pan decking to span between the girder flanges was installed, and finally the steel reinforcement was placed (Figure 5.12).



Figure 5.12: a) Formwork on bridge b) deck reinforcing steel

After about three weeks, the deck reinforcing steel was installed and the contractor was ready to cast the deck. At this time, the strain gages for the shear studs and reinforcing steel were installed as indicated in Chapter 4. The instrumentation of the deck took about three weeks and was completed by August 1st. The deck was poured 17 days later. The deck pour started from the north end and finished at the south end. The entire pour took approximately 68 cubic yards of concrete and was completed in just over 6 hours.

The data for the foil and rosette gages positioned at the girder cross sections indicated that, after the deck placement, the upper portion of the web went into compression and approximately the lower two-thirds were in tension (Figure 5.13). The stresses in the girders are shown in parenthesis below the strain values in Figure 5.13. They were calculated to estimate how close the stress was to the nominal yield stress of 50 ksi that was specified for the plates that make up the girders. Therefore, uniaxial stress in the longitudinal direction is considered. The relationship commonly known as Hooke's law given by the equation $\sigma = \varepsilon \times E$ was used. These estimates show that the highest stresses that are in the bottom flanges are less than one-half of the nominal yield stress of 50

ksi. The strain data indicated that the neutral axis of the cross section appears to be between the upper foil gage and the middle rosette gages on the web. Assuming the strains vary linearly up the webs, the neutral axis was determined to be at 31 in and 30 in. above the bottom flange for the interior and exterior girders respectively. This is lower than the calculated location of 48 in. for the girder cross-section.

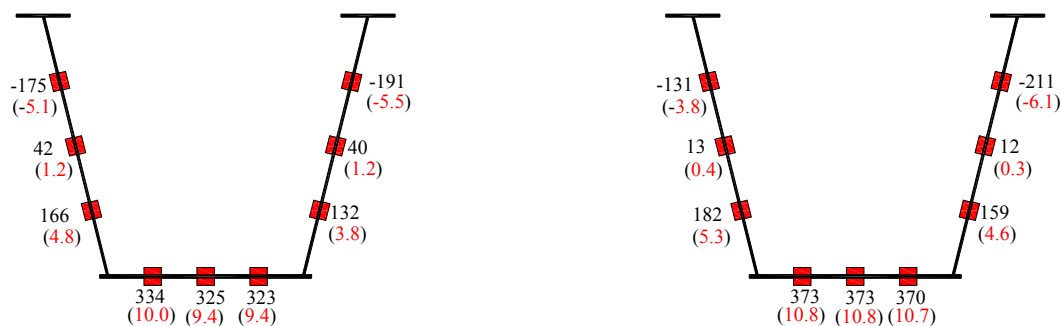


Figure 5.13: Average microstrains and stresses (ksi) south of midspan after deck casting

5.5.2 T501 RAILING

The formwork and steel reinforcement were placed for the west rail within a couple of days after the deck was cast. The west rail was cast five days after finishing the deck and was allowed to gain strength overnight. The forms were removed the next day and placed on the east side of the bridge casting the east rail the next day. The rails were finished one week after the deck had been cast.

The foil and rosette gages indicated an increase in compression in the top one-third of the web and an increase in tension in the lower two-thirds of the web in the cross sections of the girder after the rails were cast (Figure 5.14). The increase in strain observed indicated neutral axis shifted upward toward the girder

flanges after the rails were pour. Using the same assumptions in the previous section, the change was determined to be only about 1/2-in. for both girders.

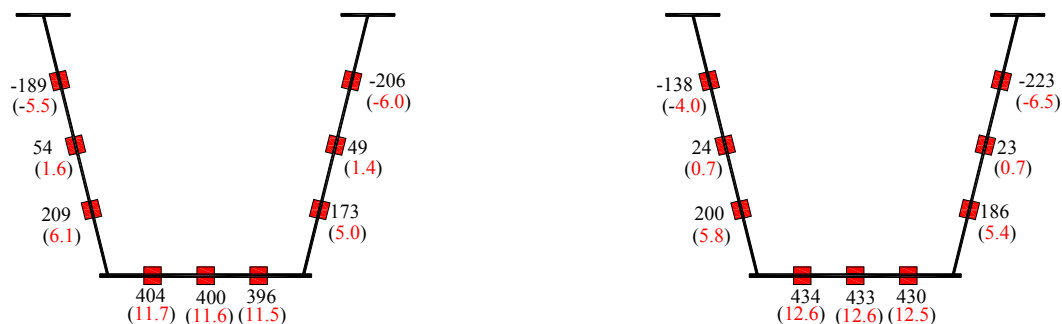
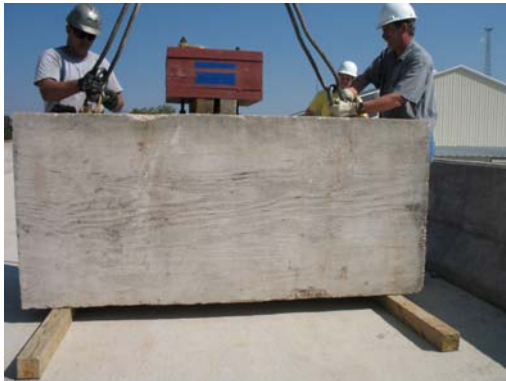


Figure 5.14: Average microstrains and stresses (ksi) after casting rails

5.5.3 LIVE LOAD

The bridge was subjected to a simulated HS-20 truck at the position that would maximize the moment and torsion in the girders. The truck axle spacing was 14 ft. for both front and rear axles. The front axle weight consisted of one concrete block, 2 ft. W × 3.33 ft. H × 7.33 ft. L, and a group of 5 steel plates, 1.5 ft. W x 0.167 ft. H x 1.67 ft. L with 4 holes 7/8-in. diameter, that were bolted together and placed on top of the block (Figure 5.15a). The truck mid and rear axle weights were simulated using AASHTO Type IV prestressed concrete beams positioned on 4 × 4 dunnage (Figure 5.15b).



(a)



(b)

Figure 5.15: a) Front axle loading b) rear axle loading

To determine the weight of each component, the pieces were lifted with a crane while a 50 kip load cell was attached between the cables of the crane and concrete pieces (Figure 5.16).



Figure 5.16: Load cell connection to crane

The strains were recorded with a Vishay, model P-3500, digital strain indicator. The load cell was calibrated in the lab to determine the appropriate gage factor to use to convert the strains into loads (Table 5.2). As load was applied to the load cell, the strain output was recorded. The calibration factor for each load was determined by using the following equation:

$$Gf = \frac{\varepsilon \times C_{Loadcell}}{2000 \times \delta_{Load}}$$

Where Gf = Calibration factor

$C_{Loadcell}$ = Capacity of load cell (lbs)

ε = strain reading

δ_{Load} = change in load (lbs)

Because the load cell readings tend to be less accurate at lower loads, the first and last load readings were not used to find the average for the gage factor.

Table 5.2: Load cell calibration

Calibrating Load Cell				
	Load (lbs)	δL (lbs)	Reading ($\mu\varepsilon$)	Output (mV/V)
Prior to load	80	0	0	
	5265	5185	426	2.05
	10046	9966	815	2.04
	15060	14980	1221	2.04
	10008	9928	811	2.04
	4999	4919	403	2.05
After load	71	-9	0	
			Calibration Factor	2.04

Once the gage factor was determined, the loads could be calculated using the strain readings recorded at the beginning of the live load test. The previous equation was rearranged with the change in load on the left and the gage factor in the denominator on the right. An additional load was added to the front axle block to bring it up to the AASHTO standard 8 kips of an HS-20 load (Table 5.3). The weight of the live load totaled to approximately 76 kips (Table 5.4). Both the front and rear axle weights were a little more than estimated, which made the load slightly larger than the target value of 72 kips.

Table 5.3: Steel ballast for front axle

<i>Additional Weight of Steel Plates for Front Axial</i>						
<i>Length (in)</i>	<i>Width (in)</i>	<i>Height (in)</i>	<i>Diameter of Hole (in)</i>	<i>Total Volume per plate (Ft³)</i>	<i>Weight per plate (Kips)</i>	<i>Total Weight (kips)</i>
20	18	2	0.88	0.41	0.20	1.01

Table 5.4: Live load weights

<i>Simulated Live Load Components</i>		
<i>Member</i>	<i>Strain reading($\mu\epsilon$)</i>	<i>Weight (Kips)</i>
1	1375	16.85
2	1400	17.16
3	1370	16.79
4	1390	17.03
5	585	7.17
6		1.01
<i>Total Weight</i>		<i>76.01</i>

The live load test was performed by placing the simulated truck in three positions across the width of the bridge to determine the response of the bridge to the lateral position of the load on the bridge. The first part of the test was to place the load 2 feet away from the rail of the interior girder with the front axle of the truck 10.33 feet forward of the centerline (Figure 5.17). The longitudinal position was found by using the general rules for simple supported beams carrying concentrated moving loads as prescribed by AISC (AISC, 2005). Once the load was in place, the data collection system was sampled once every second for approximately 5 minutes. After the data was collected, the load was moved to position 2, which is centered across the width of the bridge (Figure 5.18). Finally, the load was placed with the edge 2 feet from the exterior girder rail to produce the maximum vertical and torsional moment in the bridge (Figure 5.19). The load was removed from the bridge after the readings were taken at each position on the bridge..

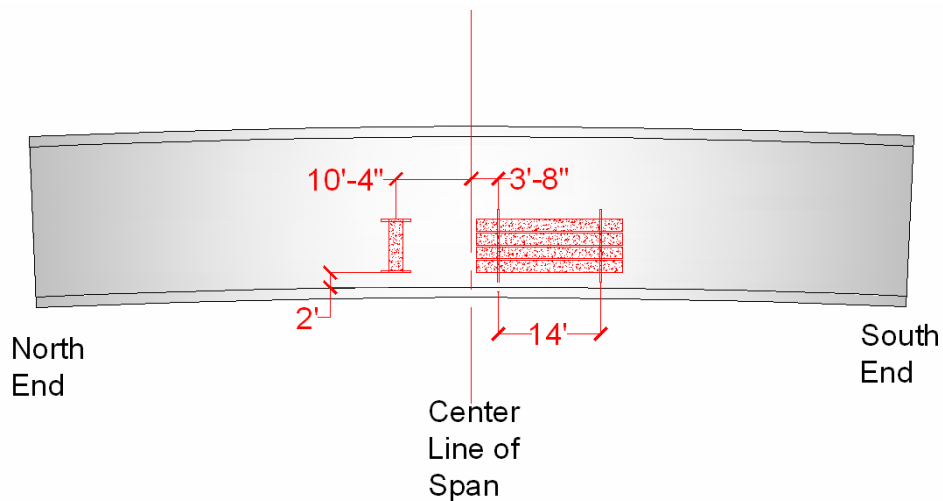


Figure 5.17: Live load position 1

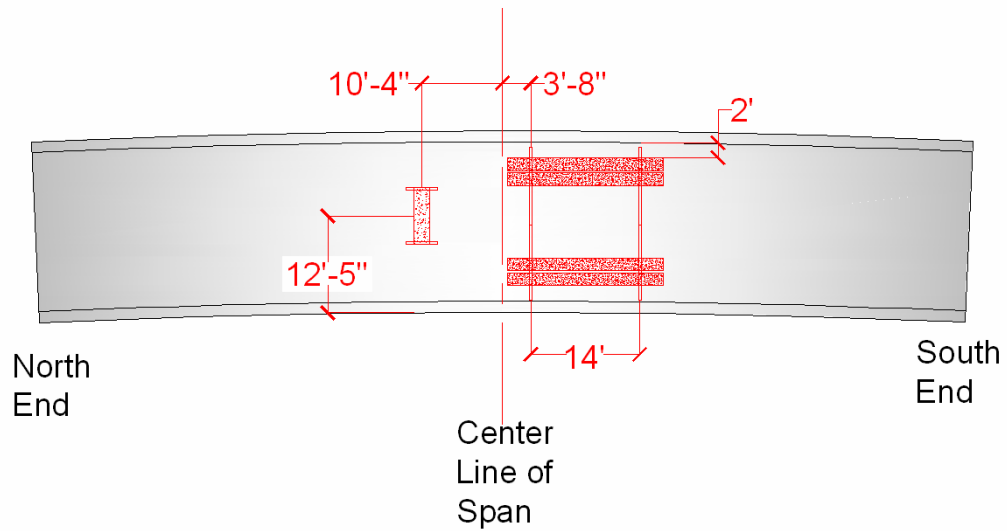


Figure 5.18: Live load position 2

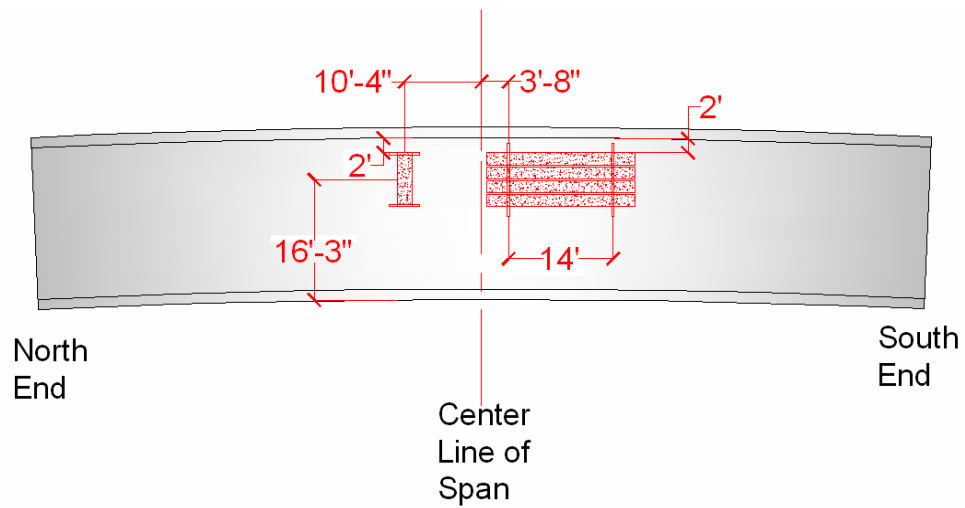


Figure 5.19: Third and final live load position

The gage response during the live load test highlighted a few problems with some of the gages. There were a total of three channels that had problems during the test. The bottom flange rosette gage of the interior girder cross section

north of the centerline experienced a constantly increasing strain in channel b that did not fluctuate with the loading and unloading cycles like all the other gages. All the gages listed below had too much noise that could not be removed by filtering the signal and were not recorded:

- a) Foil gage 16 on the inside of the interior girder bottom flange south of the center line.
- b) Channel b on rosette gage 4 located on the outside of the east web of the exterior girder.
- c) Channel b of rosette gage 16 on the outside of the east web of the interior girder north of the centerline.

These problems should be corrected as soon as possible. Also, the majority of the foil and rosette gages were left with a little residual strain at the end of the test (Figures C.11 to C.14). As mentioned earlier, the shear studs did not seem to be affected at all during the test.

The biggest change noted was the constant rise in the strain in shear stud gage 1, FS1 (Figure C.15). Also, the problems experienced in gage 11 earlier were not evident during this test. The other gages missing, 7, 13, and 14, were not connected to the high speed system because of the severity of the fluctuations in their data.

The deck reinforcing steel indicated a little change in strain at the centerline location and at the 10 feet north and south locations (Figure C.16 to C.22). Because the changes are on the order of 10 to 20 microstrains, it is hard to conclude how much is due to the load and how much is due to thermal effects. At the end of the test with the final positioning of the live load, the largest change in the system was experienced in the girders.

The strain data from the live load test show that all the foil gages were in tension after the live load was placed in its final position. The strains were

averaged, as before, and added to the dead load strains that were previously determined. The stress increased to approximately 15 ksi in interior bottom flange and 16 ksi in the exterior bottom flange, which do not include the stress from the self-weight dead load (Figure 5.20). The computed stresses from the finite element model were 16.0 ksi for the interior bottom flange and 17.7 ksi for the exterior bottom flange after subtracting the stress for the self weight of the girders. The additional strain in the east side of the interior bottom flange, highlighted by the rectangle, could not be determined because of the noise in foil gage 16 as pointed out above. Even with the additional stress of the live load, the steel is well below its estimated yield stress.

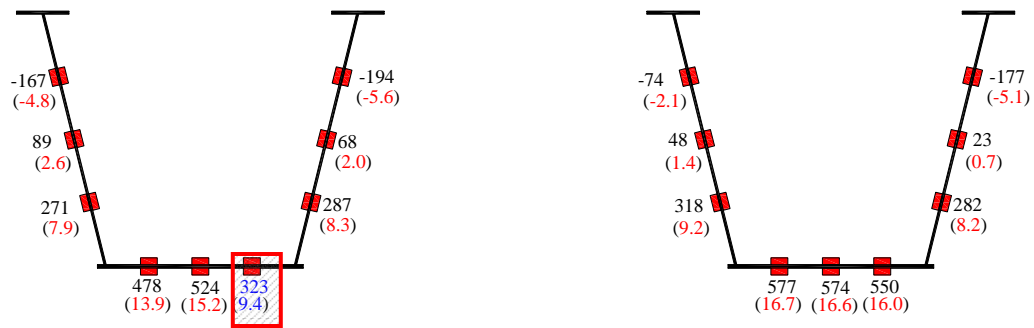


Figure 5.20: Final microstrains and stresses (ksi) prior to the fracture test

The data gathered during the construction and live load test showed the measured deflections differed from the computed finite element analysis by a maximum of 15 percent, while the stresses were within 14 percent of the interior girder and 10 percent of the exterior girder. The conclusions and future recommendation are discussed in the next section.

CHAPTER 6

Conclusion and Recommendations

6.1 SUMMARY

This report describes the process of constructing, instrumenting, and incremental static testing of a full-scale horizontally curved twin steel trapezoidal box-girder bridge segment. As stated in Chapter 1, the objectives of the research described in this report were to: 1) construct a bridge segment that represents, as close as possible, what is currently in service; 2) instrument the bridge components to capture the behavior of the bridge system before, during, and after construction; and 3) generate meaningful data that would be a useful baseline for analytical models of this type of bridge. The first goal was met by contracting with a builder familiar with TxDOT procedures and having TxDOT personnel assist in overseeing the construction. Next, the behavior of the bridge system was monitored with a network of 95 gages measuring strains in the cross-sections of the girders, both end diaphragms, steel reinforcement in the deck, and shear studs on both girder flanges. Periodic measurements of the bridge's response to different parts of construction allowed strains and deflections to be compared with expected behavior from calculations and computer analysis. A finite element model of the bridge was checked to ensure the modeling methods that were being developed were reasonably accurate in predicting stresses and deflections. These conditions were met in order to proceed with further testing of a simulated brittle fracture of the exterior girder's bottom flange. This instantaneous loss of one of the two FCMs will test the bridge's ability to transfer the load carried by the fractured member to the other components in the system.

6.2 CONCLUSIONS

The conclusions for each of the objectives are as follows:

- 1) The test bridge was built to perform in a similar manner to a typical twin steel trapezoidal box-girder bridge currently used in several areas of the state of Texas. The measurements taken of the as-built condition of the deck reinforcing steel (Chapter 3) show that the average spacing was consistent with the design drawings. The only exception was that the average haunch height on the east flange of the interior girder was 0.8 in. higher than specified. The additional height of the haunch will reduce the shear stud capacity in this area. It was calculated that the shear studs of two flanges along one-third of the longitudinal length were needed to transfer the load during the fracture test. Because the capacity of twice as many shear studs still remain, it was reasonable to assume that the additional haunch height would not affect the test results. Also, the bridge support conditions differ from actual field conditions. The test bridge was built in a simply supported configuration instead of a continuous span like the bridges in the field. The difference in support conditions means that the bridge specimen will not receive additional support from other bridge members and will undergo more rotation due to the deflections; therefore, it will represent a worst case scenario during the fracture test.
- 2) The data in Chapter 5 indicate that the instrumentation used provides reasonable measurements for most of the gages. The girder cross-section gages showed that the neutral axis of the girders was between the upper foil gage and the center rosette gage on the web. This

finding demonstrated that the bridge began working as a composite section as expected. Also, the gages in the bottom flanges were measuring stresses close to those calculated using the basic assumptions of Hooke's law.

- 3) The data collected during the project generated stresses that correlated with the finite element model being developed. The strains and deflection predicted by the finite element analyses were between 10 and 15 percent of the actual measurements recorded.
- 4) After the positioning of the simulated live load of approximately 76 kips, the bottom flanges experienced stresses that were less than one-half of the nominal yield strength of the steel.
- 5) After the high-speed data collection system was connected, there were more channels available than previously assumed. Therefore, the diaphragms could have more gages installed to more accurately determine the shear stress transferred from the exterior girder to the interior girder during the fracture test.

6.3 RECOMMENDATIONS FOR FUTURE RESEARCH

After the course of constructing, instrumenting, and monitoring the behavior of the test bridge, the following recommendations can be made for future research:

- 1) The diaphragms should have gages installed to more accurately determine how the shear will be transferred from the exterior girder to the interior girder.
- 2) If deflection readings are needed in the future, metal tabs should be welded to the ends of the outer edge of the bottom flange of both girders to use for measuring movement at the end and relative

displacement along the span of the girders. The strips of wood placed on the foundations below the girders that were used in the current study began to warp due to weathering.

- 3) Gages wires should be shielded and the heat shrink should be redone in places where wires may still be exposed to the environment in order to eliminate noise in the data collection system.
- 4) The end supports could be modified to restrain the girders to simulate continuous support conditions from other spans to allow the bridge segment to mimic service conditions more closely.
- 5) Coupons of the plate metal should be removed and tested to validate the plate properties within the computer model.
- 6) Because the issue of fracture critical members is not isolated to the bridge studied in this report, other scaled test models of other bridge systems can be constructed in the lab to calibrate other computer models to aid the engineering community.

APPENDIX A

Calculations

A.1- Elastomeric Bearing pad calculations:

The TxDOT Bridge Design Manual and the AASHTO Bridge LRFD Specifications were used to determine the requirements. The recommended steps in the TxDOT manual were used when they differed from the AASHTO specifications.

A recommended minimum bearing capacity of 1000 psi was used to determine the surface area. Pads were found in the lab that could possibly be used. The pads were constructed of 9 steel reinforcing plates 1/8-inch thick encased in layers of elastomeric material 3/16-inch thick.

Bearing Pad Dimensions:

Length = 22 in Width = 11 in Height = 3 in

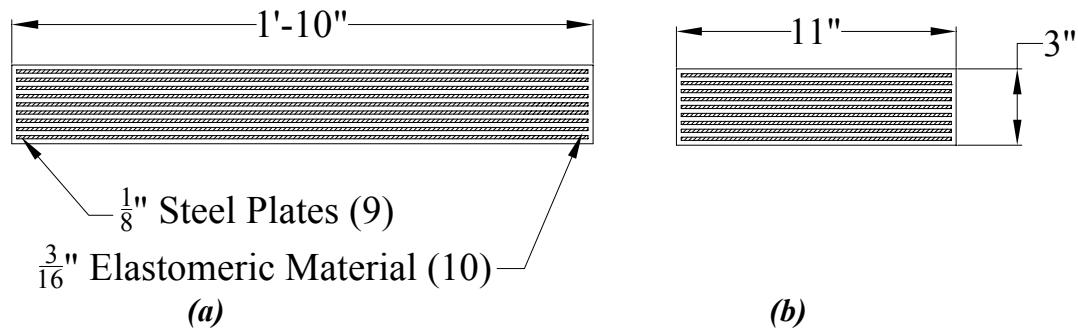


Figure A.1-1: a) plate and elastomeric layer thickness b) side view of width and height.

$$\text{Bearing capacity} = \frac{220\text{kip}}{\text{Length} \times \text{Width}}$$

$$\text{Bearing capacity} = 1000 \text{ psi}$$

Because the design load of 220 kips was factored, the bearing capacity in the pad was considered to be adequate.

Checking the translation limits in the TxDOT manual:

Translation limits for pads with no anchorage were used.

$$\text{Minimum } T = 4.8 L' A / (R_d \times F)$$

Where T = Total elastomeric thickness (in)

L' = Expanded length (ft)

A = Area of the pad (in²)

R_d = Reaction due to dead load (lbs)

F = Dead load reduction factor due to grade or slope of beams

(To simplify calculations R_d was taken as the design reaction load and no dead load reduction was taken, so F is 1.)

Maximum $T = L/3$ or $W/3$ which ever is smallest

Where L = Bearing length across beam (in)

W = Bearing length along beam (in)

Minimum $T = 0.576$ in.

Maximum $T = 3.667$ in.

Total thickness of the elastomeric material

$h_{rt} = 0.1875$ in per layer

$T_{pad} = 10$ layers \times 0.1875 in

$T_{pad} = 1.875$ in

The total thickness of the elastomeric material falls within the minimum and maximum range.

Determine bearing displacements:

The displacement that a bearing pad will experience due to thermal effects were determined by using the equation below. The TxDOT Bridge Design manual required the strain to be calculated over a temperature fluctuation of 70 degrees.

$$\text{Thermal Strain, Steel} = 6.5 \times 10^{-6} \times 70^\circ \text{ F} \times 12 = 0.0055 \text{ (in/ft)}$$

Thermal displacement of the bearing pad (Δ_T) = 0.66 in.

The expected deflection obtained from UTrap was around 7.5 inches. Assuming 7.5 inches over 60 feet to be a small angle, the expected rotation can be obtained by dividing the deflection by the length. The rotation will be approximately 0.01 radians

It can be assumed that the displacement that the bottom of the girder will undergo will be equal to the rotation of 0.01 radians times the height of the neutral axis. The girders are considered to act compositely, and the neutral axis was calculated to be approximately 48 inches above the bottom flange, which gives the following displacement value:

$$\begin{aligned} \text{Rotational displacement } (\Delta_r) &= 0.01 \times 48 \text{ in} \\ \Delta_r &= 0.048 \text{ in} \end{aligned}$$

Total displacement in the bearing pad (Δ_{Total}) = $\Delta_T + \Delta_r$

The pad must have a height-to-displacement ratio of 2 to 1. Therefore, $h_{rt} \geq 2 \times \Delta_{Total}$ must be checked.

$$1.875 > 1.416 \text{ Good.}$$

To prevent the girder from lifting off the pad, a check is made to ensure that at least 80 percent of the pad will stay in contact with the girder. To check this condition, the compression deflection was calculated and must be greater than $(.01 \times \text{Width} \times 0.8) \times 0.5$.

$$\text{Lift}_{off} = \frac{0.01 \times \text{Width} \times 0.8}{2} \quad \text{Lift}_{off} = 0.044 \text{ in}$$

The compressive deflection was determined by using performance curves in the TxDOT bridge manual (Figure A.1-2). The bearing pressure was used with the shape factor (SF) for an individual layer of elastomeric material to determine the percentage of compressive strain each layer will experience.

$$\text{Shape Factor (SF)} = \text{Length} \times \text{Width} / [2 \times (\text{Length} + \text{Width}) \times t]$$

where t = the thickness of one layer of elastomeric material

$$\text{SF} = 18.925$$

The strain percentage reads approximately 3.0 (Figure A.1-2). The total compression for the pad was determined from the following equation:

$$\varepsilon = \frac{3.0}{100} \quad \Delta_{\text{compression}} = h_{rt} \times \varepsilon$$

$$\Delta_{\text{compression}} = 0.056$$

The calculated compression deflections were larger than the lift off. The bearing pads meet all the requirements and were used to transfer the load from the girders of the test bridge.

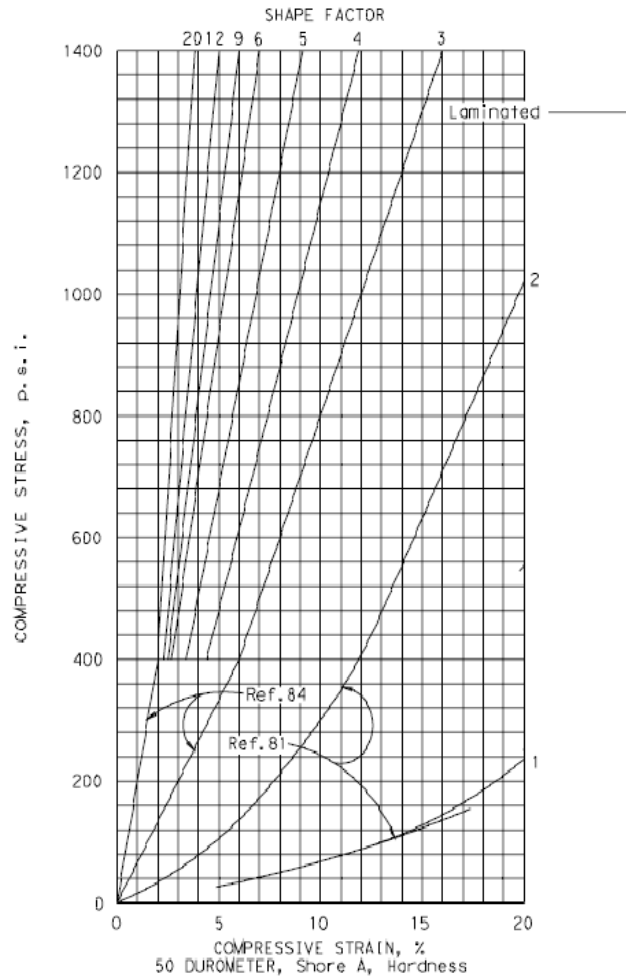


Figure A.1-2: Elastomeric Bearing Performance Chart (TxDOT Bridge Design Manual, 2006)

A.2 Pier Foundation Capacity Calculations

Material Properties and Dimensions:

$f_c = 3000$ psi Design strength

$F_y = 60$ ksi Yield strength of the steel reinforcement

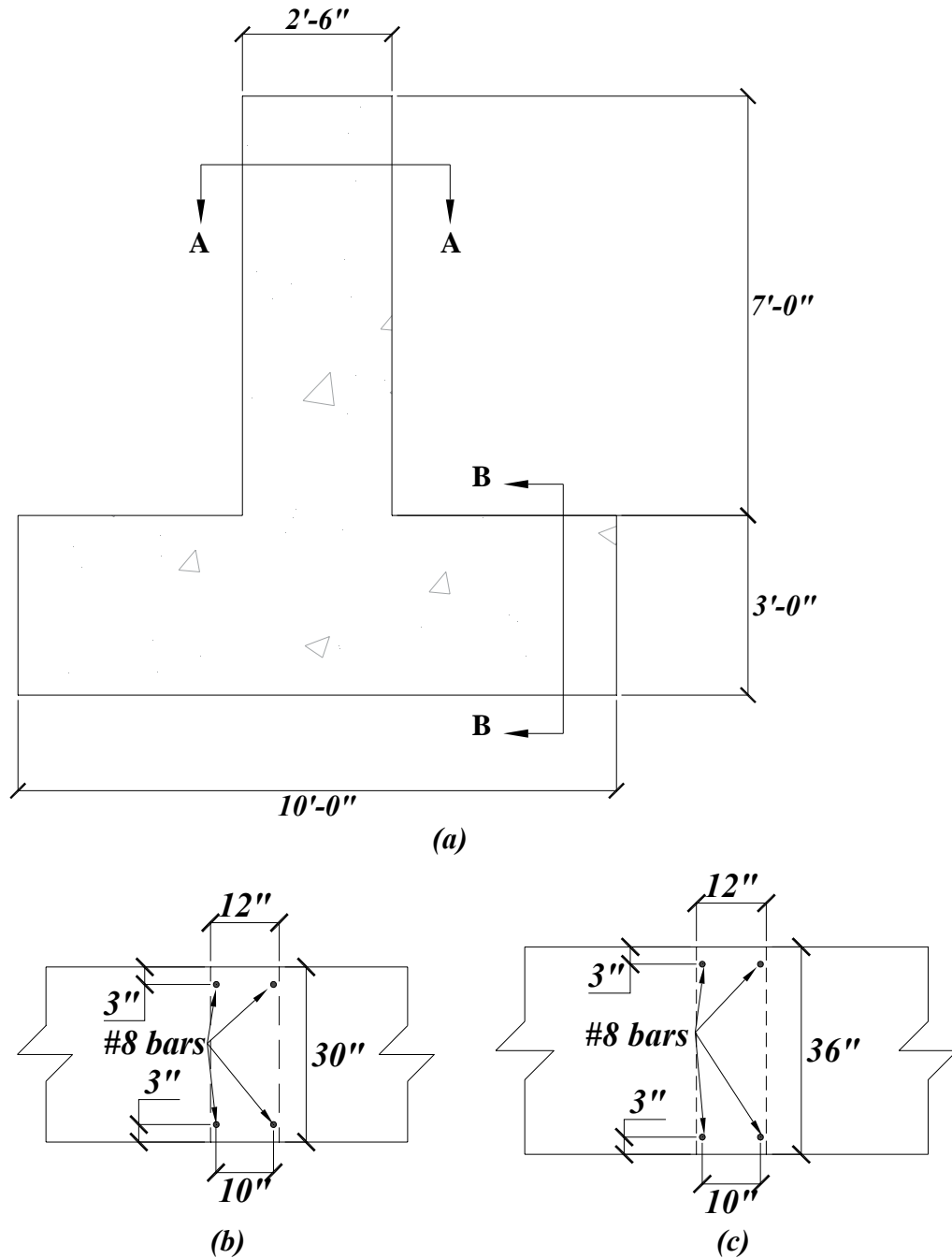


Figure A.2-1: a) Cross-sectional view; b) Cut A-A through stem wall per foot; and c) cut B-B through footing per foot

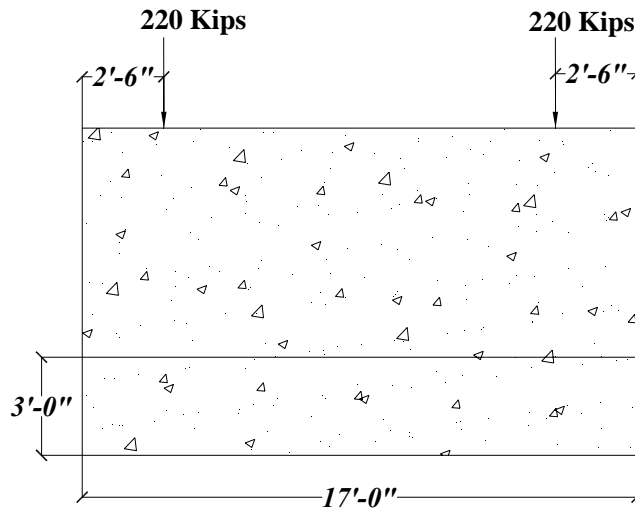


Figure A.2-2: Elevation view showing loading

Capacity of Stem Wall per foot

Axial Capacity per foot:

- A_{s_total} = Total steel in the cross-section (12.56 in²)
- A_g = Gross area of the cross-section considered (360 in²)
- P_u = Ultimate factored axial load (220 kips)
- P_n = Nominal axial capacity
- ϕ = 0.90

$$P_u \leq \phi \times P_n$$

$$P_n = 0.85 \times f'c \times (A_g - A_{s_total}) + A_{s_total} \times F_y$$

$$P_n = 1640 \text{ kips per foot}$$

1640 Kips > 220 Kips

The computations show that the axial capacity was adequate.

Moment Capacity per foot:

Due to an error in laying out the foundations, the load was offset creating some eccentricity and moment in the wall. Also, the wall was expected to experience an estimated horizontal load of 25 percent of the axial load, if the bridge collapses during the fracture test. The moments were summed around point A in Figure A.2-3. Because the horizontal and vertical loads create moments that counter each other, the larger moment was checked to ensure the capacity of the wall was adequate.

M_e = Moment due to the offset vertical load

$M_{horizontal}$ = Moment due to horizontal load

e_{wall} = Eccentricity (7.5 in.)

H_{wall} = Height of the stem wall (7 ft.)

$P_{horizontal}$ = Horizontal load (55 Kips)

$$M_e = P_u \times e_{wall}$$

$$M_e = 137.5 \text{ kip-ft}$$

$$M_{horizontal} = P_{horizontal} \times H_{wall}$$

$$M_{horizontal} = 385 \text{ kip-ft}$$

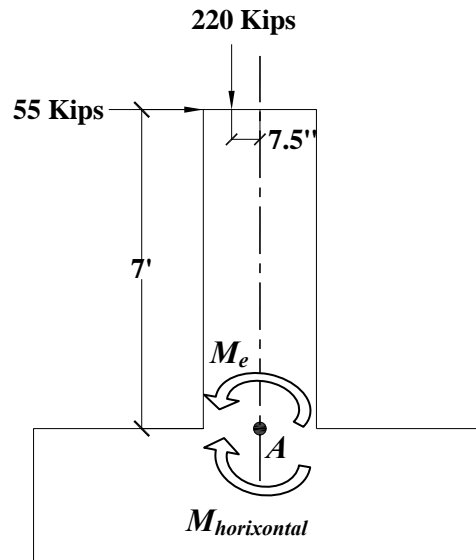


Figure A.2-3: Horizontal and vertical loads applied to foundation

The ultimate moment the base of the stem wall will have to resist is due to the horizontal load applied from the girders.

Variables:

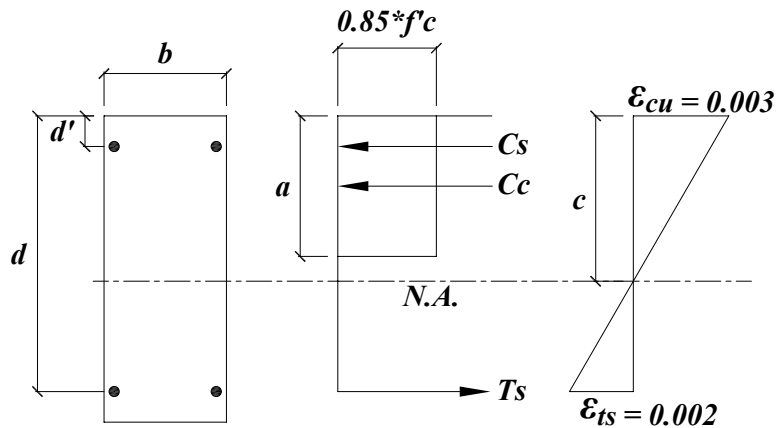
- $f'c$ = Compressive strength of concrete (3 ksi)
- β = Coefficient of 0.85 for $f'c < 4$ ksi
- a = Depth of the compressive stress block
- A_s = Area of tension steel (6.28 in²)
- c = Distance from the extreme compression fiber to the neutral axis
- b = Width of cross-section considered (12 in)
- d = Distance from the center of tension steel to the extreme compression fiber (27 in)
- d' = Distance from the center of the compression steel to the extreme compression fiber (3.5 in)
- A_s' = Area of the compression steel (6.28 in²)
- ϵ_{cu} = Maximum strain limit for concrete compression ACI 318-05 (10.3.3)
- ϵ_{ts} = Maximum strain for 60 ksi steel reinforcement in tension ACI 318-05 (10.3.3)
- C_c = Compressive force in concrete
- C_s = Compressive force in steel
- M_n = Nominal moment capacity
- M_u = Ultimate factored moment (385 kip-ft)

Required moment:

$$\phi \times M_n \geq M_u$$

$$M_n = \frac{M_u}{\phi}$$

$$M_n = 428 \text{ kip-ft}$$



Figures A.2-4: Internal forces and strains in stem wall at maximum capacity

The moment capacity was calculated about the line through the center of the tension steel.

$$c = \frac{d \times \varepsilon_{cu}}{\varepsilon_{cu} + \varepsilon_{ts}} \quad a = \beta \times c$$

$$M_n = 0.85 \times f_c \times a \times b \times \left(d - \frac{a}{2}\right) + A_s \times F_y \times (d - d')$$

$$M_n = 1460 \text{ kip-ft}$$

Based on the calculations, the moment capacity was determined to be adequate.

Moment capacity of the base footing per foot

The size and spacing for the reinforcing steel in the footing were the same as the stem wall. So, the same process for the calculating moment capacity was followed.

$$d = 33 \text{ in} \quad c = \frac{d \times \epsilon_{cu}}{\epsilon_{cu} + \epsilon_{ts}} \quad a = \beta \times c$$

$$M_n = 0.85 \times f'_c \times a \times b \times \left(d - \frac{a}{2}\right) + A'_s \times F_y \times (d - d')$$

$$M_n = 1981 \text{ kip-ft}$$

The moments created after the fracture event:

The moments generated after the fracture event were calculated about the centerline of the foundation at point A (Figure A.2-5). It was determined from simple statics that overturning would be prevented if the resultant of the soil pressure acted within a distance that was at least one-half the width of the footing.

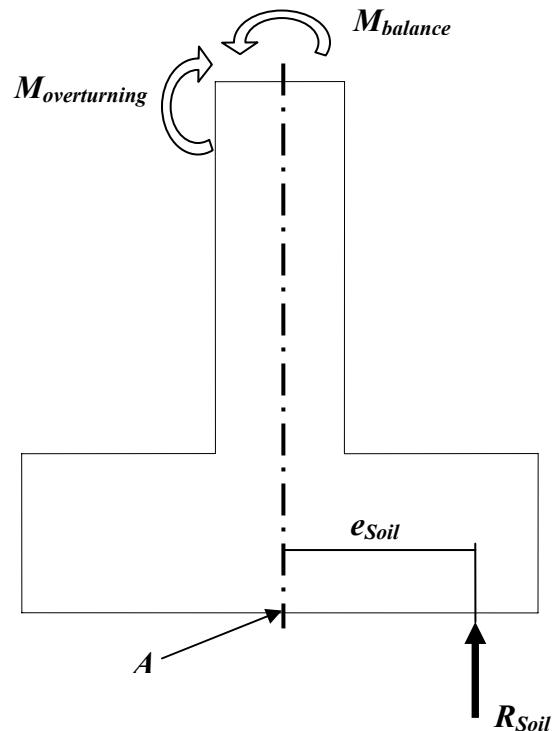


Figure A.2-5: Overturning and balancing moments

The resultant force of the soil was calculated by assuming an eccentricity for the soil to be at the edge of the base of the footing, 60 in. from point A. Because the resultant force of the soil was dependent upon the contact area of the footing and the soil, the contact area needed to be found. The required contact area was the product of the width of the footing and a tributary length along the footing (Figure A.2-6). The tributary length required to generate a resultant soil force large enough to prevent overturning was calculated below:

Variables:

$M_{overturning}$ = Moment due horizontal load

$M_{balance}$ = Moment due to vertical load remaining after fracture

R_{soil} = Resultant reaction of the soil to moments

e_{soil} = Eccentricity of resultant of soil (60 in. minimum)

q_{soil} = Soil bearing pressure (3000 psf)

$l_{tributary}$ = Tributary length of footing

$w_{footing}$ = Width of footing

W_{pier} = Weight of pier per foot

$$P_{vertical} = 0.97 \times P_u \quad P_{horizontal} = 0.25 \times P_u$$

$$M_{overturning} = P_{horizontal} \times (H_{wall} + h_{footing})$$

$$M_{balance} = P_{vertical} \times e_{wall}$$

$$M_{overturning} = 550 \text{ kip-ft}$$

$$M_{balance} = 103.3 \text{ kip-ft}$$

$$R_{soil} = \left(\frac{M_{overturning} - M_{balance}}{e_{soil}} \right)$$

$$R_{soil} = 83.3 \text{ kips}$$

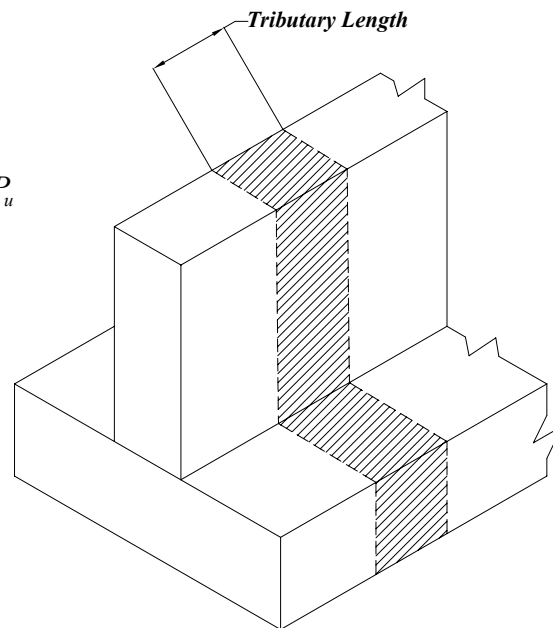


Figure A.2-6: Tributary length

$$l_{tributary} = \left(\frac{R_{soil}}{q_{soil} \times w_{footing} - W_{pier}} \right)$$

$$l_{tributary} = 3.4 \text{ ft.}$$

Assuming that the only half of the foundation participated, a tributary length of 8.5 ft. would be available to develop the resultant soil force. Therefore, because the tributary length required to develop the resultant soil force was less than the length available, the foundation overturning was not considered to be a concern.

Resistance to sliding

The ability of the foundation to prevent sliding along the ground was determined using a coefficient of friction of 0.45, (Hassoun, 1998), and assuming one-half of the foundation would contribute to the force.

Variables:

μ = Coefficient of friction for coarse-grained soils on concrete (0.45)

$$F_{sliding} = [(W_{pier} \times 8.5 \text{ ft.}) + P_{vertical}] \times \mu \quad F_{sliding} = 116.8 \text{ kips}$$

Based on the calculations, the force available to prevent sliding was determined to be over twice the amount needed to prevent sliding of the foundation along the ground if the assumed horizontal force of 55 kips was applied.

APPENDIX B

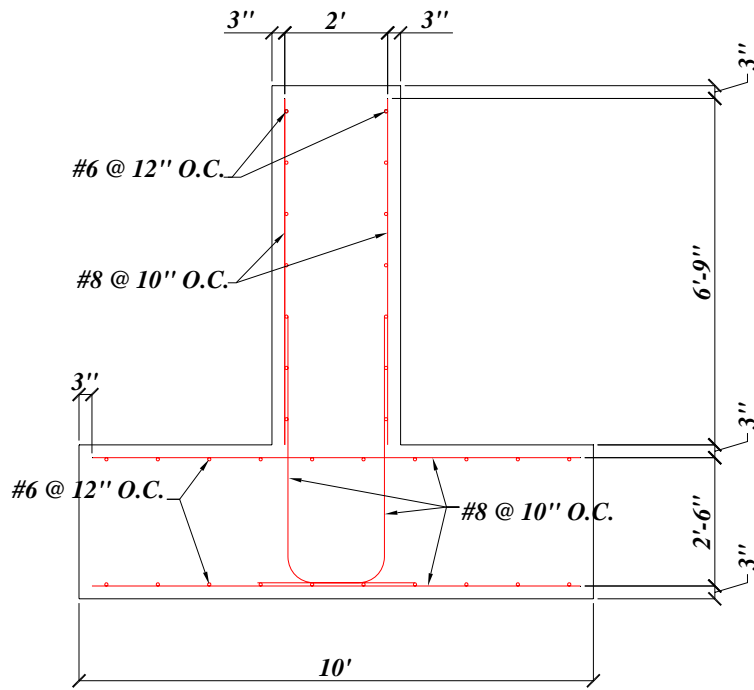
Drawings and Plans



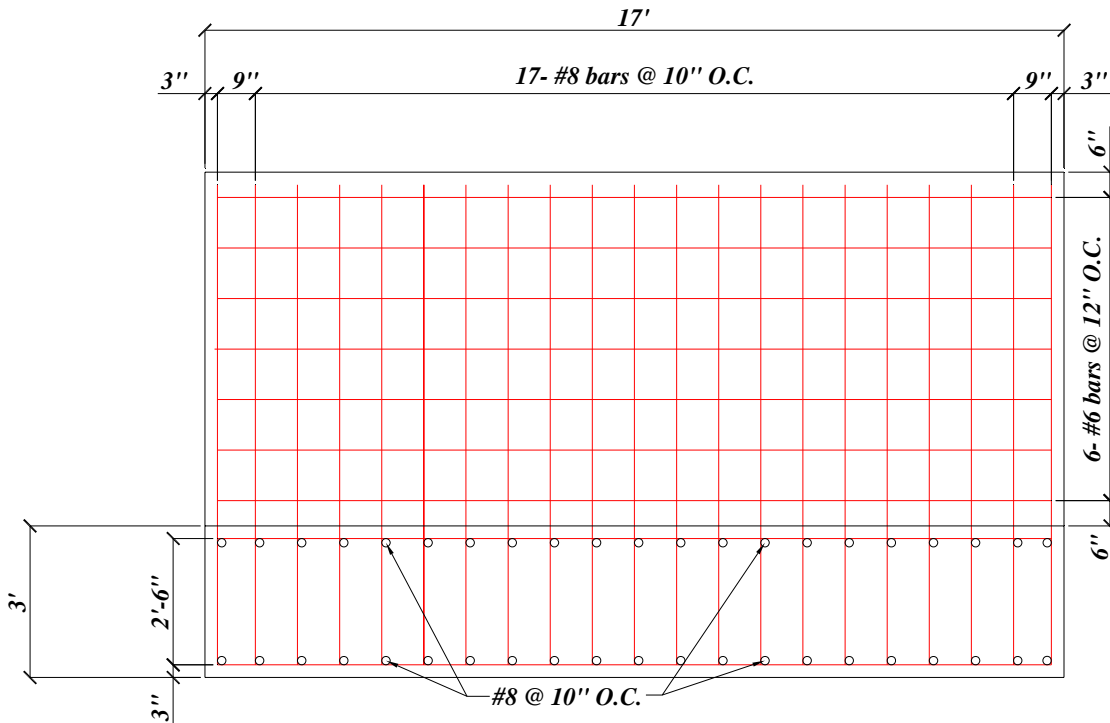
(a)



Figure B.1: a) Site Plan of Bridge Test site at Ferguson Structural Engineering Laboratory b) benchmark location



(a)



(b)

Figure B.2: a) Cross section of Pier Foundation for Test Bridge b) elevation view

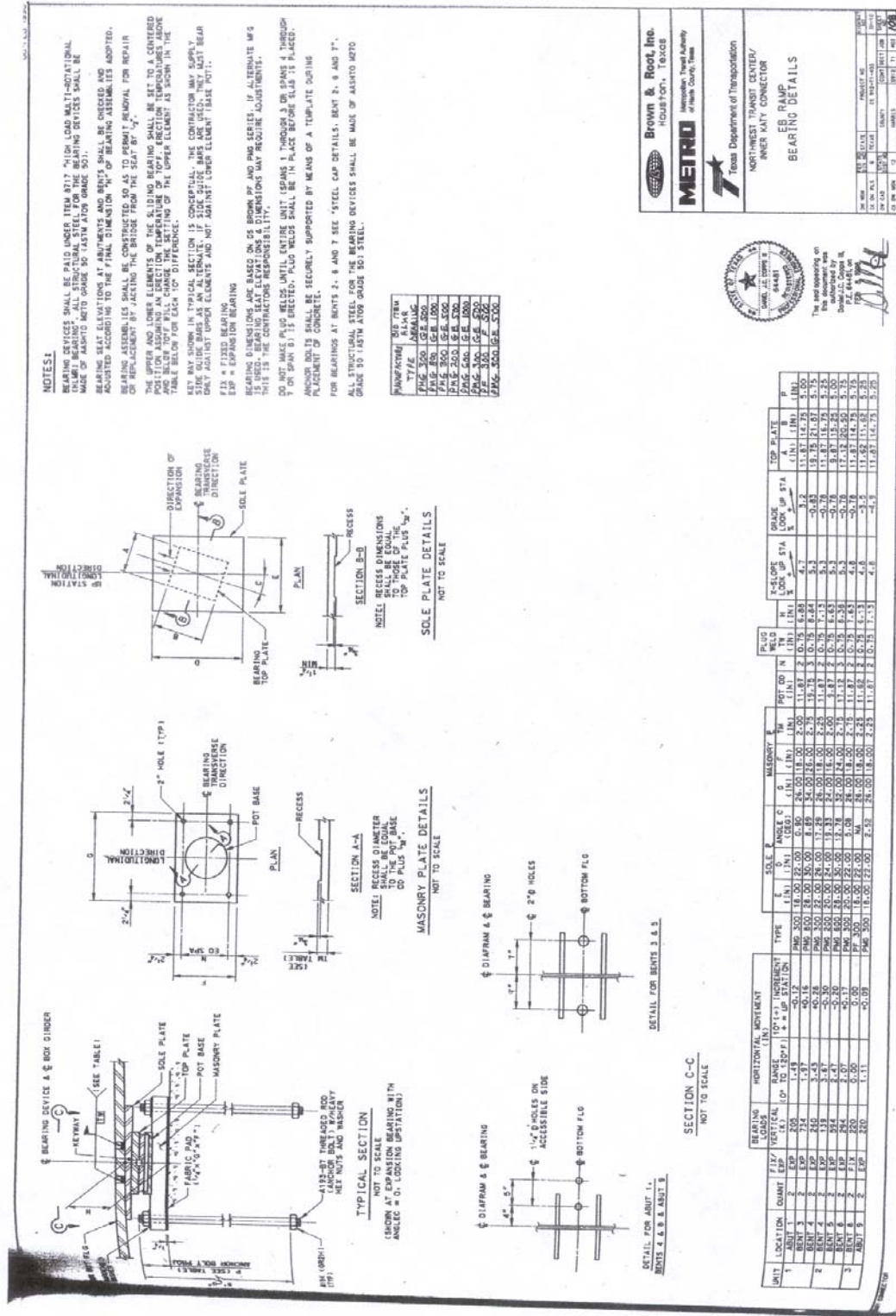
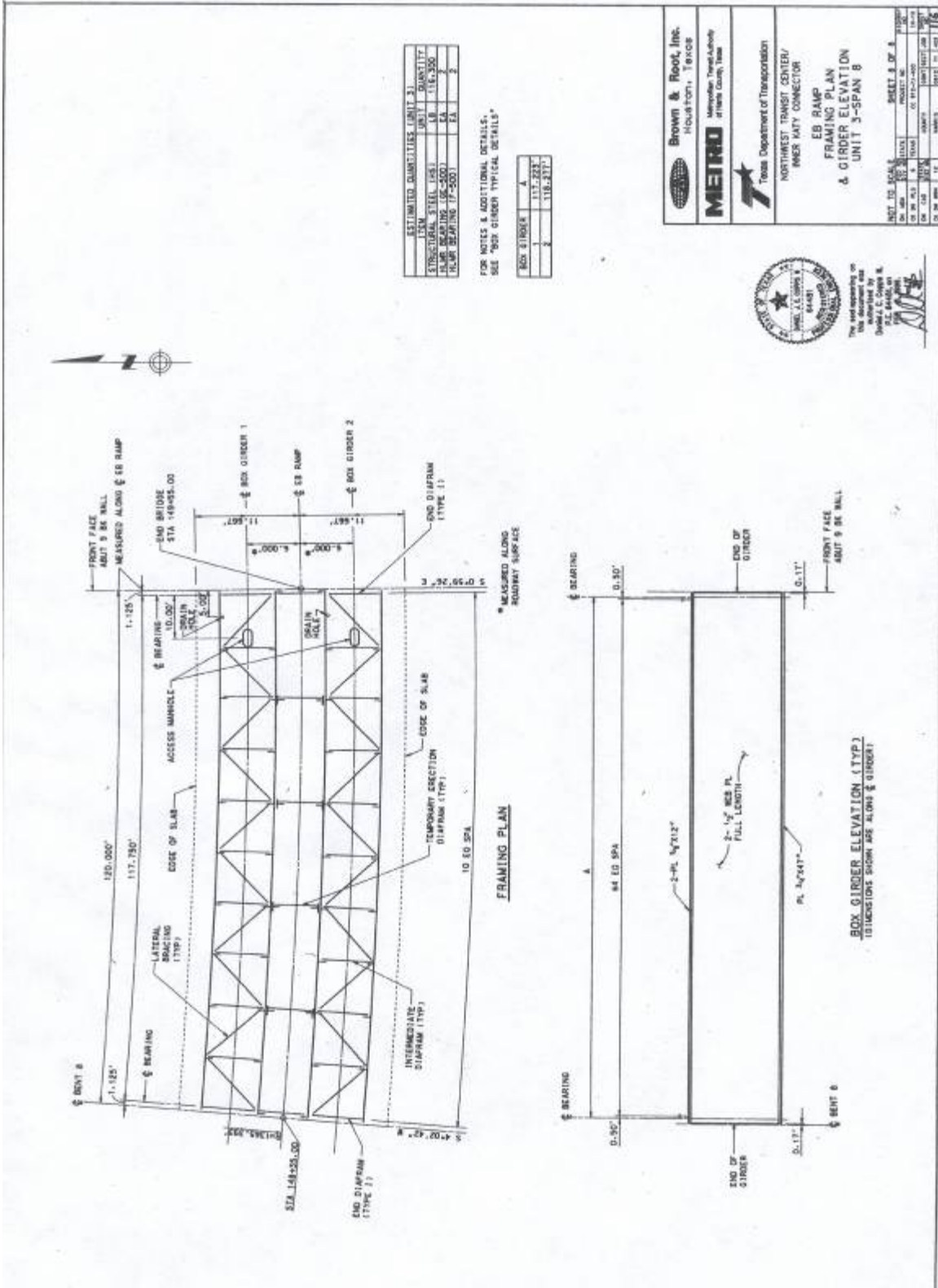


Figure B.3-1: Bearing details from design drawings



ESTIMATED QUANTITIES (UNIT 3)			
STRUCTURAL STEEL (L&S)	EA	118.277	
SLAB BEARING (L&S)	EA	118.250	
PLATE BEARING (L&S)	EA	2	

FOR NOTES & ADDITIONAL DETAILS, SEE "BOX GIRDER TYPICAL DETAILS"

BOX GIRDER	A
1	117.277
2	118.277

Brown & Root, Inc.
Houston, Texas

MEIRO
Metropolitan Transportation Authority
11000 Katy, Houston, Texas

Texas Department of Transportation
NORTHWEST TRANSPORT CENTER/
INNER KATY CONNECTOR

EB RAMP
FRAMING PLAN
& GIRDER ELEVATION
UNIT 3-SPAN 8

SHEET 8 OF 8

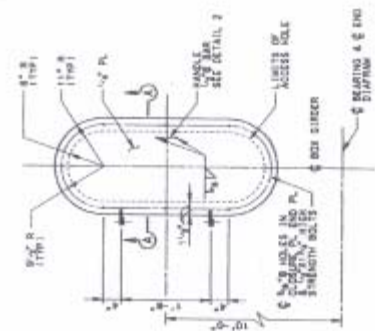
DATE	NOV 10 2011	SCALE	AS SHOWN
BY	W. J. GIBBS	PROJECT NO.	00 812-2-200
CHECKED	J. L. GIBBS	DATE	11/10/11
DATE	11/10/11	DESIGNED	W. J. GIBBS
DATE	11/10/11	DRAWN	W. J. GIBBS
DATE	11/10/11	CHECKED	J. L. GIBBS
DATE	11/10/11	APPROVED	W. J. GIBBS



Figure B.3-2: Framing details from design drawings

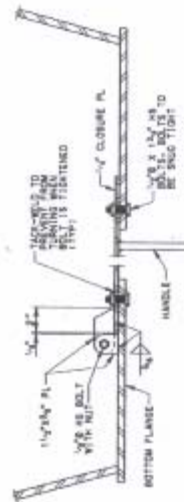
NOTES:

- 1. STRUCTURAL STEEL FOR WEB AND FLANGES OF THE GIRDER SHALL BE A1015, A1015-11, OR A36. ALL STEEL SHALL BE GRADE 50 STEEL. THE GIRDER SHALL BE GRADE 50 STEEL. THE GIRDER SHALL BE GRADE 50 STEEL. THE GIRDER SHALL BE GRADE 50 STEEL.
- 2. GIRDERS SHALL BE DESIGNED AS ONE MEMBER WITH ALL JOINTS AND THE JOINTS WITH FLANGE OVERLAP ETC.
- 3. FOR BEARING AT THE CAP AND JOINTS, THE GIRDER SHALL BE GRADE 50 STEEL.
- 4. ALL STEEL SHALL HAVE PAINT PROTECTION SYSTEM THAT INCLUDES THE JOINTS OF THE GIRDER. THE GIRDER SHALL BE GRADE 50 STEEL.

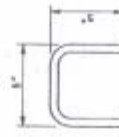


ACCESS MANHOLE DETAIL

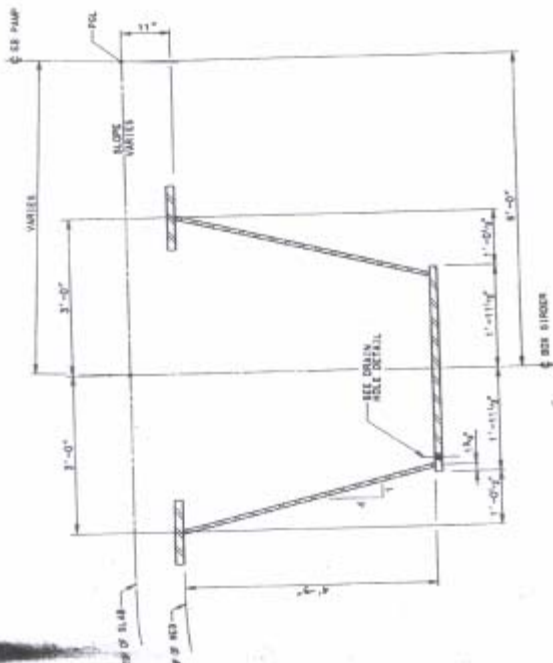
SCALE: 1/8\"/>



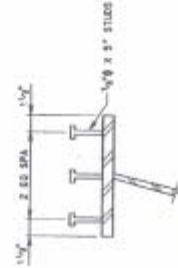
SECTION A-A
TOILET 3'-0\"/>



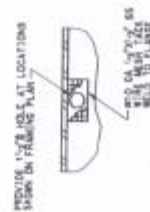
DETAIL 2
SCALE: 3/4\"/>



TYPICAL GIRDER
SECTION
SCALE: 1/8\"/>



SHEAR CONNECTOR DETAIL
N/A



DRAIN HOLE DETAIL
N/A

Brown & Root, Inc.
Houston, Texas

MEIRO
Mechanical Thermal & Electrical
Analysis Group, Inc.

Texas Department of Transportation
NORTHWEST TRANSIT CENTER/
INNER RAMP CONNECTOR
EB RAMP
BOX GIRDER
TYPICAL DETAILS

SCALE: 1/8\"/>



The seal appearing on
this document has
been prepared by
David L. Jones, P.E.
No. 84481, State of Texas.

D.L. Jones

Figure B.3-3: Box-girder cross section details from design drawings

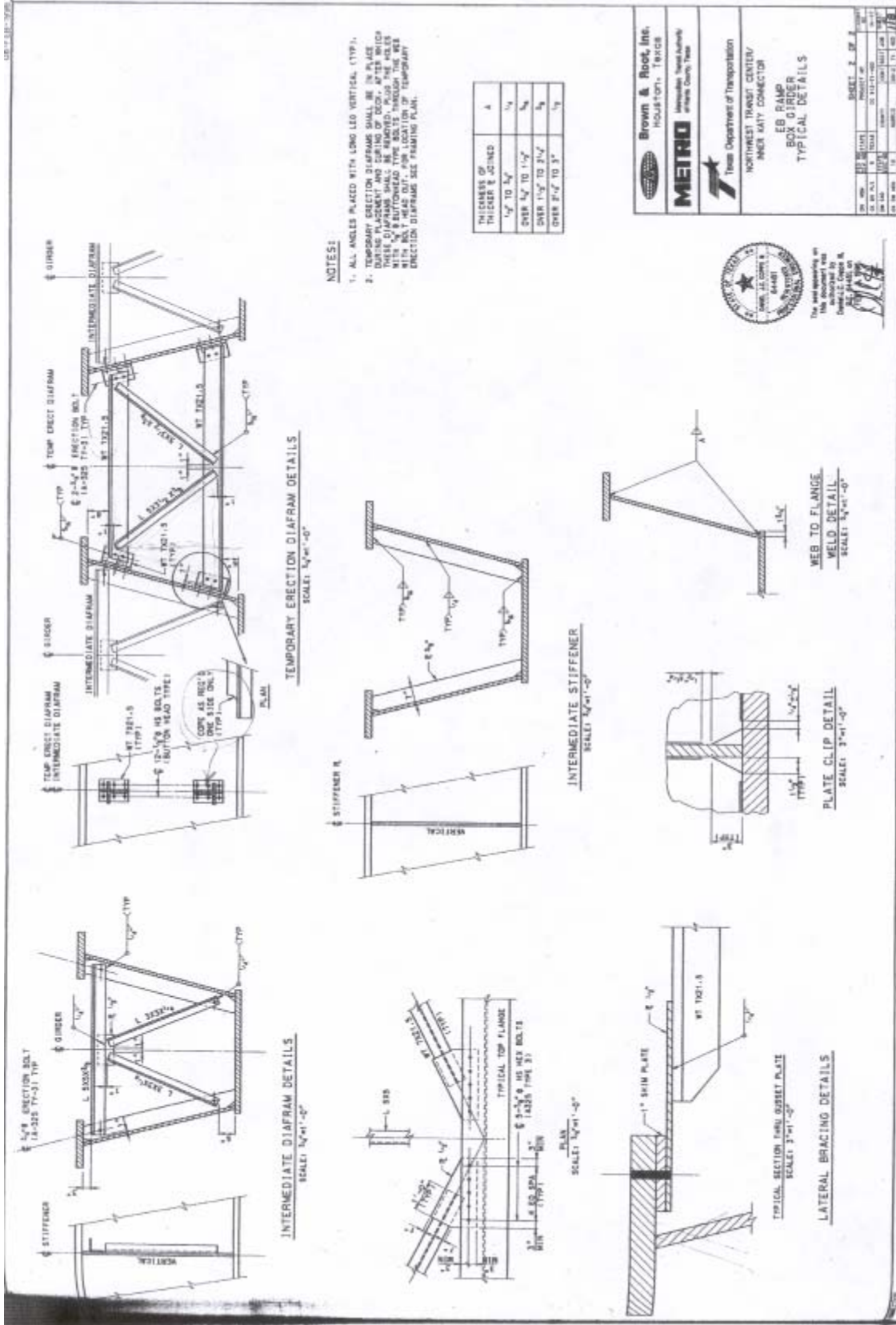


Figure B3-4: Internal and external bracing details from design drawings

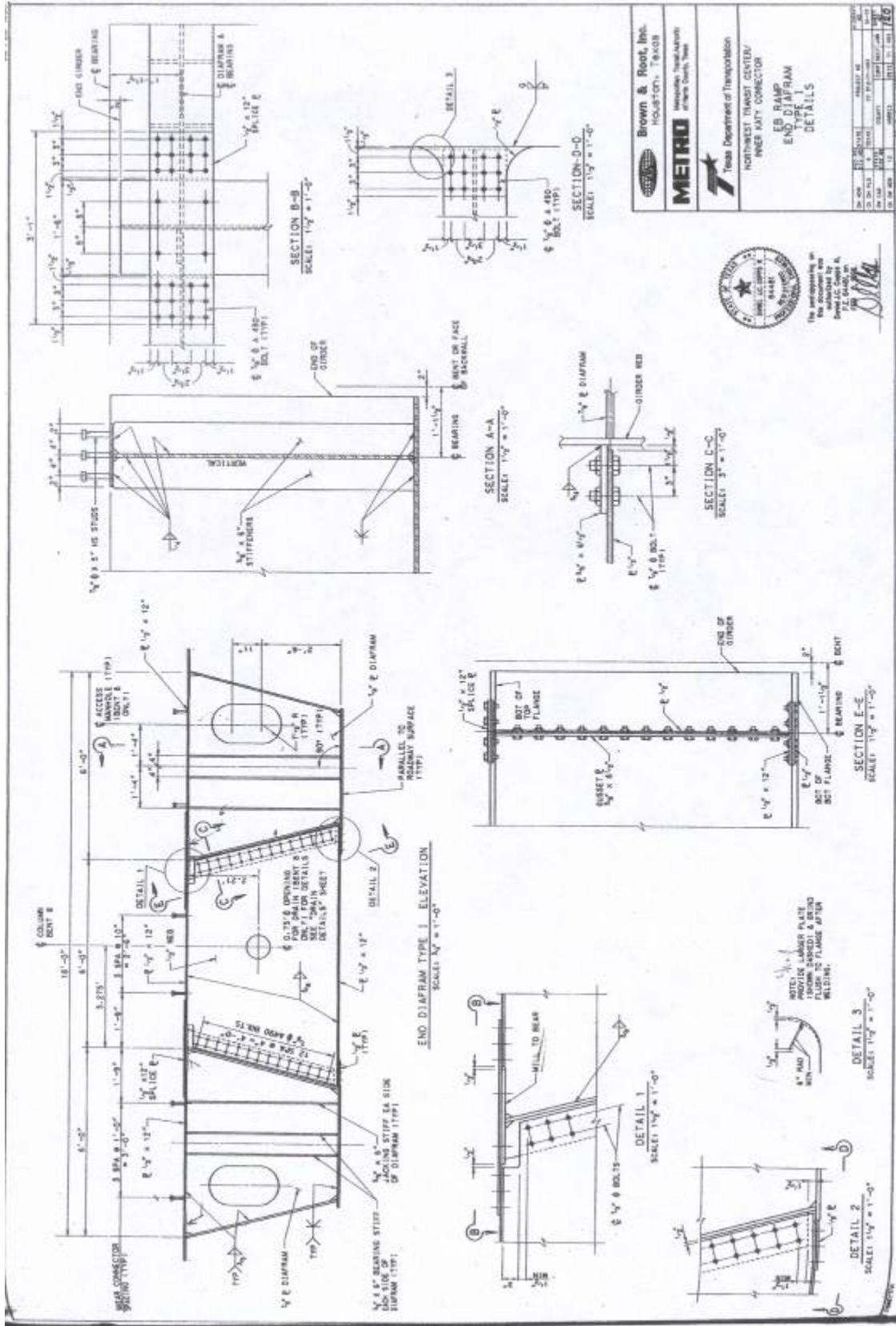


Figure B.3-5: End diaphragm, flange, and stiffener details

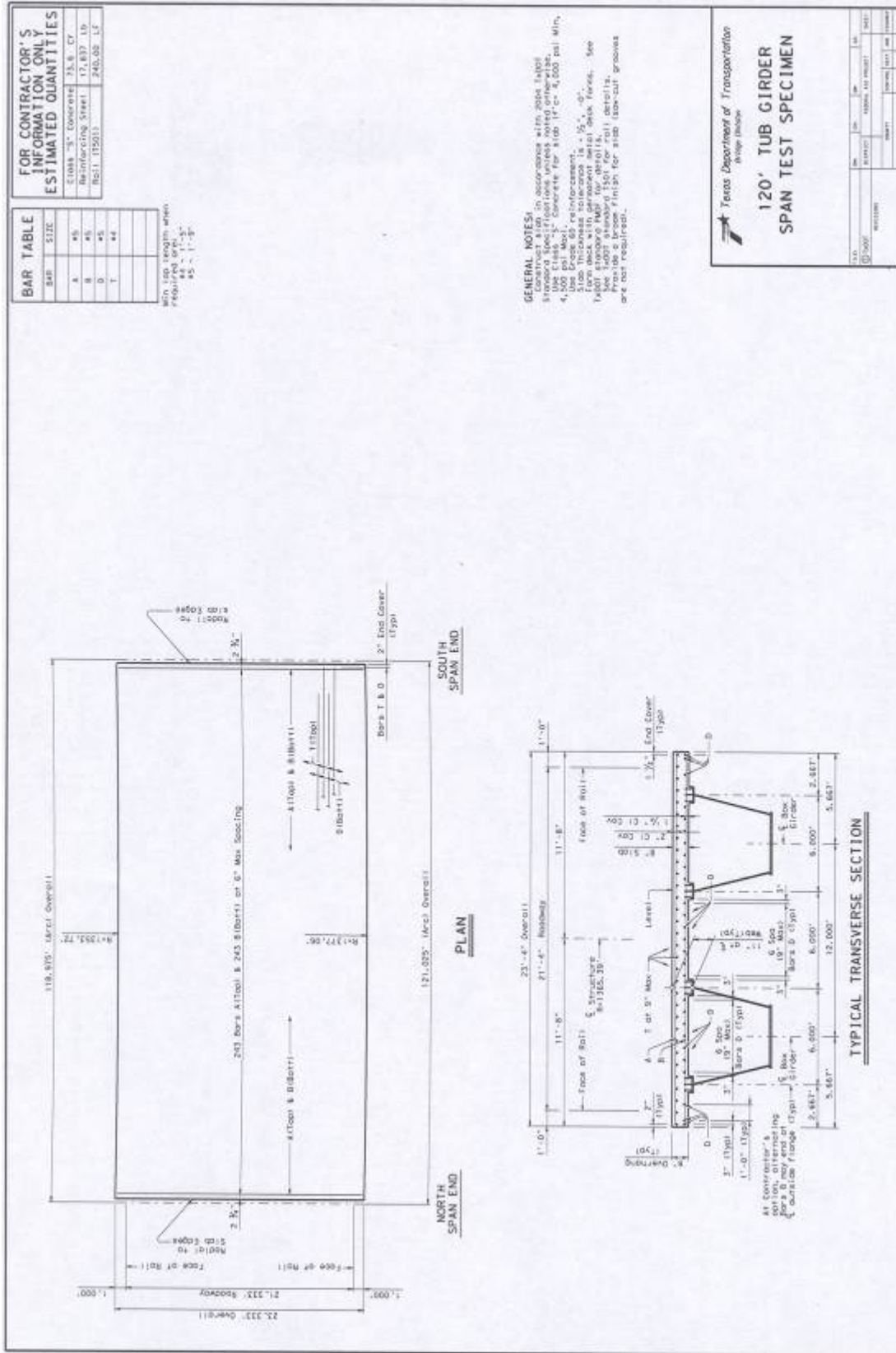


Figure B.4-1: Deck details

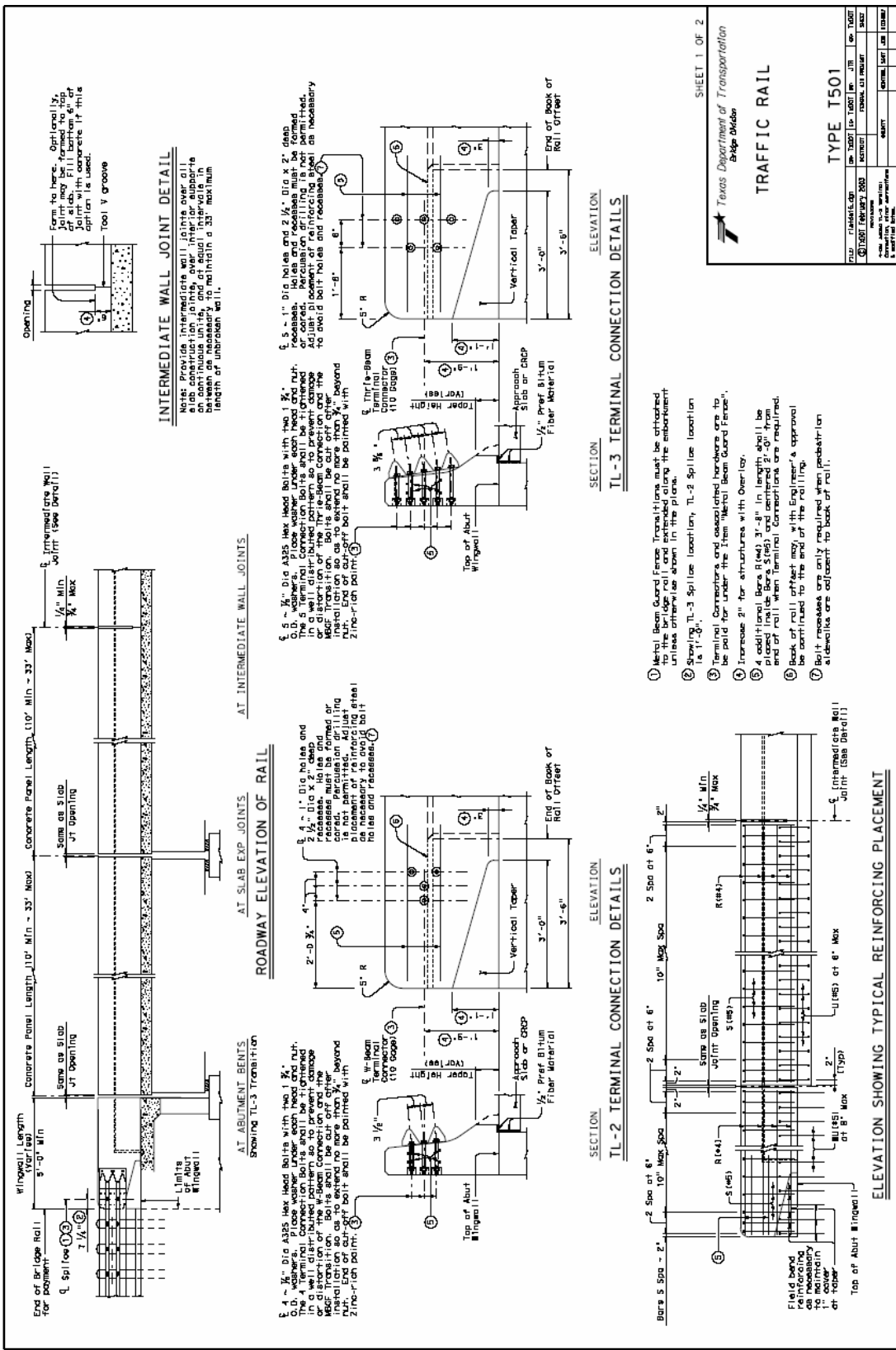


Figure B.5-1: Standard T501 Railing drawings

SHEET 1 OF 2

Texas Department of Transportation
Bridge Division

TRAFFIC RAIL

TYPE T501

FILE NO.	PROJECT NO.	SECTION NO.	DATE
DESIGNED BY	CHECKED BY	APPROVED BY	
DATE	SCALE	BY	DATE

APPENDIX C

Instrumentation Graphs

Interior Girder Average Strains Foil Gages

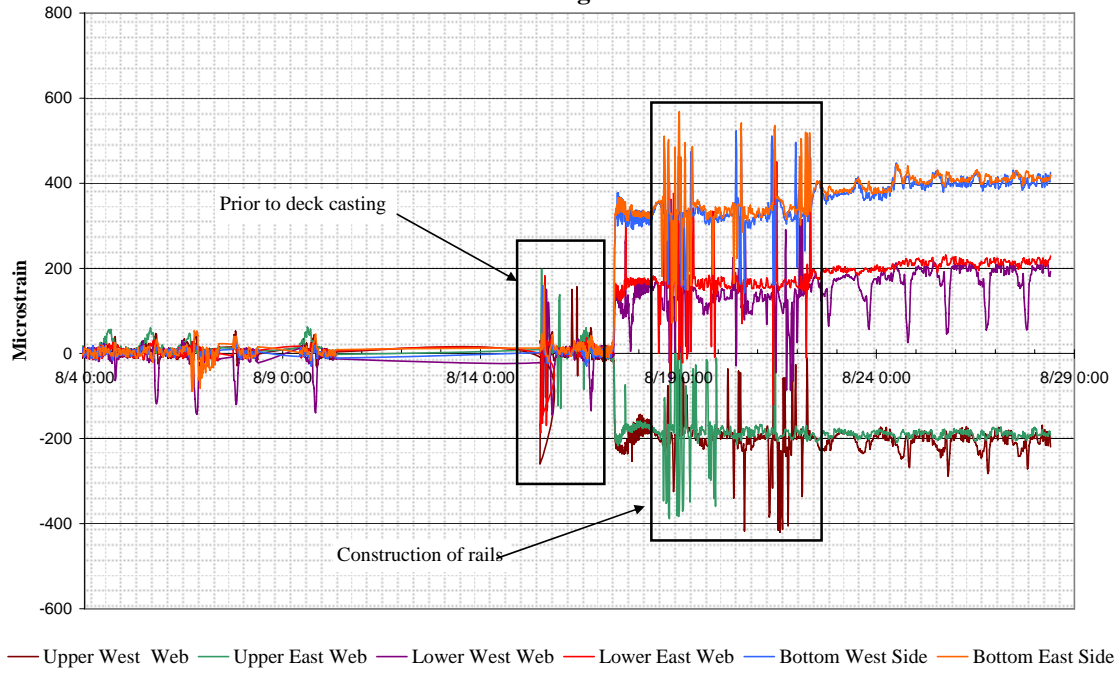


Figure C.1: Noise in strain data

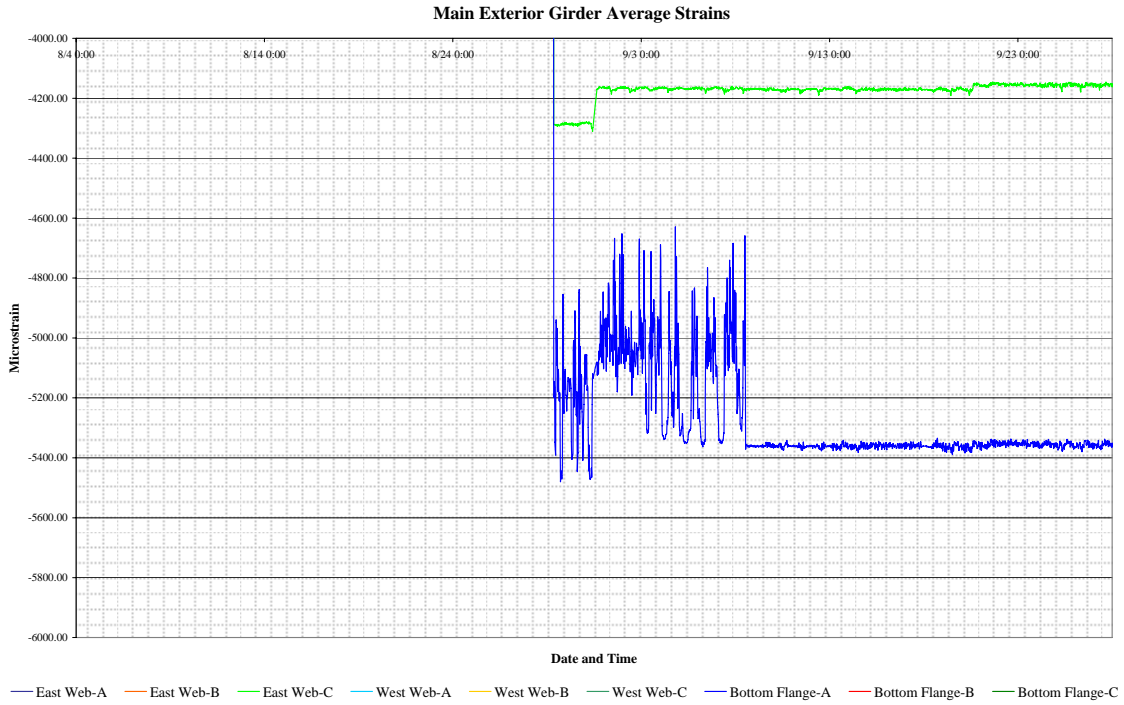


Figure C.2: Average strains at the main cross-section of the exterior girder

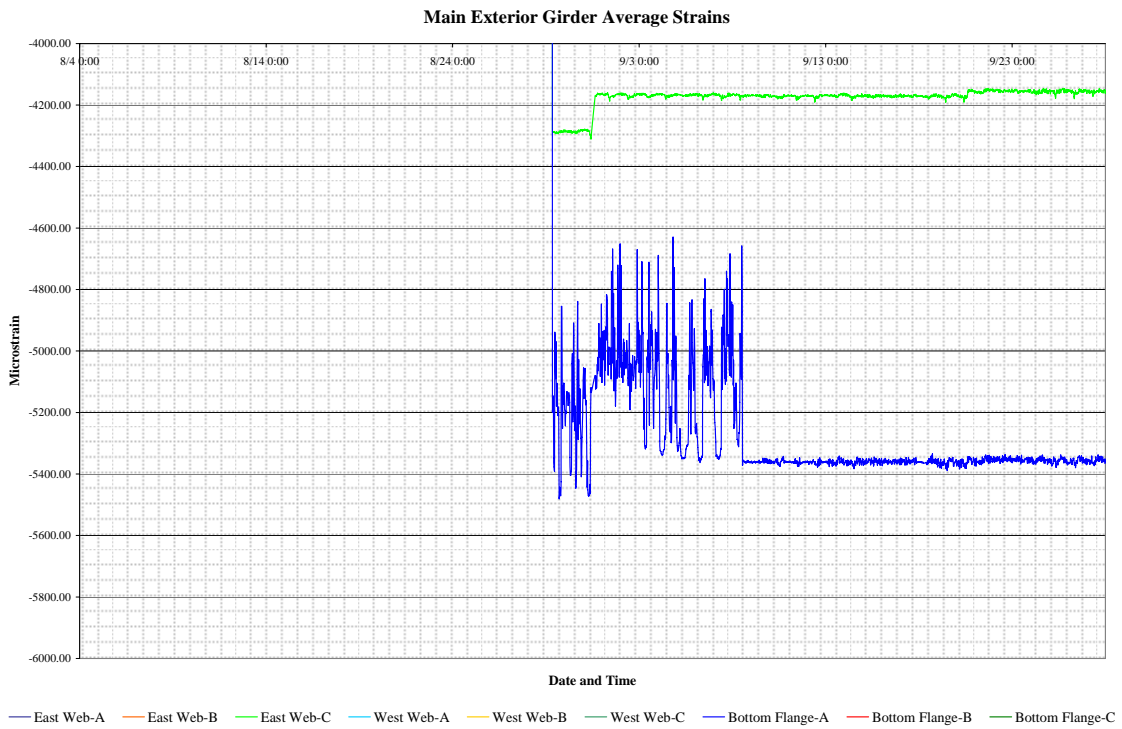


Figure C.3: Sudden drop in the average strains level out and remain steady

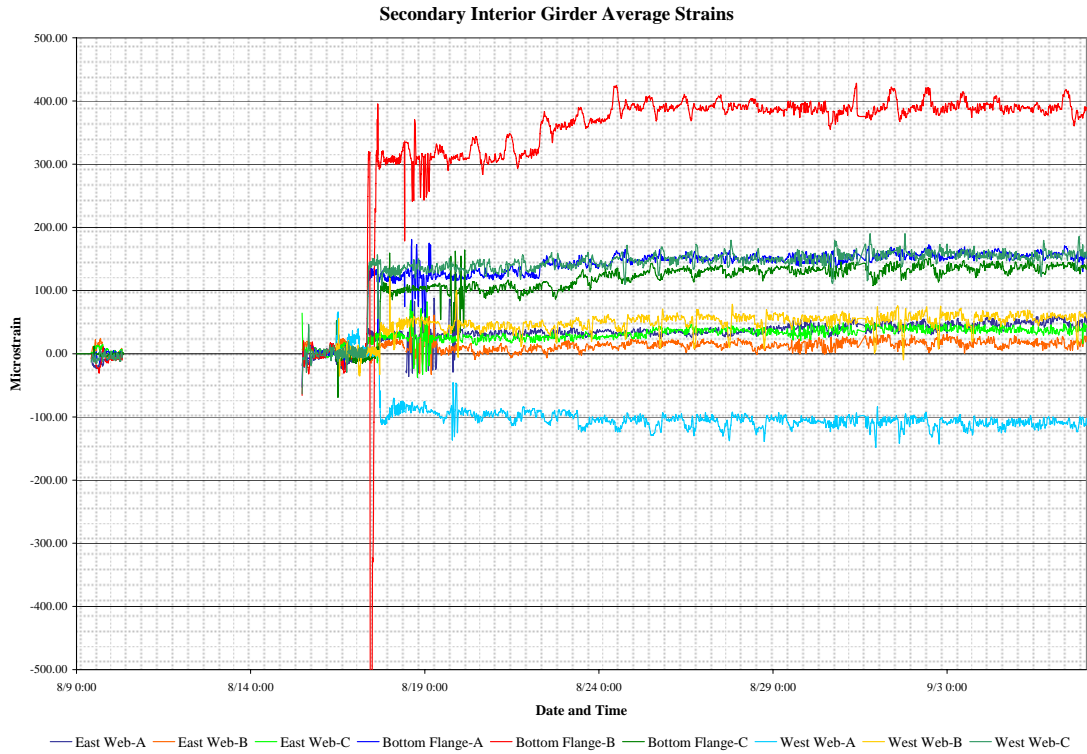


Figure C.5: Average strains at the secondary cross-section of the interior girder.

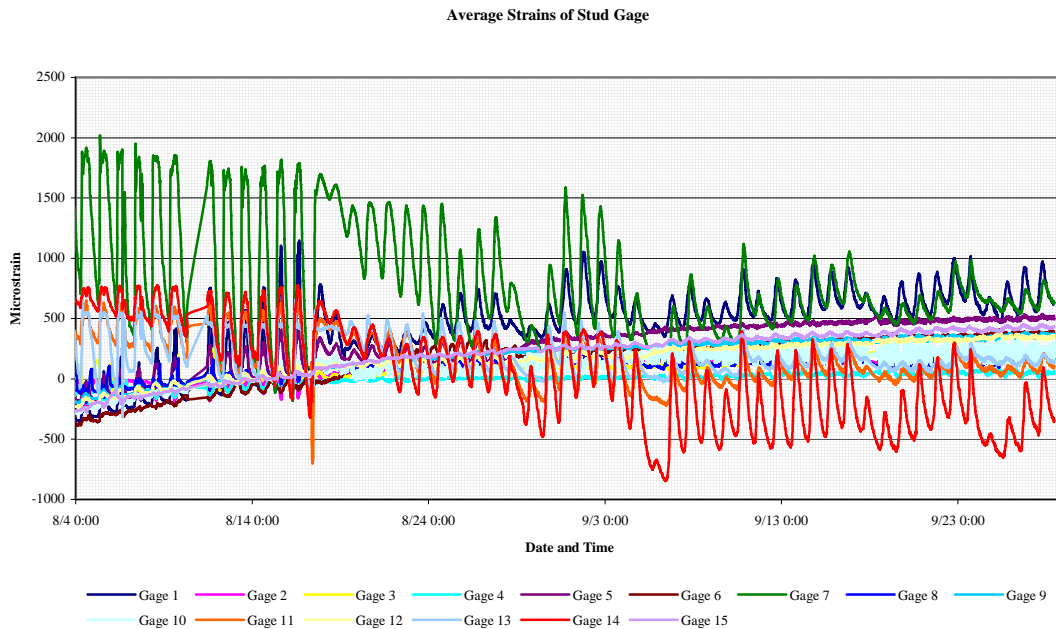


Figure C.6: Average strain in shear studs

Average Strains of Stud Gage

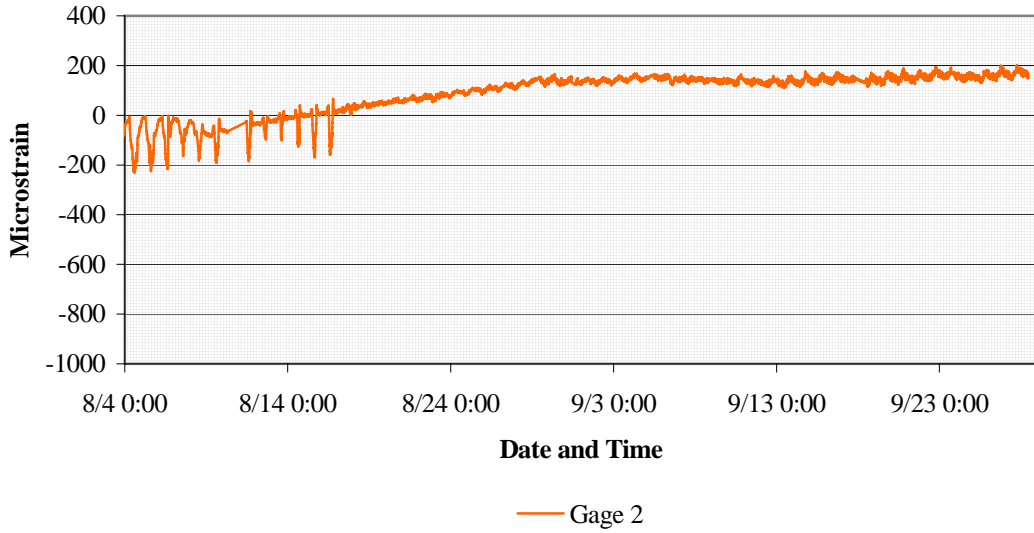


Figure C.7: Strains in shear stud No. 2

Average Strains of Stud Gage

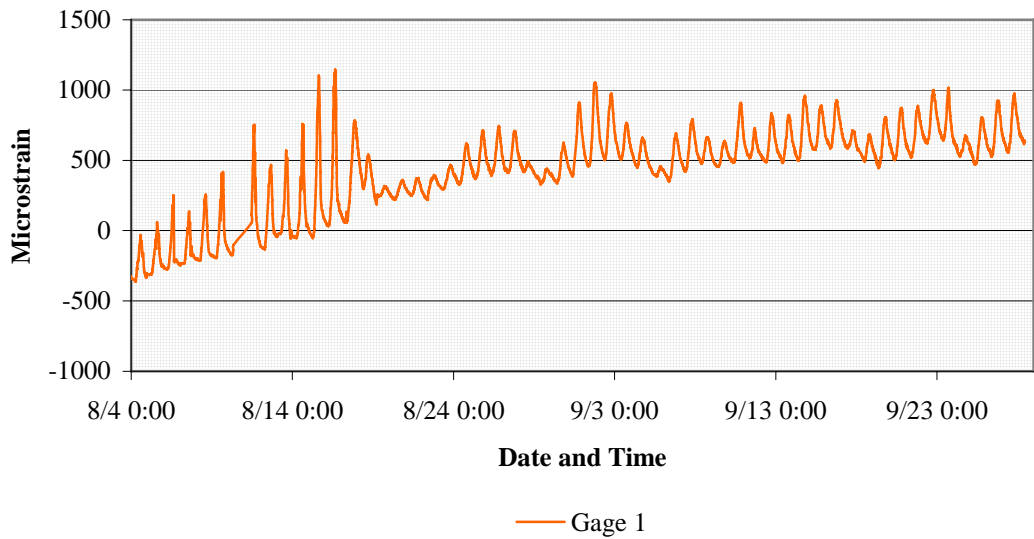


Figure C.8: Large fluctuations in strain data in shear stud No. 1

Average Strains of Stud Gage

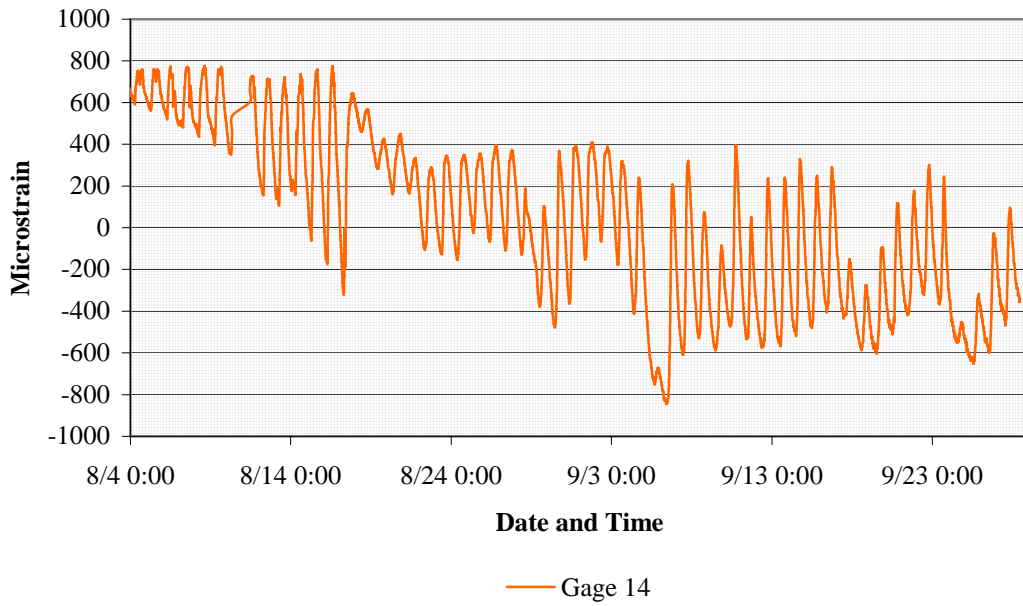


Figure C.9: Extreme fluctuations in strain in shear stud No. 14

Interior Girder Average Strains

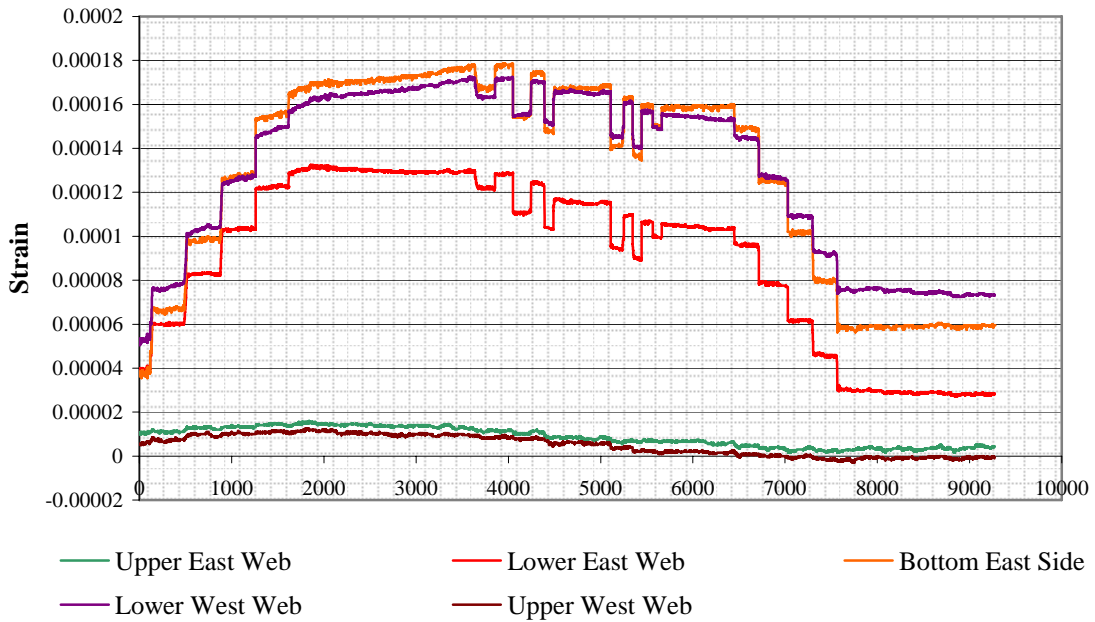


Figure C.10: Interior girder foil gage response during live load testing

Exterior Girder Average Strains

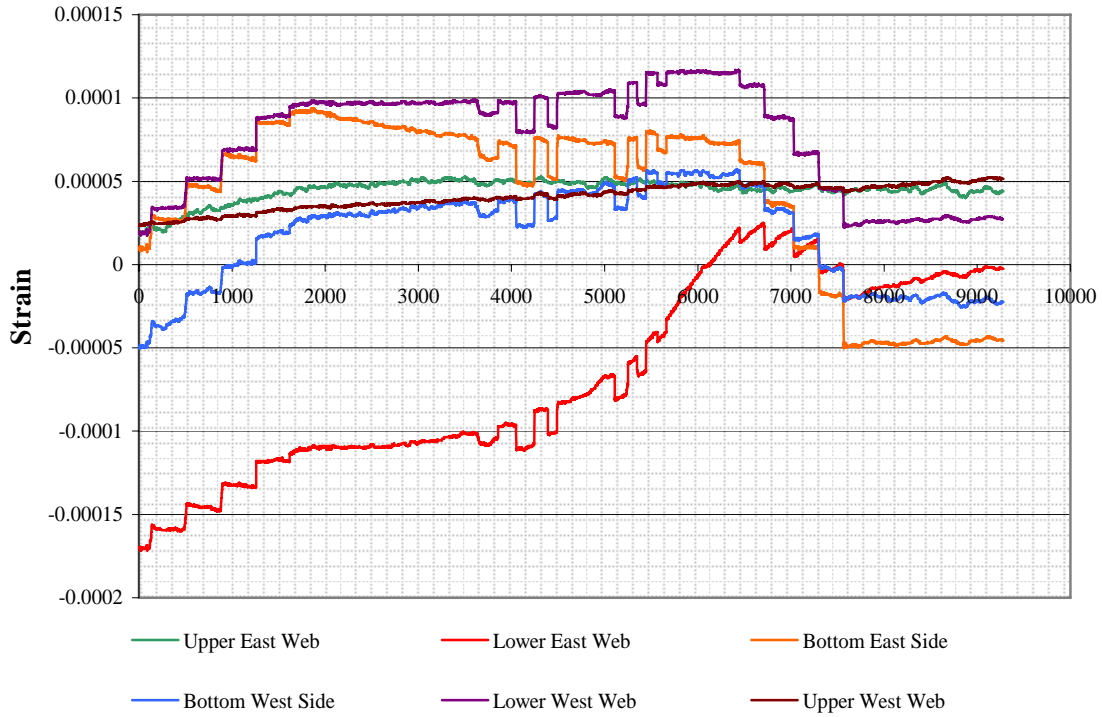


Figure C.11: Exterior girder foil gage response during live load testing

Interior Gider Live Load Test

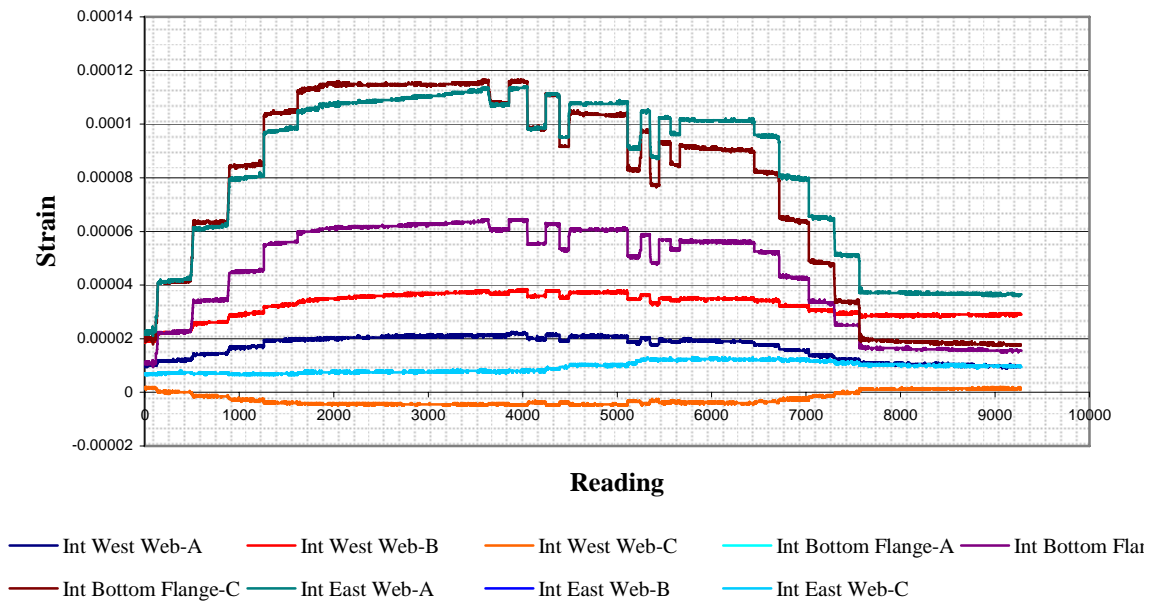


Figure C.12: Interior girder rosette gage response during live load testing

Exterior Gider Live Load Test

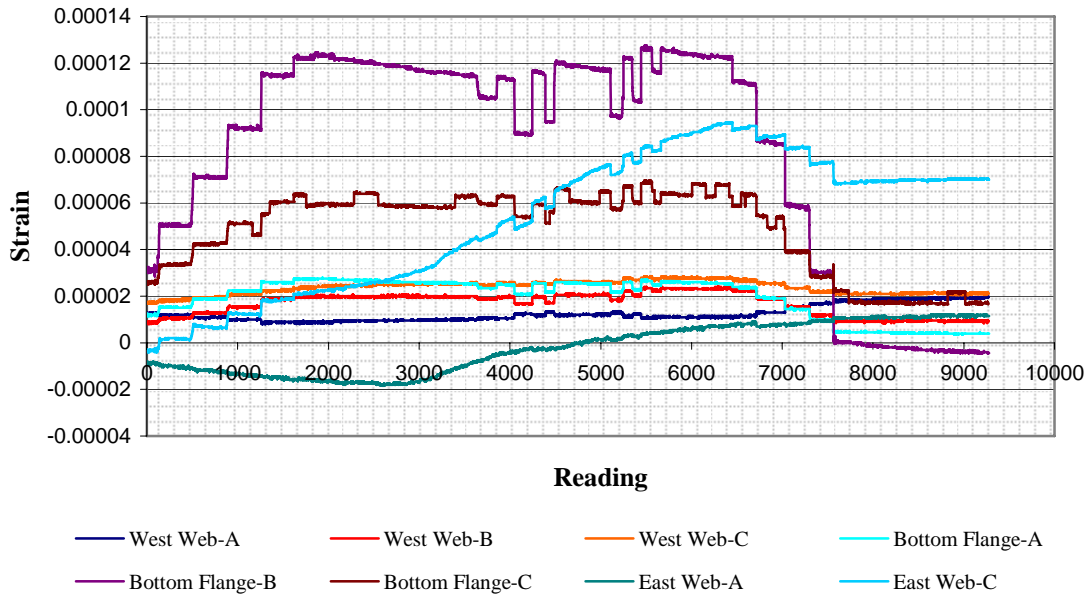


Figure C.13: Exterior girder rosette gage response during live load testing

Secondary Interior Gider Live Load Test

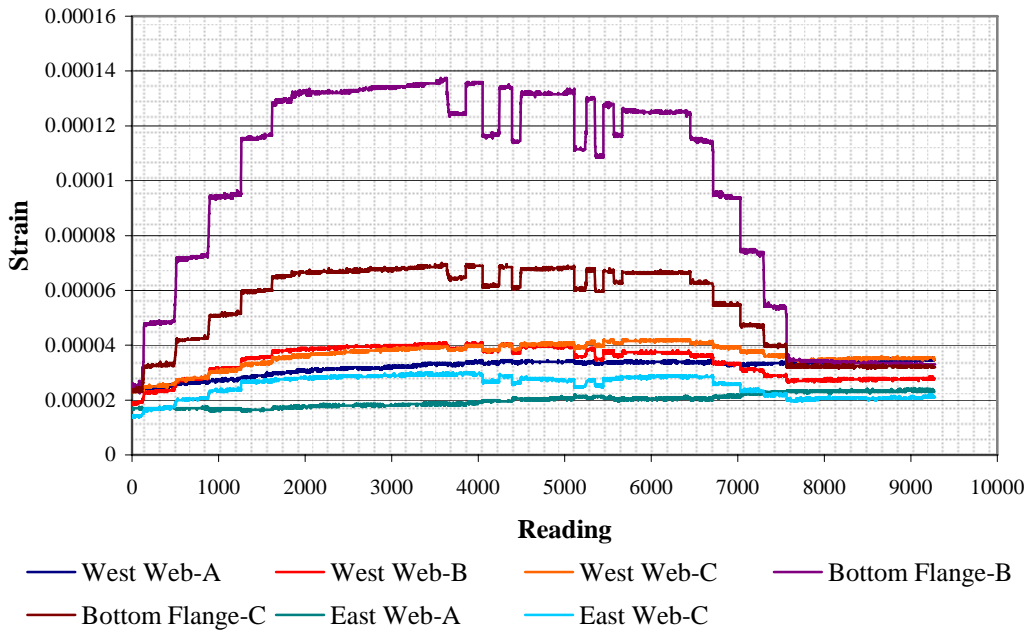


Figure C.14: Interior girder rosette gage response north of midspan during live load testing

Stud Gages During Final Live Load

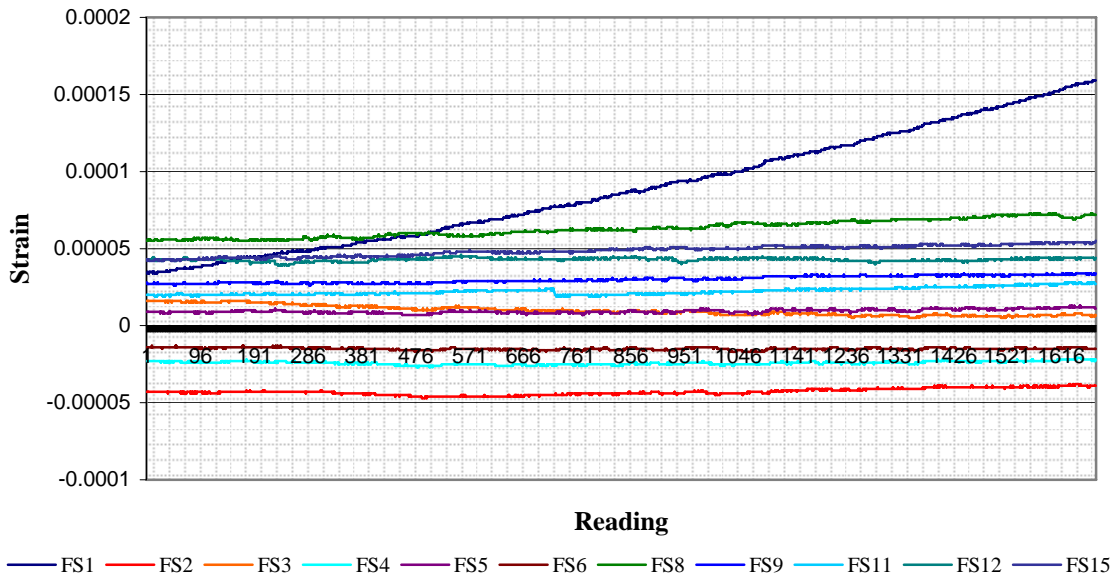


Figure C.15: Shear stud gage response during live load testing

40' North of Center line

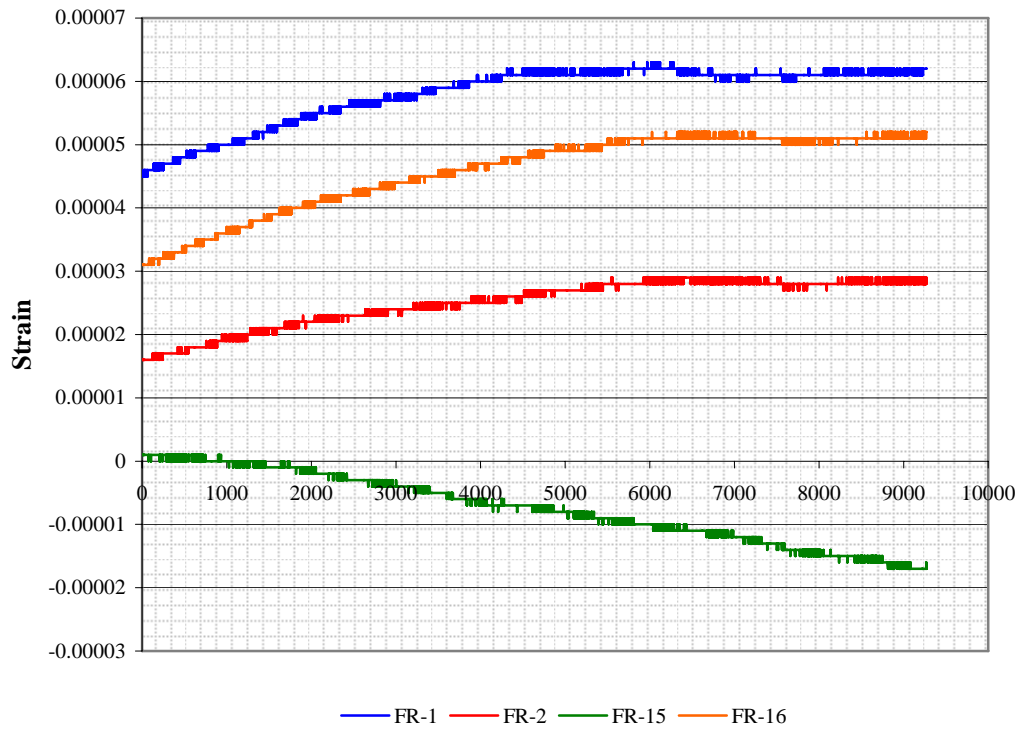


Figure C.16: Rebar gage response 40' North of center line during live load testing

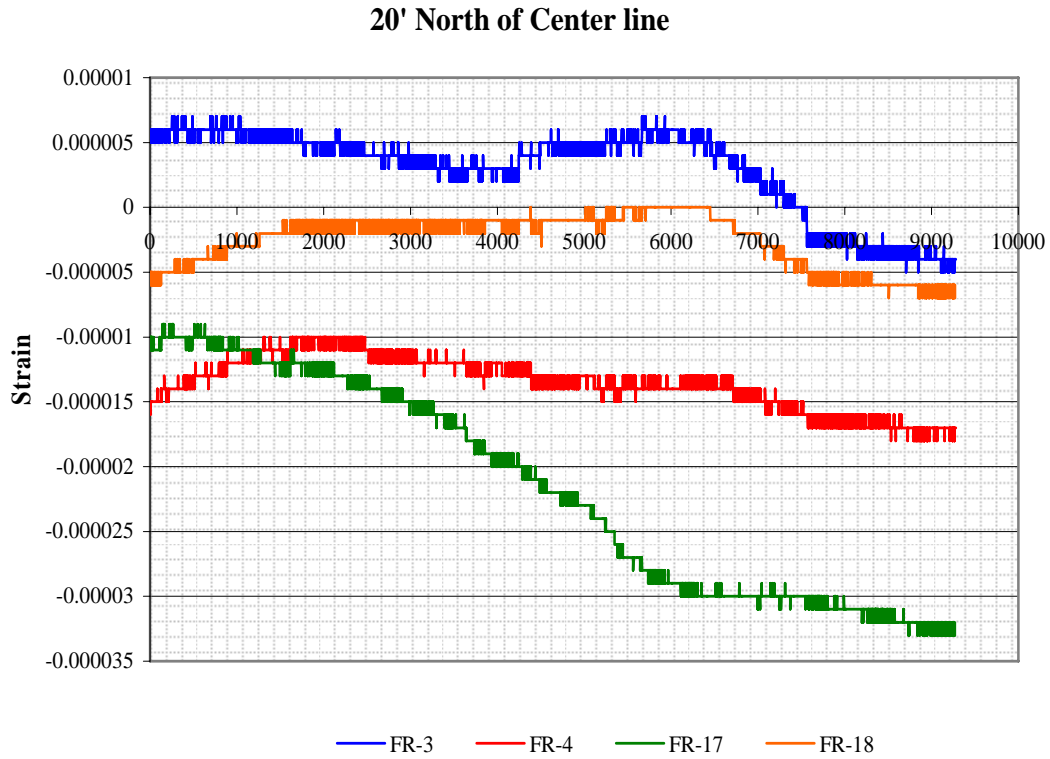


Figure C.17: Rebar gage response 20' North of centerline during live load testing

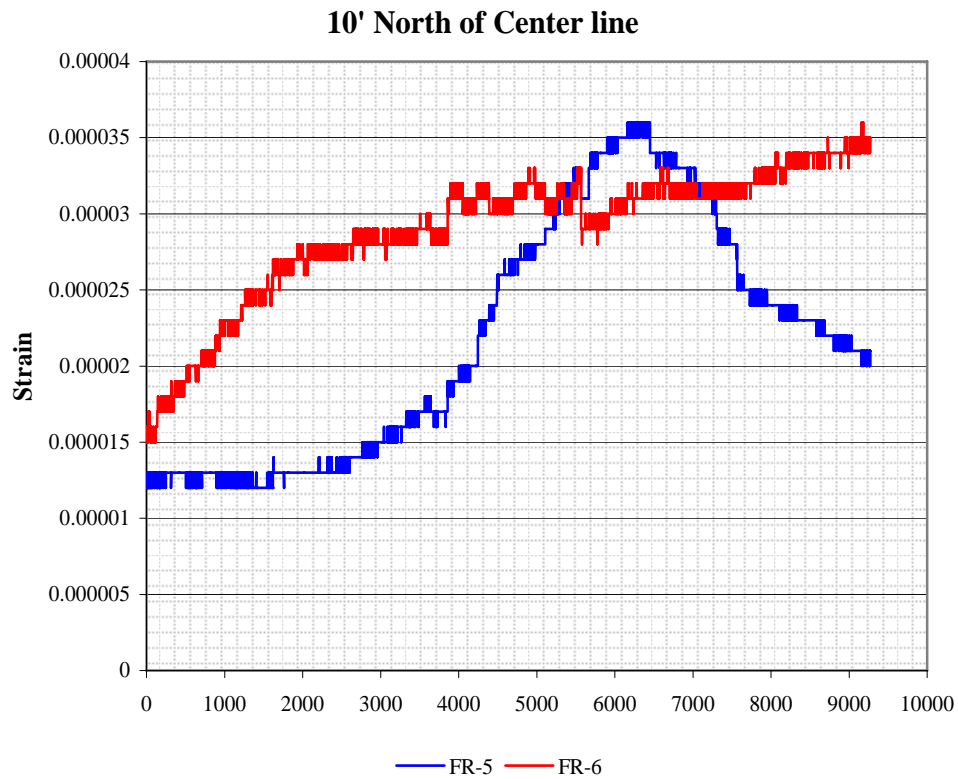


Figure C.18: Rebar gage response 10' North of centerline during live load testing

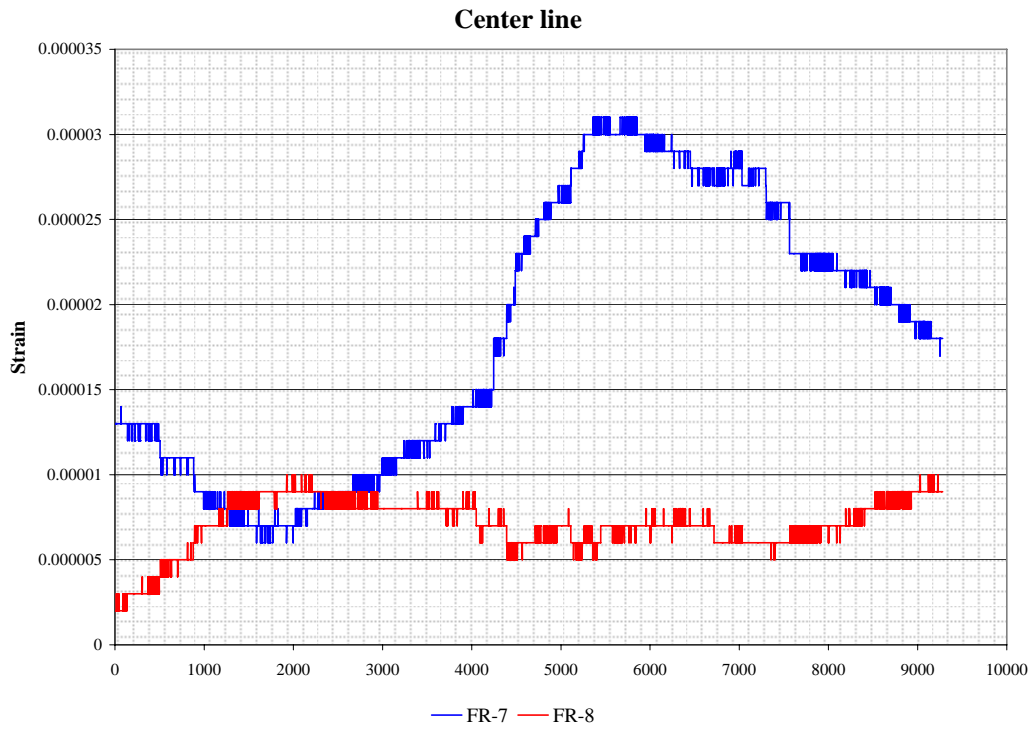


Figure C.19: Rebar gage response at centerline during live load testing

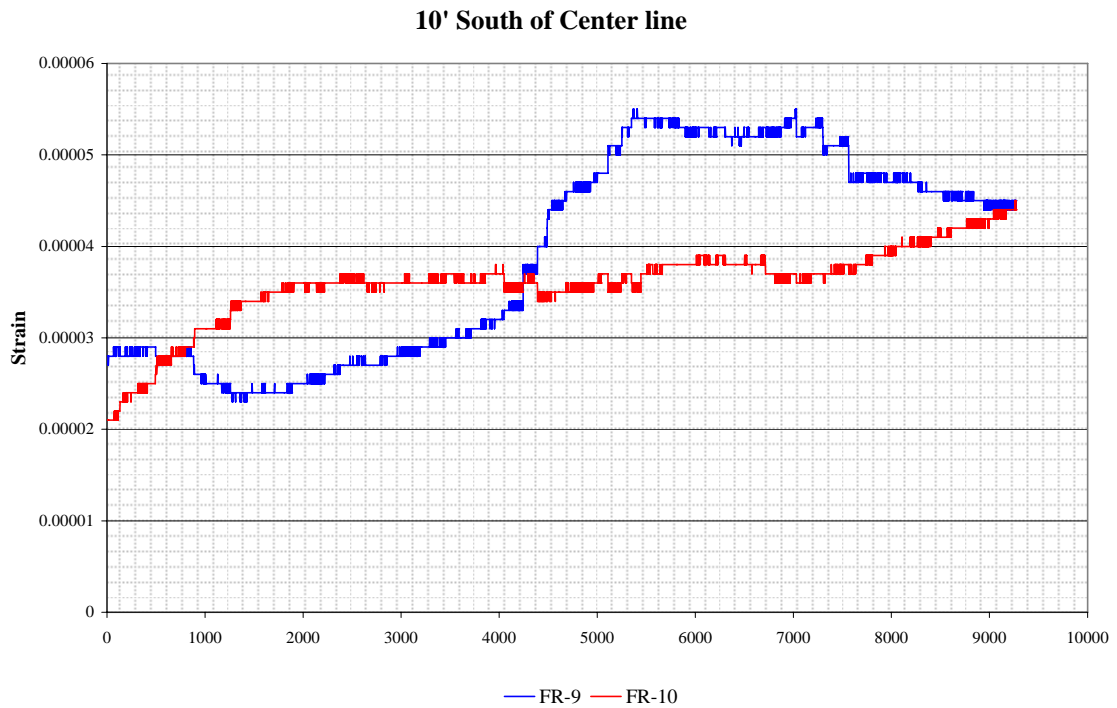


Figure C.20: Rebar gage response 10' South of center line during live load testing

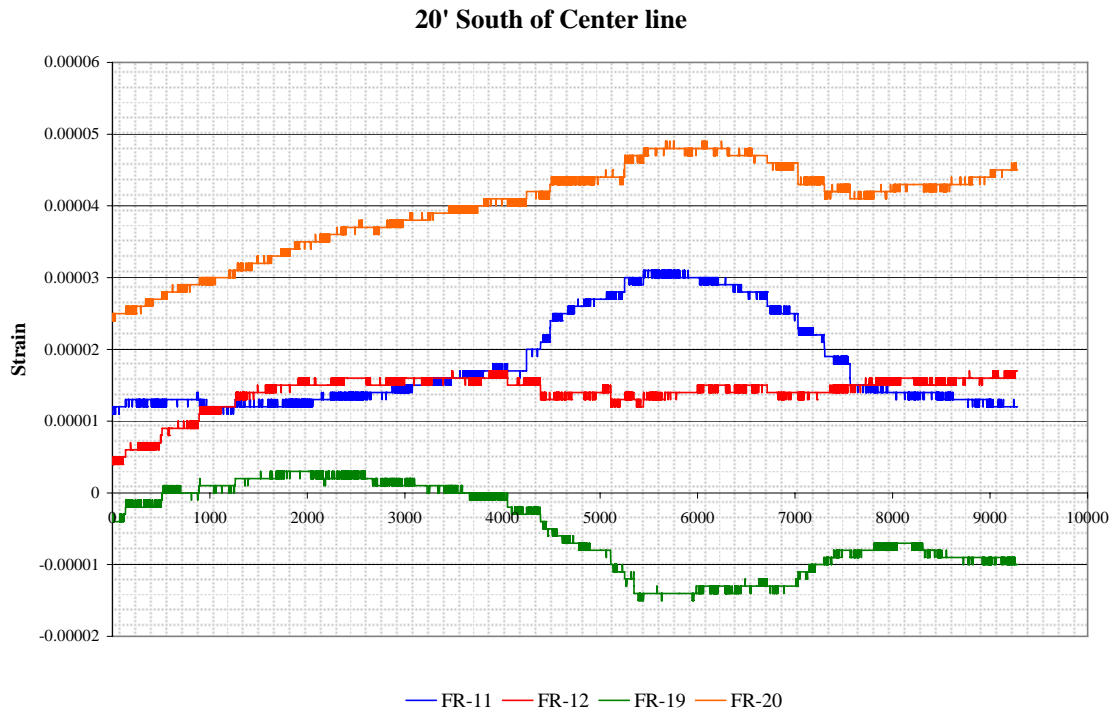


Figure C.21: Rebar gage response 20' South of center line during live load testing

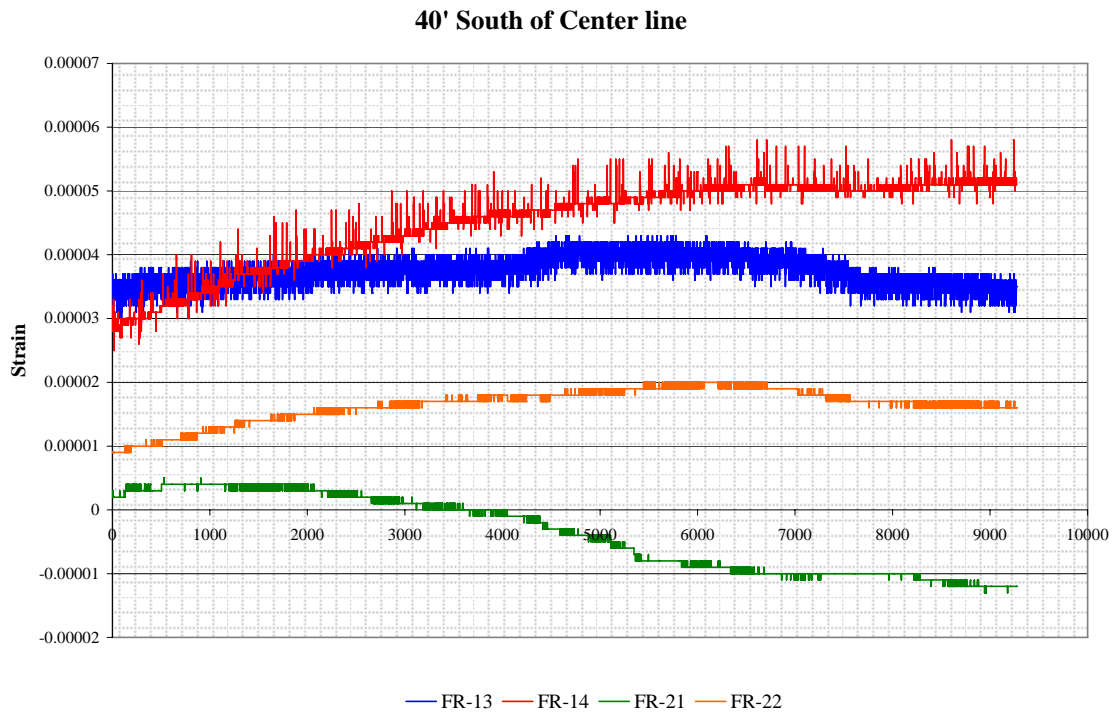


Figure C.22: Rebar gage response 40' South of center line during live load testing

Average Foil Strains During Live Load

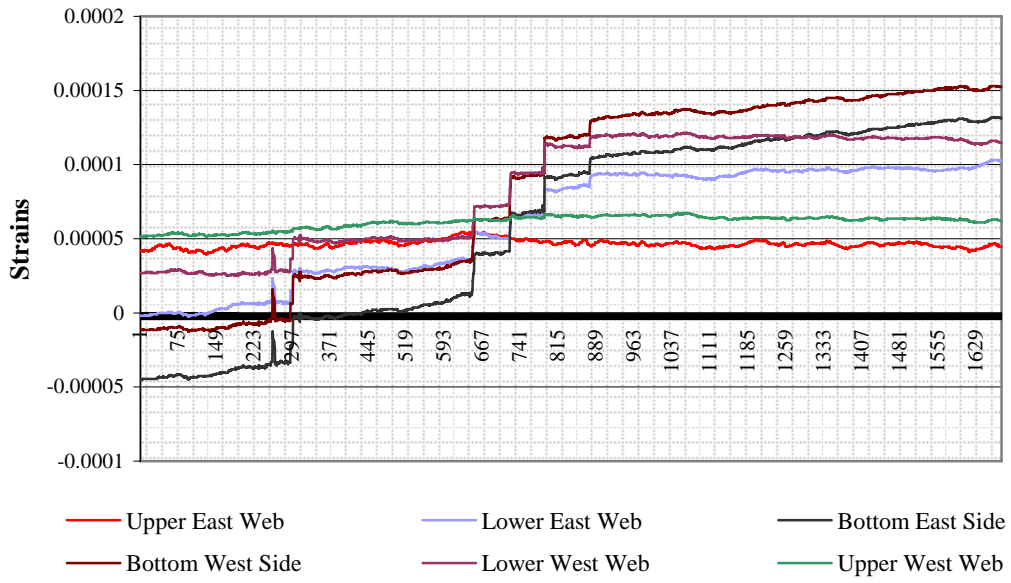


Figure C.23: Average Foil gage strains at final live load placement

APPENDIX D

Pictures

D.1 FOUNDATION CONSTRUCTION



Figure D.1-1: North foundation base



Figure D.1-2: South foundation stem wall

D.2 GIRDER ERECTION



Figure D.2-1: Interior girder placement



Figure D.2-1: North diaphragm placement



Figure D.2-3: South diaphragm placement



Figure D.2-4: Exterior girder placement



Figure D.2-5: Girders in place on foundations

D.3 ASSYMBLING



Figure D.3: Diaphragm bolted connections

D.4 BRACING



Figure D.4: Bracing installation

D.5 STUD REPLACEMENT

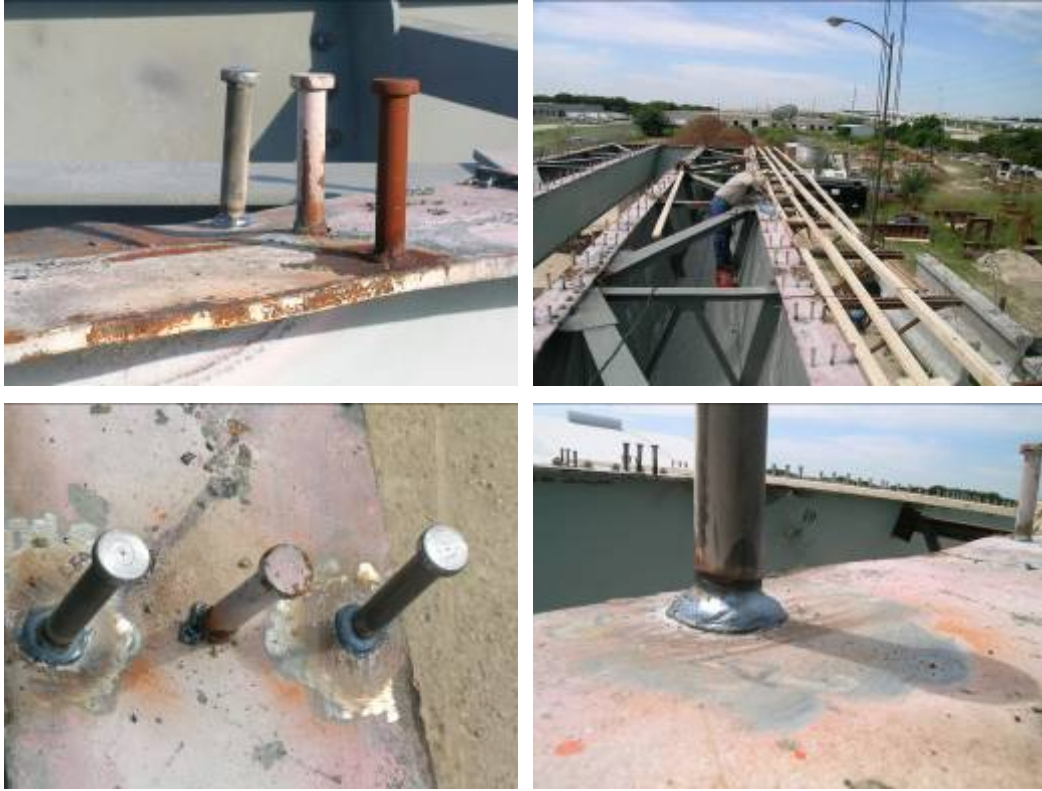


Figure D.5: Stud replacement

D.6 GIRDRIDGE INSTRUMENTATION

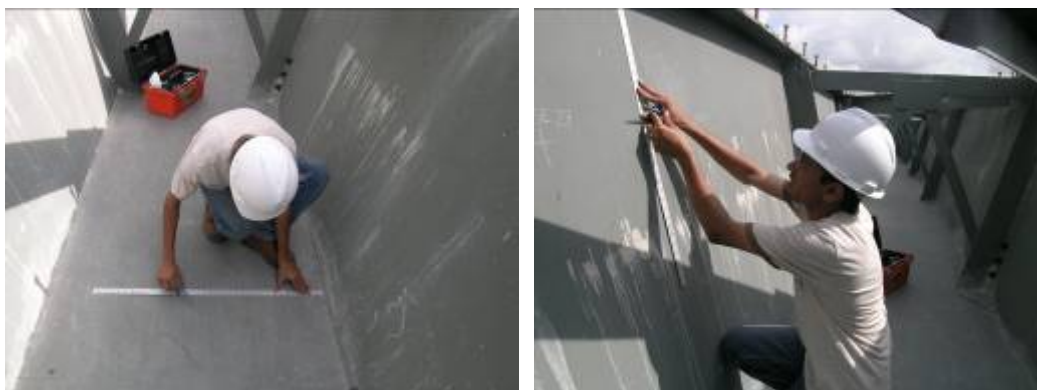


Figure D.6-2: Measuring the girder for proper gage placement



Figure D.6-2: Preparing the surface for gages



(a)

(b)



(c)

Figure D.6-3: a) Installing a rosette gage, b) checking the resistance to ensure proper reading, and c) protecting the gages from moisture with wax



Figure D.6-4: External gages on the girder cross-section

D.7 DECK CONSTRUCTION



Figure D.7-1: Bracket placement on the girders



(a)



(b)

Figure D.7-2: a) Permanent metal decking installation b) edge built up for proper haunch height



Figure D.7-3: Deck reinforcing steel placement

D.8 INSTRUMENTING DECK



Figure D.8-1: Gages located in the center of the flange and the wires were routed under the bars for protection

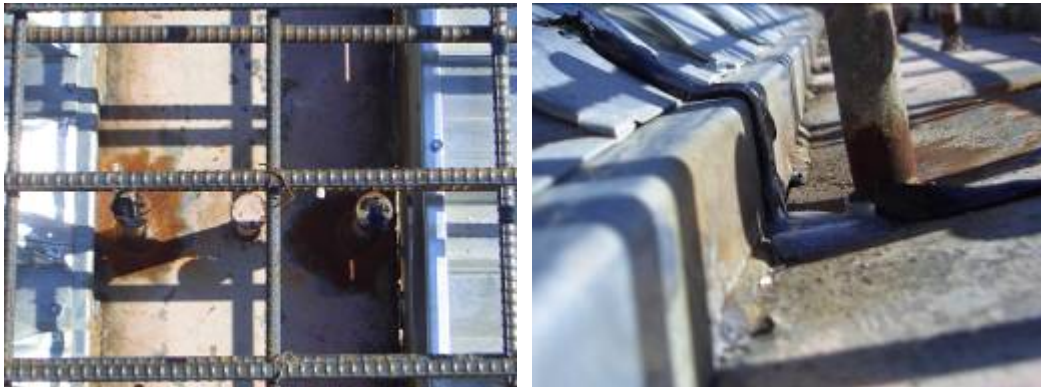


Figure D.8.2: Shear stud gage wiring protected by soft adhesive bituminous material and silicone

D.9 DECK CASTING



Figure D.9-1: Deck casting starting from the north end using screen



Figure D.9-2: Contractor provided a broom finish



Figure D.9-3: Deck was sprayed with sealing compound and covered with wet blankets and plastic to cure

D.10 CASTING RAILS



Figure D.10-1: Rail construction



Figure D.10-2: Rails after forms were removed

D.11 DATA ACQUISITION SYSTEM



Figure D.11-1: Wiring coming from bridge to the data acquisition storage shed



Figure D.11-2: Wiring routed to multiplexers and connected



Figure D.11-3: Data logger unit used to collect data during construction phase of the project

D.12 LIVE LOAD



Figure D.12-1: Attaching plates to load cell to allow it to be hooked to crane cable



Figure D.12-2: Cables with load cell attached are placed on the crane hook



Figure D.12-3: Concrete beam being attached to crane with load cell to determine weight



Figure D.12-4: Beams were numbered to keep track of strain from load cell and position on the bridge deck during testing



(a)



(b)

Figure D.12-4: a) Live load test position 1 front axle position b) rear axle position



(a)



(b)

Figure D.12-5: a) Live load test position 2 front axle position b) rear axle position



Figure D.12-6: Position 3 during live load testing and the final position for fracture testing

REFERENCES

- ACI Committee 318, 2002, *Building Code Requirements for Structural Concrete (ACI 318-02)*, American Concrete Institute, Farmington Hills, MI., pp. 379-405.
- ACI Committee 318, 2005, *Building Code Requirements for Structural Concrete (ACI 318-05)*, American Concrete Institute, Farmington Hills, MI., pp. 121.
- American Association of State Highway Transportation Officials (AASHTO), 2004, *AASHTO LRFD Bridge Design Specifications*, AASHTO, Washington, DC, pp. 1-2, 210-212.
- American Institute for Steel Construction (AISC), 2004, *Specification for Structural Joints using A325 and A490 Bolts*, Research Council on Structural Connections, Chicago, Illinois, pp. 16.4-48.
- American Institute for Steel Construction (AISC), 2003, *Manual of Steel Construction: Load and Resistance Factor Design*, 13th Edition, AISC, pp. 5-177.
- Bradberry, T. E.; Cotham, J. C.; and Medlock, R.D., 2005, "Elastomeric Bearings for Steel Trapezoidal Box Girder Bridges," *Transportation Research Record No. 1928*, pp. 27-38.
- Charleston Daily Mail, 2006, <http://www.dailymail.com/static/specialsections/lookingback/lb0208c.htm> (accessed December 1, 2006).
- Connor, Robert J.; Dexter, Robert; and Mahmoud, Hussam, 2005, "Inspection and Maintenance of Bridges with Fracture-Critical Details," *NCHRP Synthesis 354*, National Research Council, TRB, Washington, DC, pp. 1, 13-15, and 30.
- Electronic Code of Federal Regulations (e-CFR), 2006, *Title 23, Part 650, Subpart C: National Bridge Inspection Standards*, U.S. Government Printing Office, Washington DC, <http://ecfr.gpoaccess.gov/cgi/t/text/text-idx?c=ecfr;sid=c0278a8e9bb21e847152c57feb8a95ff;rgn=div5;view=text;node=23%3A1.0.1.7.28;idno=23;cc=ecfr#23:1.0.1.7.28.3.1.3> (accessed December 1, 2006).

- Ghosn, Michel and Moses, Fred, 1998, "Redundancy in Highway Bridge Superstructures," *NCHRP Report 406*, National Research Council, TRB, Washington, DC, pp. 1-42.
- Hassoun, M. Nadin, 1998, "*Structural Concrete*," Menlo Park, California, pp. 435
- Idriss, R.L; White, K.R.; Woodward, C.B.; and Jauregui, D.V., 1995, "Evaluation and testing of a Fracture Critical Bridge," *NDT&E International*, V. 28, No. 6, pp. 339-347.
- International Code Council (ICC), 2003, *International Building Code (IBC)*, ICC, Falls Church, Virginia, pp. 426.
- Kowalik, Alan, 2006, Correspondence through electronic mail.
- Lovejoy, Steve C., 2003, "Determining Appropriate Fatigue Inspection Intervals for Steel Bridge Members," *Journal of Bridge Engineering*, V. 8, No. 2, pp. 66.
- Texas Department of Transportation, 2001, "Bridge Design Manual," TxDOT, pp. 9-83 to 9-88.
- Texas Department of Transportation, 2006, "Bridge Railing Manual," TxDOT, pp. 2-23.
- Trimble Navigation Limited, 2006, <http://trl.trimble.com/docushare/dsweb/Get/Document-256481/Datasheet%20-%20LL400%20Laser%20-%20English.pdf> (accessed December 1, 2006).

VITA

Timothy J. Barnard was born in Little Rock, Arkansas on March 3, 1967, son of Thomas and Wanda Barnard. He is the brother of Thomas and James Barnard. He graduated high school in 1985 from Sheridan High in Sheridan, Arkansas. After high school, he entered into the United States Air Force where he served as an Aircraft Systems Mechanic for 11 years and an Engineering Assistant for 2 years before being accepted into the Reserve Officer Training Corp program at Florida State University. In December of 2001 he was awarded the degree of Bachelor of Science in Civil Engineering and reentered the Air Force as a commissioned officer. After graduating, he was stationed at Eielson Air Force Base, Alaska where he worked as a maintenance engineer for the 325th Civil Engineering Squadron. In July of 2005, he was selected by Air Force leadership to attend graduate school to obtain an advanced degree in civil engineering. In August of 2005, he entered The Graduate School at The University of Texas to pursue a Master of Science degree in Engineering. While pursuing his graduate degree, he worked at the Ferguson Structural Engineering Laboratory under the supervision of Prof. Eric B. Williamson and Prof. Karl H. Frank.

Permanent Address: 807 Jones Drive

Sheridan, Arkansas 72150

This report was typed by the author.